Assessing biomass and architecture of tropical trees with terrestrial laser scanning

Alvaro Ivan Lau Sarmiento

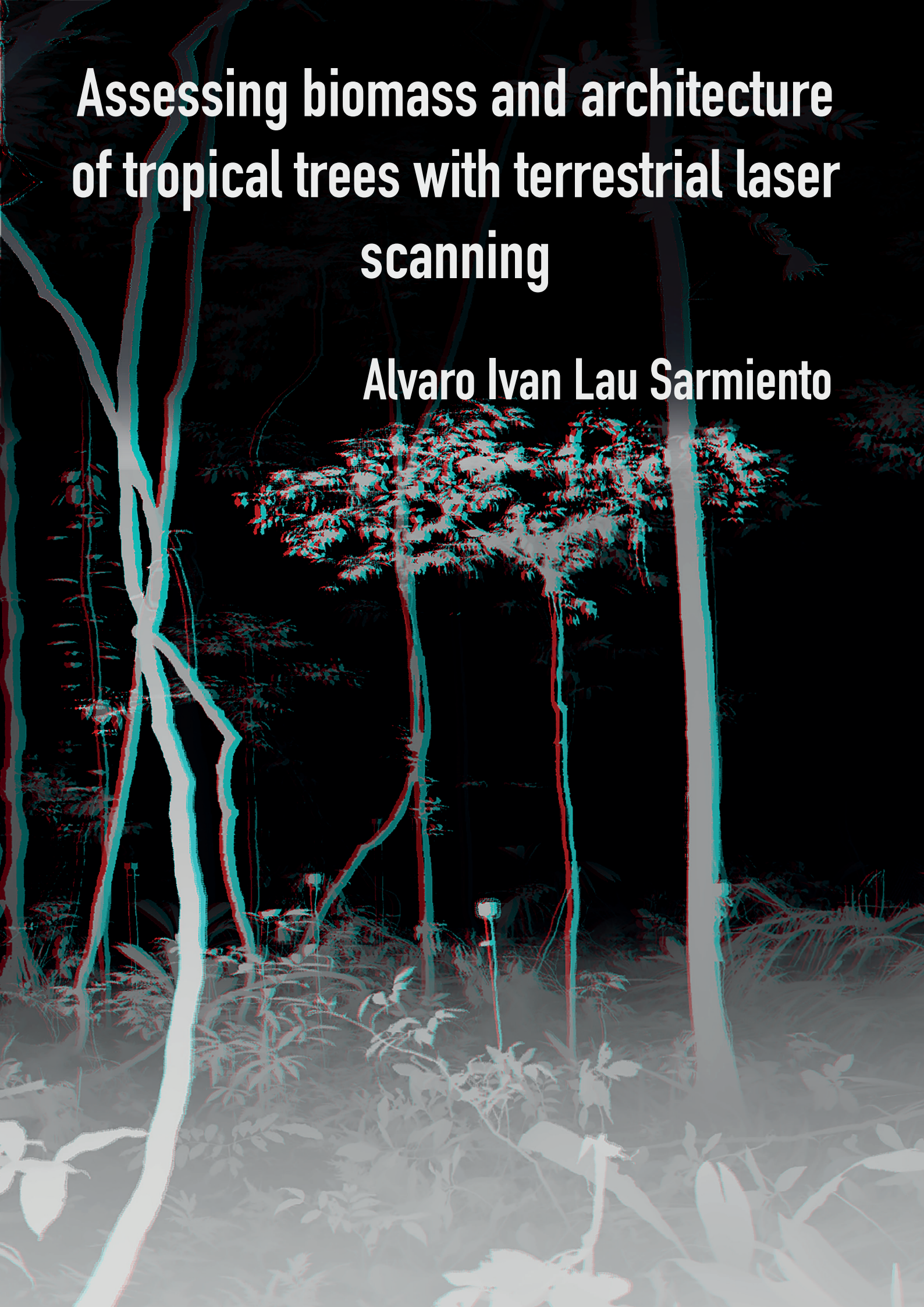

Assessing biomass and architecture of tropical trees with terrestrial laser scanning

Alvaro Ivan Lau Sarmiento

Thesis committee

Promotor
Prof. Dr M. Herold
Professor of Geo-information Science and Remote Sensing
Wageningen University & Research

Co-promotors
Dr H. Bartholomeus
Assistant professor, Laboratory of Geo-information Science and Remote Sensing
Wageningen University & Research

Dr K. Calders
Researcher, CAVElab - Computational & Applied Vegetation Ecology
Ghent University, Belgium

Other members
Prof. Dr P.A. Zuidema, Wageningen University & Research
Prof. H. Verbeeck, Ghent University, Belgium
Prof. E. Næsset, Norwegian University of Life Sciences, Ås, Norway
Dr N. Barbier, Institute of Research for Development, Montpellier, France

This research was conducted under the auspices of the C.T. de Wit Graduate School of Production Ecology & Resource Conservation (PE&RC)

Assessing biomass and architecture of tropical trees with terrestrial laser scanning

Alvaro Ivan Lau Sarmiento

Thesis
submitted in fulfilment of the requirements for the degree of doctor
at Wageningen University
by the authority of the Rector Magnificus,
Prof. Dr A.P.J. Mol,
in the presence of the
Thesis Committee appointed by the Academic Board
to be defended in public
on Tuesday 30 October 2018
at 4 p.m. in the Aula.

Alvaro Ivan Lau Sarmiento
Assessing biomass and architecture of tropical trees with terrestrial laser scanning,
158 pages.

PhD thesis, Wageningen University, Wageningen, the Netherlands (2018)
With references, with summaries in English and Spanish
ISBN 978-94-6343-472-0
DOI: 10.18174/455128

Summary

Over the last two decades, terrestrial light detection and ranging (LiDAR), also known as terrestrial laser scanning (TLS) has become a valuable tool in assessing the woody structure of trees, in a method that is accurate, non-destructive, and replicable. This technique provides the ability to scan an area, and utilizes specialized software to create highly detailed 3D point cloud representations of its surroundings. Although the original usage of LiDAR was for precision survey applications, researchers have begun to apply LiDAR to forest research. Tree metrics can be extracted from TLS tree point clouds, and in combination with structure modelling, can be used to extract tree volume, above-ground biomass (AGB), growth, species, and to understand ecological questions such as tree mechanics, branching architecture, and surface area. TLS can provide a robust and rapid assessment of tree characteristics. These characteristics will improve current global efforts to measure forest carbon emissions, understand their uncertainties, and provide new insight into tropical forest ecology. Thus, the main objective of this PhD is to explore the use of 3D models from terrestrial laser scanning point clouds to estimate biomass and architecture of tropical trees. TLS-derived biomass and TLS-derived architecture can potentially be used to generate significant quality data for a better understanding of ecological challenges in tropical forests.

In this thesis, a dataset of forest inventory with TLS point clouds and destructive tree harvesting were created from three tropical regions: Indonesia, Guyana, and Peru. A total of 1858 trees were traditionally inventoried, 135 trees were TLS scanned, and 55 trees were destructively harvested. In this thesis, procedures to estimate tree metrics such as tree height (H), diameter at breast height (D), crown diameter (CD), and the length and diameter of individual branches were developed using 3D point clouds and 3D modelling. From these tree metrics, I infer AGB, develop allometric models, and estimate metabolic plant scaling of individual tropical trees. All these metrics are validated against a traditional forest inventory data and destructively harvested trees.

Chapter 2 presents a procedure to estimate tree volume and quantify AGB for large tropical trees based on estimates of tree volume and basic wood density. The accurate estimation of AGB of large tropical trees (diameter $> 70\,\text{cm}$) is particularly relevant due to their major influence on tropical forest AGB variation. Nevertheless, current allometric

models have large uncertainties for large tree AGB, partly due to the relative lack of large trees in the empirical datasets used to create them. The key result of this chapter is that TLS and 3D modelling are able to provide individual large tree volume and AGB estimates that are less likely to be biased by tree size or structural irregularities, and are more accurate than allometric models.

Chapter 3 focuses on the development of accurate local allometric models to estimate tree AGB in Guyana based solely on TLS-based tree metrics (H, CD, and D) and validated against destructive measurements. Current tropical forest AGB estimates typically rely on pantropical allometric models that are developed with relatively few large trees. This leads to large uncertainties with increasing tree size and often results in an underestimation of AGB for large trees. I showed in Chapter 2 that AGB of individual large trees can be estimated regardless of their size and architecture. This chapter evaluates the performance of my local allometric models against existing pantropical models and evidenced that inclusion of TLS-based metrics to build allometric models provides as good as, or even better, AGB estimates than current pantropical models.

Chapter 4 provides an insight into the architecture and branching structure of tropical trees. In Chapter 2, I demonstrated the potential of TLS to characterize woody tree structure as a function of tree volume, but little is known regarding their detailed architecture. Previous studies have quantitatively described tree architectural traits, but they are limited to the intensity of quantifying tree structure *in-situ* with enough detail. Here, I analysed the length and diameter of individual branches, and compared them to reference measurements. I demonstrated that basic tree architecture parameters could be reconstructed from large branches (> 40 cm diameter) with sufficient accuracy. I also discuss the limitations found when modelling small branches and how future studies could use my results as a basis for understanding tree architecture.

Chapter 5 describes an alternative approach to estimating metabolic scaling exponents using the branching architecture derived from TLS point clouds. This approach does not rely on destructive sampling and can help to increase data collection. A theory on metabolic scaling, the West, Brown & Enquist (WBE) theory, suggests that metabolic rate and other biological functions have their origins in an optimal branching system network (among other assumptions). This chapter demonstrates that architecture-based metabolic scaling can be estimated for big branches of tropical trees with some limitations and provides an alternative method that can be implemented for large-scale assessments and provides better understanding of metabolic scaling.

The results from this thesis provide a scientific contribution to the current development of new methods using terrestrial LiDAR and 3D modelling in tropical forests. The results can potentially be used to generate significant quality data for a better understanding of ecological challenges in tropical forests. I encourage further testing of my work using more samples including other types of forests to reduce inherent uncertainties.

Resumen

Por más de dos décadas, "*terrestrial light detection and ranging*" o LiDAR (por su acrónimo en inglés), conocido también como escáner de laser terrestre (TLS) se ha convertido en una herramienta valiosa en la evaluación de la estructura leñosa de árboles de una manera precisa, no destructiva y replicable. Esta técnica me permite capturar el entorno que escanea y utiliza software especializado para crear una representación en tres dimensiones muy detallada del mismo entorno en forma de una nube de puntos. Aunque el uso original del LiDAR fue para topografía de precisión, investigadores empezaron a utilizar LiDAR en la investigación forestal. De esta nube de puntos, puedo extraer métricas de árboles y, en combinación con modelamiento de estructuras, inferir el volumen del árbol, la biomasa aérea (AGB), el crecimiento del árbol, la identificación de especies y comprender los retos ecológicos como la mecánica de árboles, la arquitectura de ramas y el área de la superficie leñosa. El TLS puede proveer de una evaluación robusta y rápida de las características del árbol, lo que mejorará los presentes esfuerzos globales para medir las emisiones de carbono de los bosques, sus incertidumbres y proporcionar nuevos conocimientos sobre la ecología de los bosques tropicales. Por lo tanto, el objetivo principal de esta tesis doctoral es explorar el uso de modelos tridimensionales a partir de nubes de puntos del TLS para estimar la biomasa y la arquitectura de árboles tropicales. La biomasa y arquitectura derivada del TLS se podrán utilizar potencialmente para generar suficientes datos cuantitativos para una mejor comprensión de los desafíos ecológicos en los bosques tropicales.

Para esta tesis, fue elaborado un repositorio de inventario forestal que contiene nubes de puntos de TLS y cosecha destructiva de árboles de tres regiones tropicales: Indonesia, Guyana y Perú. Un total de 1858 árboles se inventariaron, 135 árboles se escanearon con el TLS y 55 árboles se talaron. En esta tesis, usé la nube de puntos para desarrollar métodos para estimar las medidas de árboles, como la altura (H), el diámetro a la altura del pecho (D), el diámetro de la corona (CD), la longitud y el diámetro de ramas individuales y el volumen de árboles de manera individual. A partir de estas métricas, puedo inferir biomasa aérea (AGB), modelos alométricos y calcular el escalamiento metabólico de plantas en árboles tropicales de manera individual. Todas estas métricas están validadas con el inventario forestal tradicional y los árboles talados.

El Capítulo 2 presenta un procedimiento para estimar el volumen de los árboles y cuantificar el AGB de árboles tropicales grandes en base a estimaciones de volúmenes de árboles y la densidad de madera específica. La estimación precisa del AGB de árboles tropicales grandes (con diámetro $> 70\,\text{cm}$) es importante debido a su gran influencia en la variación del AGB en bosques tropicales. Sin embargo, los modelos alométricos actuales presentan grandes incertidumbres en la estimacíón del AGB en árboles grandes, en parte debido a la relativa falta de información de árboles grandes en los datos empíricos utilizados para crearlos. El resultado clave de este capítulo es que el TLS y el modelado en 3D pueden proporcionar estimaciones individuales de volúmenes de los árboles grandes y que el AGB estimado tiene menos probabilidades de ser sesgadas por el tamaño del árbol o irregularidades estructurales y ser más precisas que los modelos alométricos.

El Capítulo 3 se centra en el desarrollo de modelos alométricos precisos a nivel local para estimar el AGB de árboles en Guyana basándose únicamente en las mediciones de los árboles escaneados con el TLS (H, CD, y D) y validado con las mediciones de los árboles talados. Las estimaciones actuales del AGB en bosques tropicales generalmente se basan en modelos alométricos pantropicales que se desarrollan con relativamente pocos árboles grandes. Esto conduce a grandes incertidumbres con el aumento del tamaño de los árboles y, a menudo, da como resultado una subestimación del AGB en árboles grandes. Demostré en el Capítulo 2 que el AGB de árboles grandes se puede estimar independientemente de su tamaño y arquitectura. Este capítulo evaluó el rendimiento de nuestros modelos alométricos locales frente a los modelos pantrópicales existentes y demostró que la inclusión de métricas basadas en TLS para construir modelos alométricos proporciona tan buenas, e incluso mejores, estimaciones del AGB que los modelos pantrópicos actuales.

El Capítulo 4 brinda una idea de la arquitectura y la estructura de las ramas en árboles tropicales. En el Capítulo 2 demostré el potencial del TLS para caracterizar la estructura de los árboles leñosos en función del volumen del árbol, pero poco se sabe sobre su detallada arquitectura. Estudios previos han descrito cuantitativamente los rasgos arquitectónicos de los árboles, pero se encuentran limitados debido a la dificultad en la cuantificación de la estructura del árbol *in-situ* con suficiente detalle. Aquí, analicé la longitud y el diámetro de ramas individuales y las comparé con medidas de referencia. Demostré que los parámetros básicos de arquitectura de árbol se pueden reconstruir a partir de ramas grandes (con diámetro $> 40\,\text{cm}$) con suficiente precisión. También discutí las limitaciones encontradas al modelar ramas pequeñas y cómo los futuros estudios podrían usar nuestros resultados como base para entender la arquitectura de los árboles.

El Capítulo 5 describe un enfoque alternativo para estimar los exponentes de escala metabólica utilizando la arquitectura de ramas derivadas de las nubes de puntos TLS. Este enfoque no se basa en el muestreo destructivo y puede ayudar a aumentar los datos recopilados. Una teoría sobre la escala metabólica, la teoría de West, Brown & Enquist

(WBE) sugiere que la tasa metabólica y otras funciones biológicas tienen su origen en un óptimo sistema de ramificaciones (entre otras suposiciones). Este capítulo demuestra que la escala metabólica basada en la arquitectura puede estimarse para las grandes ramas de árboles tropicales con algunas limitaciones. Aunque nuestra muestra fue pequeña, proporciona un método alternativo que puede implementarse para evaluaciones a gran escala y proporciona una mejor comprensión del metabolismo de escala.

Los resultados obtenidos en esta tesis doctoral proveen una contribución científica al presente desarrollo de nuevos métodos usando el LiDAR terrestre y el modelamiento en 3D en bosques tropicales. Los resultados de esta tesis doctoral pueden potencialmente ser usados para generar información con suficiente calidad que puede ser usada para el mejor entendimiento de los retos ecológicos en bosques tropicales. Aliento que se realicen más pruebas de mi trabajo con más muestras en otros tipos de bosques para reducir la incertidumbre inherente del análisis.

Contents

East Berbice-Corentyne, Guyana

Chapter 1

Introduction

1.1 Background

Tropical forests cover only 7 % of Earth's land surface (Zuidema et al., 2013); yet, they are one of the most biologically diverse ecosystems on Earth (Lewis et al., 2009). Tropical forests play an important role in carbon exchange with the Earth's atmosphere via photosynthesis, growth, respiration, death, and decay (Goodman & Herold, 2014). Trees use the energy from the sun and water from the soil to convert carbon dioxide (CO_2) from the atmosphere into sugars, water, and oxygen via photosynthesis. These sugars are used by trees for respiration or are converted to more complex molecules. These complex molecules are used later for the growth of woody tissues, such as leaves, stem or roots, often referred to as "biomass". Trees also respire, releasing CO_2. This process is inverse to photosynthesis and; while photosynthesis occurs when specific conditions are satisfied (enough light and soil moisture), respiration always occurs. Photosynthesis usually exceeds respiration, making trees a natural net carbon sink (Goodman & Herold, 2014).

Photosynthesis and respiration are also influenced by the three-dimensional organization of the tree (Rosell et al., 2009; Malhi et al., 2018). The architecture form of a tree is a combination of its genetics and its adaptive response to its environment (Malhi et al., 2018), and can lead to changes in carbon and water storage within the tree. The combined structure of the trees within a forest influence the temporal distribution of light in the stand, affecting ecological processes within the tree (Seidel et al., 2011) and with their environment. Metabolic scaling theories suggest general underlying principles that govern and link these processes (West et al., 1997; West, 1999a). Therefore, an accurate description of the architecture of trees is key for understanding these processes (Kempes et al., 2011; Malhi et al., 2018) and the magnitude of carbon stored (Saatchi et al., 2011).

Tropical trees in forests serve as a global carbon sink, accounting for 55 % of global stocks in forests (Doetterl et al., 2015). When forests are cleared or degraded, their carbon stocks are released as CO_2 to the atmosphere (Gibbs et al., 2007). Tropical trees deforestation accounts for 6 % to 17 % of global anthropogenic CO_2 (Baccini et al., 2012). The protection of current carbon stocks contained in tropical forests and its potential as future carbon sink made their preservation a global policy priority (Mitchard et al., 2014). Mechanisms like Reducing Emission from Deforestation or Degradation (REDD) are a step forward towards the development of a mechanism to reduce emissions from deforestation and forest degradation (De Sy et al., 2012). For that, data and methodologies to estimate greenhouse gas are key for REDD (De Sy et al., 2012) and considerable efforts have been made to quantify accurately the AGB in tropical forests (Saatchi et al., 2011; Baccini et al., 2012; Avitabile et al., 2016). Nevertheless, large uncertainties remain in the quantification of AGB at different spatial scales (Baccini et al., 2012; Molto et al., 2013).

1.2 How do we measure trees?

To understand the role of tropical forests in global carbon storage, assessing deforestation emissions, land-use planning, and its response to climate change, an accurate quantification of the carbon stocks is needed (Zhao et al., 2012; Mitchard et al., 2014). Currently, carbon stocks are not measured directly, but derived from AGB estimates in forest inventory plots (without accounting belowground biomass due to the difficulty of quantifying it in the field; Djomo & Chimi, 2017) or from remote sensing estimates calibrated with plot-based AGB (Gibbs et al., 2007). Allometric models are regression models that convert the tree parameters from the forest inventory plots into an estimate of AGB (Chave et al., 2005; Clark & Kellner, 2012).

The relevance of an allometric model relies on the empirical data used for its development, as it can potentially be the biggest source of uncertainty (Chave et al., 2004). Measurements are limited by the method available and the efficiency with which it can be taken (Newnham et al., 2015). Thus, most allometric models are based on easy-to-measure attributes, such as diameter at breast height (D) and wood density (WD). Although recent studies have shown the importance of other tree attributes, such as height (H; Feldpausch et al., 2012) and crown diameter (CD; Goodman et al., 2014); these attributes are not widely used due to the difficulty to measure them in the field.

Figure 1.1: Direct measurement of tree stem in Indonesia (left), tree destructive sampling in Guyana (centre), and weighing fresh biomass in Indonesia (right).

For other tree attributes, such as volume, canopy, or whole tree structure, there is no direct measurement. Currently, volume assessments are mainly based on destructive sampling (Thies et al., 2004; Saatchi et al., 2011). Destructive sampling is time-consuming, requires heavy manual labour (Figure 1.1), and requires a qualified team to sample large quantities (Henning & Radtke, 2006). Moreover, some tree species cannot be destructively sampled, because it is illegal, costly or non-practical *in-situ*. Canopy assessments are very difficult because sampling the spatial characteristic of the canopy cannot be done with direct measurements nor with indirect approaches (Seidel et al., 2011). Finally, to determine tree structure, destructive sampling is not a practical approach. Destructive sampling

implies the modification of branch and crown structure due to the felling process, thus detailed measurements of tree structure could be compromised.

1.3 Terrestrial laser scanning and 3D modelling of trees

Terrestrial Light Detection and Ranging (LiDAR), also known as terrestrial laser scanning (TLS) is a non-destructive, remote sensing technique that measures distances (Rosell et al., 2009). This active remote sensing technique is based on the emission and reception of a monospectral laser beam pulse, mostly in the near-infrared or visible part of the spectrum (Grau et al., 2017; Malhi et al., 2018). Hundreds of thousands of pulses are being emitted per second and propagated hundreds of meters from the instrument. When the pulse hits a target and is reflected back to the instrument, its sensors record the reflected signal and the processor calculates the distance between the target and the instrument in a three-dimensional space (Malhi et al., 2018). All TLS datasets in this thesis were acquired using a RIEGL VZ-400® terrestrial LiDAR (RIEGL Laser Measurements Systems, GmbH, Horn, Austria; Figure 1.2). This scanner is a discrete multiple-return laser scanner with a 1550 nm wavelength beam. The scan range is 360° in the azimuth and 100° in the zenith.

Figure 1.2: RIEGL VZ-400 terrestrial LiDAR mounted on a tripod surrounded by 5 cm cylindrical reflectors in Madre de Dios, Peru.

The TLS instruments were originally developed for urban and mining surveys, where a precise mapping of a target or an area is needed (Malhi et al., 2018). With time, TLS instruments became more robust, lighter, and smaller with improved range precision and accuracy. Moreover, with a wide range of commercial TLS available, instruments became cheaper, which facilitated the adoption of TLS by foresters, remote sensing scientists, and ecologists as part of their research (Malhi et al., 2018; Wilkes et al., 2017; Disney et al., 2018). TLS has become an automated, accurate, non-invasive, objective, and replicable option to assess forest structure, and eventually, individual tree stands (Calders et al., 2015b; Newnham et al., 2015). In the field, a forest plot can be scanned from multiple locations to acquire point clouds that can be co-registered into a highly detailed 3D point cloud of the instrument's surrounding using specialized software (Wilkes et al., 2017).

A 3D point cloud is a high dense uninterpreted collection of points and structural attributes (either at plot-level or tree-level) that cannot be directly extracted (Bremer et al., 2013). Several approaches initially aimed to extract plot-level attributes (Côté et al., 2012; van Leeuwen et al., 2011; Dassot et al., 2011; Newnham et al., 2015). At tree-level, several approaches were developed to reconstruct the detailed structure of trees (Pfeifer et al., 2004; Thies et al., 2004; Dassot et al., 2012; Raumonen et al., 2013; Hackenberg et al., 2015a). Among these, *TreeQSM* - a 3D quantitative structure model (QSM) reconstruction method (Raumonen et al., 2013; Åkerblom, 2017) - has been valued as a promising tool for topological and structural assessment of individual trees (Calders et al., 2015b; Disney et al., 2018).

TreeQSM is a quick and automatic approach to reconstruct tree trunks and branches from point clouds and record topological branching structures (Raumonen et al., 2013). *TreeQSM* fits multiple cylinders of varying length and diameter to an individual tree point cloud (Figures 1.3a and 1.3b) and reconstructs the whole tree topological structure and shape (Figure 1.3c). From these cylinders, one is able to calculate surface, volume, and reconstruct topology. The output, a QSM, is a hierarchical collection of enclosed connected cylinders that closely resemble the tree point cloud it was based on. TLS, in combination with *TreeQSM*, evidenced to be an accurate method to estimate tree attributes, such as diameter at breast height (Burt et al., 2013), tree height (Krooks et al., 2014), and indirect parameters such as stem volume, (Burt et al., 2013; Saarinen et al., 2017) and AGB (Calders et al., 2015b; Stovall et al., 2017). Other studies focused on root reconstruction, (Smith et al., 2014a; Paynter et al., 2016), tree species recognition, (Åkerblom et al., 2017), AGB comparison (Kaasalainen et al., 2014), and canopy change if the same area is scanned in different period (Olivier et al., 2017).

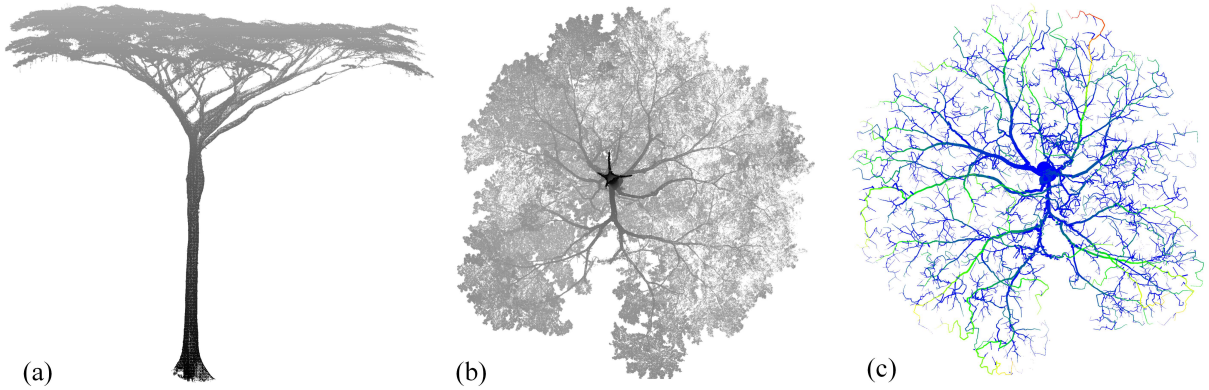

Figure 1.3: *Parkia pendula* tree scanned in Guyana. Tree point cloud from (a) side view, (b) bottom view and coloured by height from bottom (black) to top (light grey), and (c) Top view of *TreeQSM* modelled after the point cloud and coloured by branching order from low (blue) to high (red).

1.4 Research gaps

The approaches for estimating tree attributes mentioned above were mostly based on temperate trees in leafless conditions and comparative low canopy height. Few publications have been published reviewing their initial experience with TLS in tropical forests and discussing the opportunities and challenges of bringing TLS instruments into tropical and temperate forests (Wilkes et al., 2017; Rahman et al., 2017; Momo Takoudjou et al., 2018; Disney et al., 2018; Malhi et al., 2018). Nevertheless, research regarding estimating tree attributes such as diameter, height, crown diameter, and tree volume from tree point clouds of tropical trees remains very limited.

TLS, along with 3D modelling, can be useful tools in estimating these tree attributes in an objective and replicable approach without the need for destructive sampling. These TLS-derived attributes would increase the present collection of available tropical tree datasets. Moreover, TLS and 3D models can be helpful to estimate AGB from large trees ($D >$ 70 cm). As of 2014, only 7 % of the total available pantropical biomass datasets were related to large trees (Chave et al., 2014). Despite studies indicating that AGB estimates vary greatly with tree size (Goodman et al., 2014; Calders et al., 2015b); there is lack of harvested data due to the difficulty of harvesting large trees.

Scanning in tropical environments is challenging (Wilkes et al., 2017) and the information regarding an efficient scanning methodology is limited. The experience and knowledge about the potential of scanning with TLS and its limitations has improved with the efforts from the "Terrestrial LiDAR Scanning Research Coordination Network - TLSRCN" (`http://tlsrcn.bu.edu`) to connect TLS researchers. There are many unknowns about TLS being used in the tropics and the methods used to estimate tropical tree parameters

remain open among the TLS-related scientific community.

1.5 Research objective

The main objective of this thesis is to explore the use of 3D models from TLS point clouds to estimate above-ground biomass and architecture of tropical trees. TLS-derived AGB and TLS-derived architecture can potentially be used to generate significant quality data for a better understanding of ecological challenges in tropical forests. For that, I developed procedures to estimate accurate tropical tree information using terrestrial laser scanning. To achieve this objective, I asked the following research questions:

1. How accurately can above-ground biomass of tropical trees be estimated from TLS point clouds?
2. What is the capability of non-destructive TLS-based methods to derive allometric models for tropical trees?
3. Can the branching architecture of tropical trees be linked to 3D models using their topological features?
4. Does TLS-based branching architecture relate to metabolic scaling in tropical trees?

1.6 Thesis overview and fieldwork campaigns

This thesis consists of six chapters, including this introductory chapter. Chapters 2 to 5 address the research questions presented in section 1.5 and the outline of the chapters is presented in Figure 1.4.

Chapter 2 introduces an approach to estimate tree volume and quantify AGB for large tropical trees based on estimates of tree volume and basic wood density in Peru, Indonesia, and Guyana. I estimated AGB using tree point clouds from TLS and 3D modelling. This approach was tested on 20 tropical trees and validated with nine trees from three different regions (Research Question 1).

Chapter 3 adapts the methodology from Chapter 2 to estimate AGB from point clouds. With tree metrics (D, H, and CD) estimated from 72 trees point clouds; five allometric models are developed without any prior tree information. The AGB estimated from the TLS-based allometric models are compared against AGB from 26 destructively harvested trees and pantropical biomass models. This chapter is of relevance because allometric models can be built from terrestrial LiDAR point clouds without the need of destructively harvesting any tree (Research Question 2).

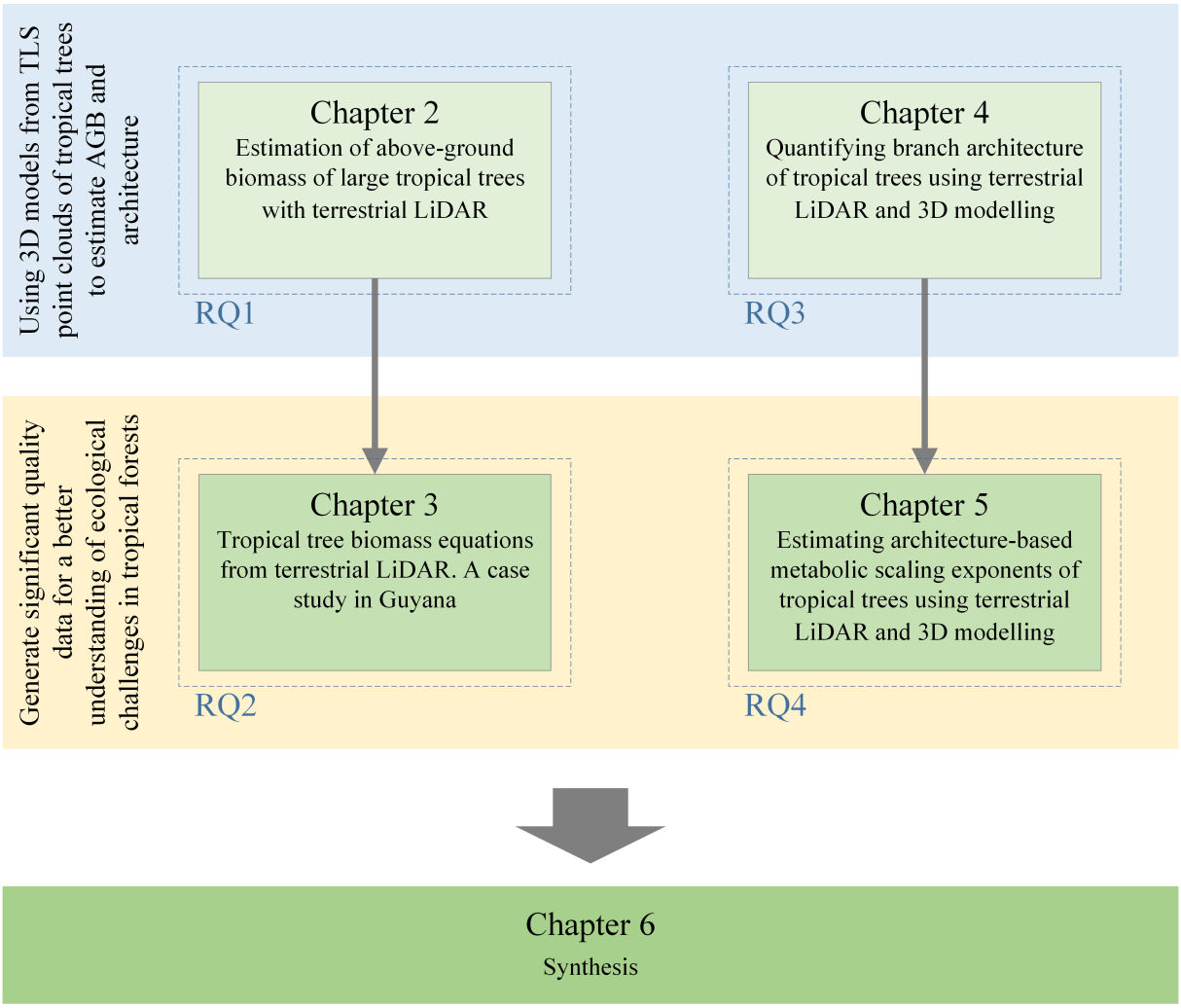

Figure 1.4: Flowchart for the chapters of this thesis in relation to the main objectives and the research questions (RQ).

Chapter 4 investigates the architecture and branching structure of tropical trees. Chapters 2 and 3 demonstrated the potential of TLS to characterize tree structure as a function of tree volume, but not much is known regarding their detailed architecture. This chapter presents a method to estimate basic branching architecture metrics, such as branch diameter, branch length, and branching order from TLS point clouds. Then, the TLS-derived metrics were compared against 279 branches from 10 destructively harvested trees (Research Question 3).

Chapter 5 describes an alternative approach to estimate metabolic scaling exponents using the branching architecture derived from TLS point clouds. A theory on metabolic scaling, the West, Brown & Enquist (WBE) theory suggests that metabolic rate and other biological functions have their origins on an optimal external branching network. I used the radius and length of TLS-derived measurements from Chapter 4 to estimate radius

and length scaling exponents and from these exponents, derived metabolic scaling rate. To validate these, I compared the TLS-derived scaling exponents against scaling exponents from field measurements and theoretical values (Research Question 4). This chapter is of relevance because estimating metabolic scaling exponents is key to understand the ecological processes of plant metabolism.

Chapter 6 presents the major findings of this thesis, addresses the findings in relation to the research questions above, proposes a reflection of this thesis, and an outlook of present and future developments.

My research involved four TLS fieldwork campaigns across three tropical regions (Figure 1.5; Wilkes et al., 2017). The first one, in the southwest region of Madre de Dios in Peru is featured in Chapter 2. This area is a lowland tropical moist *terra firme* forest. Here, I inventoried a total of 763 trees and destructively harvested 9 trees. The second fieldwork campaign, also featured in Chapter 2, is located in a peat swamp forest in central Kalimantan, Indonesia. Here, I inventoried 381 trees and destructively harvested 10 trees. The third fieldwork campaign is located in a lowland tropical moist forest in central Guyana. In this fieldwork campaign, I inventoried 608 trees and destructively harvested 10 trees. This fieldwork campaign is featured in Chapters 2, 4 and 5. The last study area, on which Chapter 3 is based, was located also in Guyana, in the East Berbice-Corentyne Region. In this mixture of white sand and mixed forest, I inventoried and scanned 106 trees, and destructively harvested 26 trees. Specific characteristics on the study sites are explained further in their respective chapters.

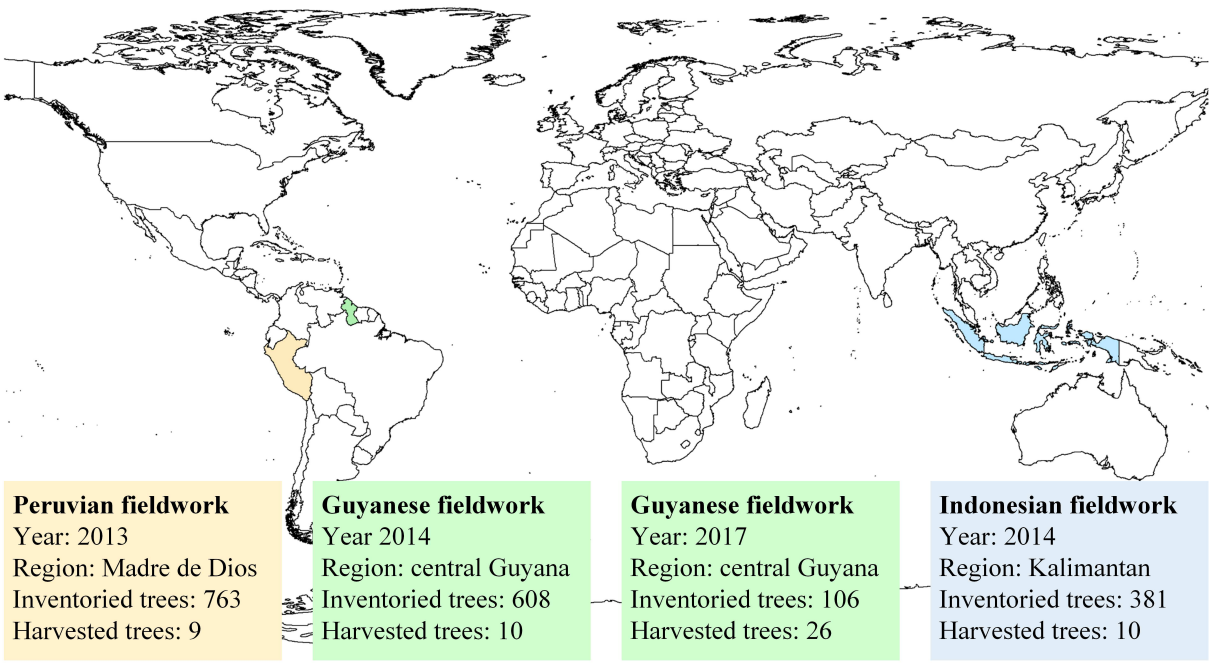

Figure 1.5: Location of TLS fieldwork campaigns for this thesis.

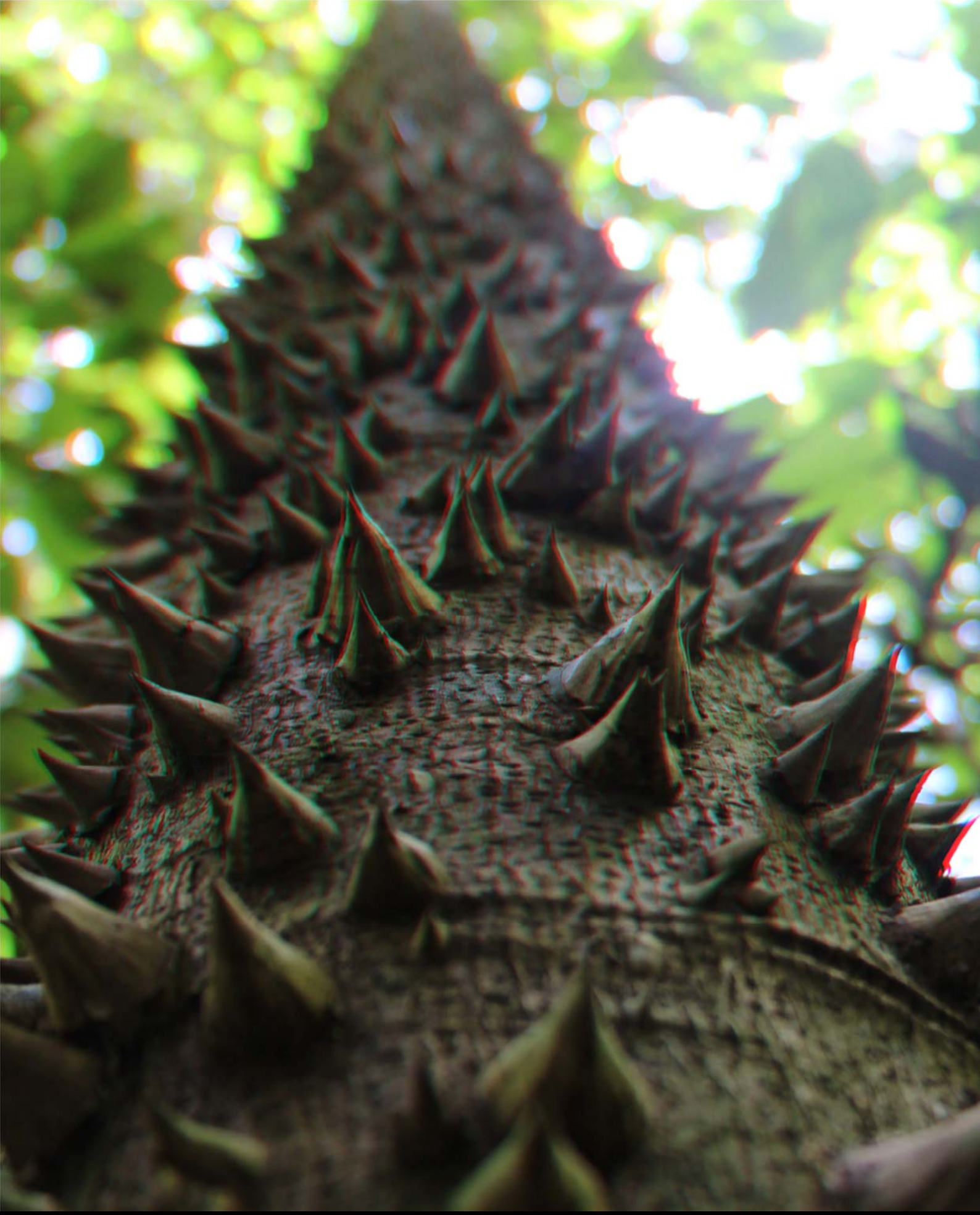

Tambopata National Reserve, Peru

Chapter 2

Estimation of above-ground biomass of large tropical trees with Terrestrial LiDAR

This chapter is based on:

Gonzalez de Tanago, J., Lau, A., Bartholomeus, H., Herold, M., Avitabile, V., Raumonen, P., Martius, C., Goodman, R. C., Disney, M., Manuri, S., Burt, A. and Calders, K. Estimation of above-ground biomass of large tropical trees with Terrestrial LiDAR. *Methods in Ecology and Evolution.* 2017, 1-12. DOI: 10.1111/2041-210X.12904.

Supplementary materials to this chapter can be found in the online publication.

Abstract

Tropical forest biomass is a crucial component of global carbon emission estimations. However, calibration and validation of such estimates require accurate and effective methods to estimate *in-situ* above-ground biomass (AGB). Present methods rely on allometric models that are uncertain for large tropical trees. Terrestrial laser scanning (TLS) tree modelling has demonstrated to be more accurate than allometric models to infer forest AGB in temperate forest. Nevertheless, applying TLS methods on tropical large trees is still challenging. We propose a method to estimate AGB of large tropical trees by 3D tree modelling of TLS point clouds. Twenty-nine plots were scanned with a TLS in three study sites (Peru, Indonesia and Guyana). We identified the largest tree per plot (mean diameter of 73.5 cm, extracted its point cloud and calculated its volume by 3D modelling its structure using quantitative structure models (QSM) and converted to AGB using species-specific wood density. We also estimated AGB using pantropical and local allometric models. To assess the accuracy of our and allometric methods, we harvested the trees and took destructive measurements. AGB estimates by the TLS-QSM method showed the best agreement in comparison to destructive harvest measurements (28.37 %) CV-RMSE and Concordance Correlation Coefficient (CCC) of 0.95, outperforming the pantropical allometric models tested (35.6 % to 54.95 % CV-RMSE and CCC of 0.89 to 0.73). TLS-QSM showed also the lowest bias (overall underestimation of 3.7 %) and stability across tree size range, contrasting with the allometric models that showed a larger bias (overall underestimation ranging 15.2 % to 35.7 %) systematic linearly increasing with tree size. The TLS-QSM method also provided accurate tree wood volume estimates (CV RMSE of 23.7 %) with no systematic bias regardless of the tree structural characteristics. Our TLS-QSM method accounts for individual tree biophysical structure more effectively than allometric models, providing more accurate and less biased AGB estimates for large tropical trees, independently of their morphology. This non-destructive method can be further used for testing and calibrating new allometric models, reducing the current under-representation of large trees in, and enhancing present and past estimates of forest biomass and carbon emissions from tropical forests.

2.1 Introduction

The above-ground carbon in tropical forests represents 40 % of the total carbon stocked in forests globally (Gibbs et al., 2007). However, the estimation of tropical forest carbon stocks presents large uncertainties (Mitchard et al., 2013, 2014). Forest carbon stocks are not measured directly, but derived either from interpolation or extrapolation of point estimates of the above-ground biomass (AGB) contained in forest inventory plots, or from measurements of remote sensing proxies calibrated with plot-based AGB estimates (Gibbs et al., 2007).

The only way to truly and directly measure forest AGB implies cutting and weighing the mass of all trees in the plot, which is costly and causes a negative impact, and is thus seldom executed (Clark & Kellner, 2012). Instead, plot AGB is estimated from aggregation of individual tree AGB estimates. These tree AGB estimates are indirectly derived from easily measured tree parameters (diameter at breast height (D), height and wood density derived from tree species identification) by means of allometric models, which relate these tree parameters with real tree AGB measured in destructive sampling studies (Chave et al., 2005). This indirect estimation approach introduces an error propagation chain. The biggest source of error is derived from the allometric models, hence its appropriate selection is the most important aspect to improve the accuracy of AGB estimates (Molto et al., 2013).

The uncertainty in the tree AGB estimation is even greater for large tropical trees ($D > 70$ cm because AGB in large trees varies more than in small trees (Chave et al., 2005; Slik et al., 2013; Goodman et al., 2014; Ploton et al., 2016), and due to the presence of buttresses is prone to larger measurement error (Chave et al., 2014). Moreover, it is particularly relevant to accurately estimate AGB of large trees because of their major influence on the tropical forest AGB variation (Stegen et al., 2011; Slik et al., 2013).

As an alternative, remote sensing systems can be used to estimate tropical forest carbon stocks. One of the most promising remote sensing approaches to estimate forest AGB is via light detection and ranging (LiDAR), either via spaceborne platforms (e.g. ICESat), airborne laser scanning (ALS) or terrestrial laser scanning (TLS). Laser pulses from LiDAR instruments can penetrate the forest canopy providing good estimates of forest canopy heights and structure, from which AGB along the vertical profile and canopy cover can be estimated (Goetz & Dubayah, 2011).

TLS data provide the highest level of three-dimensional (3D) detail of forest and tree structure (Newnham et al., 2015). Currently, TLS data are being used to model 3D structure of individual trees allowing direct measurements of forest and tree structural parameters such as D (Bauwens et al., 2016), tree height (Király & Brolly, 2007), crown dimensions (Holopainen et al., 2011) and individual branches (Raumonen et al., 2011).

Several review articles provide additional information about the characteristics of TLS and its use for forestry surveying (Newnham et al., 2015).

Several approaches estimate forest AGB by exploiting the capability of TLS data to characterize forest structure at tree level. A simple approach is to measure tree structural parameters from a TLS 3D point cloud and apply allometric models to relate the measured parameters with AGB (e.g. Yao et al. 2011). However, this method still relies on allometric models. A different kind of approach has been developed to reconstruct the complete 3D tree architecture from TLS data rather than a single or few structural parameters. Quantitative structure models (QSMs; Raumonen et al., 2013; Delagrange et al., 2014; Hackenberg et al., 2015b) are architectural tree models reconstructed from the TLS point cloud of individual trees and allow volume measurements. The estimated tree volume is converted to tree AGB by multiplying it by the specific wood density (Hackenberg et al., 2015b; Calders et al., 2015b). Thus, this method estimates AGB based on the biophysical modelling of specific tree structure rather than the allometric models which are based on empirical relationships from a sample of trees and rely on a limited number of tree structural parameters.

The QSM reconstruction method developed by Raumonen et al. (2013) has been applied for wood volume estimation and AGB estimation in boreal and temperate forest (Raumonen et al., 2015) and in more structurally complex tropical forests in Gabon (Disney et al., 2014). AGB estimates derived from this approach in Australia showed a higher agreement with reference values from destructive sampling (CV RMSE = 16.1 %) compared to AGB estimates derived by allometric models (CV RMSE = 46.2 % to 57 %; Calders et al., 2015b). However, the accuracy of AGB estimates in tropical forest trees has not been investigated yet with reference data.

Several challenges arise when one wants to estimate tree AGB in a tropical forest using QSM. First, for very large and complex trees there is a lack of reference data to validate the 3D reconstruction models from TLS. Further, the structural complexity of a tropical forest can potentially have a large influence on acquired TLS data. This requires careful design of an appropriate scanning pattern to diminish vegetation occlusion and to allow accurate reconstruction of the 3D structure of trees (Wilkes et al., 2017).

Here, we assess the potential and accuracy of volume reconstruction using QSMs for estimating AGB of large tropical forest trees. For this, 29 plots were scanned with TLS and one large tree per plot was destructively sampled afterwards. With the TLS data acquired, we (i) optimized the QSM tree volume reconstruction method based on a subsample of nine of the 29 trees. After each tree was scanned and harvested, we (ii) performed in situ destructive measurements to independently estimate tree volume for comparison with model estimates and calculate their accuracy. Finally, using the independent tree dataset (remaining 20 trees non-used in point i) we (iii) compared the accuracy of the AGB estimates based on QSMs with the accuracy of the AGB estimates based on pantropical

and local allometric models.

2.2 Material and methods

2.2.1 Study area

We acquired field data from 29 plots across three tropical forest sites in: Peru, Indonesia and Guyana. Table 2.1 shows the description of each site.

Table 2.1: Study sites description.

Site Description	Peruvian Site	Indonesian Site	Guyanese Site
Number of plots	9	10	10
Forest type	Lowland tropical moist *terra firme* forest	Peat swamp forest	Lowland tropical moist forest
Region	Madre de Dios. South western Amazon	Mentaya River (Central Kalimantan)	Vaitarna Holding's concession
Lat/Long	−12.27 lat, −69.10 long	−2.41 lat, 113.13 long	6.04 lat, −58.70 long
Mean elevation	312 masl	22 masl	117 masl
Mean yearly rainfall[a]	2074 mm	2616 mm	2195 mm
Mean stem density (trees with density >10cm)	565 stem ha^{-1}	1314 stem ha^{-1}	516 stem ha^{-1}
Mean D harvested tree (standard deviation)	90.0 cm (22.2 cm)	58.4 cm (18.2 cm)	73.7 cm (12.0 cm)

[a]from Muñoz & Grieser (2006)

2.2.2 TLS sampling and field data collection

Plots were established around a tree to be harvested after the laser scanning. Plot spatial design and tree selection are detailed in Supporting Information (S1). Once the plots were set up, we scanned the plot with TLS, performed a forest inventory, harvested the selected tree, and measured the geometric structure of the harvested tree.

TLS data acquisition

TLS datasets were acquired using a RIEGL VZ-400® 3D terrestrial laser scanner. This scanner is a discretized multiple-return LiDAR scanner and its specifications are shown in Table 2.2. Details of the sampling design are described in the Supporting Information (S2).

Table 2.2: Terrestrial laser scanning specifications.

Wavelength	1550 nm
Beam divergence	0.35 mrad
Scan range	360° in azimuth 100° in zenith
Scan resolution	0.06°

Forest inventory data collection

For each tree we measured D (or diameter above buttresses), tree height, height of first branch and crown width. We measured D with a forestry tape and tree height with a Nikon "Forestry-Pro" laser hypsometer with precisions of 0.01 m and 0.2 m respectively. An experienced taxonomist (specialist of the local flora) identified the trees at species level.

Harvested tree reference measurements

We measured the geometry of the stem, buttresses, and branches of each harvested tree. As in Figure 2.1.1, tree stem diameters (1a) were measured at every meter along the stem (1b) following the approach of Kankare et al. (2013). For trees with buttresses or major irregularities we measured as in Figure 2.1.2. Finally, we measured all branches until tapered diameter ≤ 10 cm by measuring each internode independently as in Figure 2.1.3.

2.2.3 Volume and biomass estimation

Tree wood volume estimation from 3D QSM

We co-registered each individual TLS scan into a single plot point cloud using RiScan Pro software [RIEGL Laser Measurement Systems GmbH, Horn, Austria, `www.riegl.com`, version 2.0] and the accuracy of our co-registration was kept below 1 cm.

We reconstructed the woody structure of trees using the QSM method developed by Raumonen et al. (2013) and further developed by Calders et al. (2015b) and Raumonen et al. (2015). The method first segments the TLS point cloud reconstructing the whole tree topological branching architecture and then reconstructs the surface and volume of the segments by fitting cylinders to each of the segments (Figure 2.2). The resulting cylinder models are used for automatic calculation of the volume of the whole woody

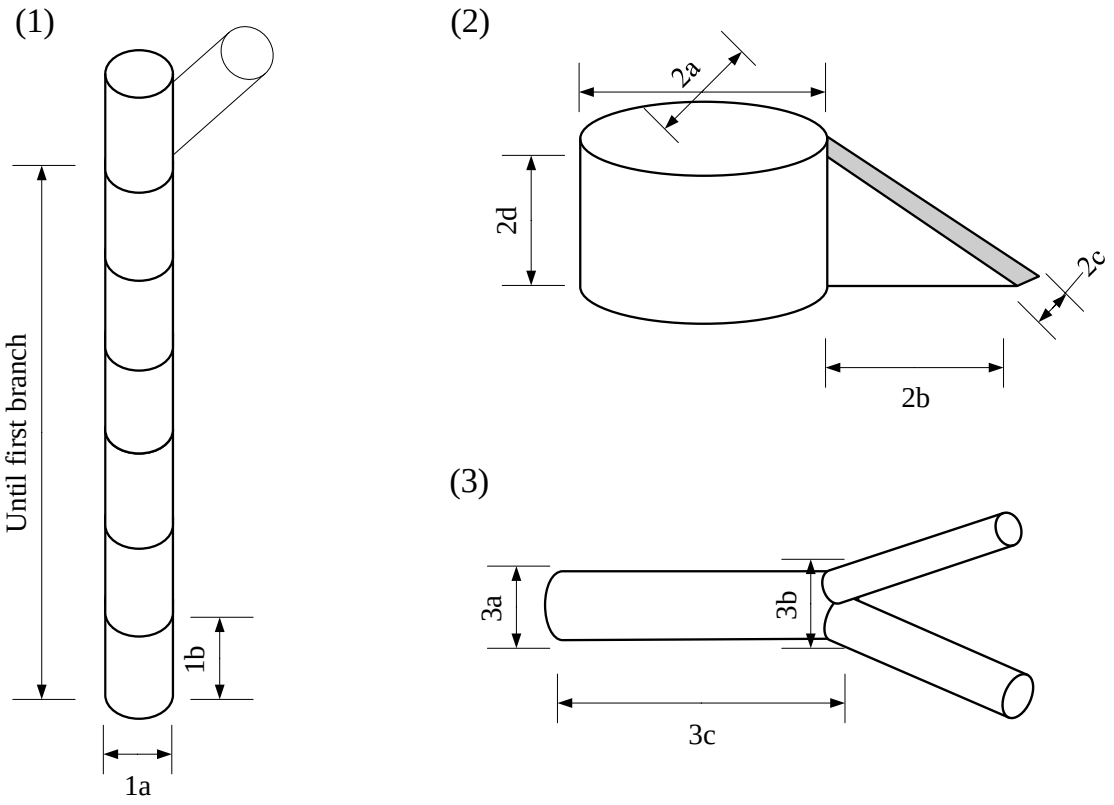

Figure 2.1: Tree geometry measurements. (1) Stem diameter (1a) every meter (1b) until start of first branch. For trees with buttresses (2): diameter in two orthogonal directions (2a) and for each buttress horizontal length (from the furthest point to the stem, (2b), width (mean width between the tip and the buttress intersection with the stem, (2c), and height (from the ground to the highest insertion point of the buttress into the stem, (2d). For branches (3): proximal diameter at the base of each internode and above flaring (3a), distal diameter at the tip of each internode and below flaring of the next node (3b) and branch length from the base to the tip of each internode (3c).

fraction of individual trees (trunk and branches). More details are provided in Supporting Information (S3).

We filtered out cylinders with diameter $< 10\,\text{cm}$ from resulting QSMs to be consistent with the reference volume estimation and we calculated the total tree volume by summing the volume of all remaining cylinders. Due to the random generation of the QSM patches (point cloud partition into small segments; Raumonen et al., 2015; Calders et al., 2015b), for each parameter set used we reconstructed 20 QSM's and averaged the volume of the 20 model realizations.

Figure 2.2: Example of one tree TLS point cloud from Guyana dataset (left, in dark red), and the same tree modelled by QSM (right, in green). Figure from (Gonzalez de Tanago et al., 2016).

Sensitivity analysis and independent estimation of QSM accuracy.

We split our tree population into two independent sub-datasets using stratified random sampling without replacement: a tree dataset of nine trees (three from each study area) for the sensitivity analysis of a QSM parameter value, and a second tree dataset of 20 trees (the remaining six trees for Peru and seven for Guyana and Indonesia) for independent estimation of tree volume and AGB estimates accuracy.

The reconstruction of the QSMs requires a few input parameters, of which the size of the point cloud segments -expressed by the "surface patches diameter" (hereafter *"PatchDiam"*)- had the most influence on the outcome (Calders et al., 2015b). A detailed ex-

planation of the QSM parameters and QSM sensitivity to them is provided in Supporting Information and in Raumonen et al. (2013, 2015) and Calders et al. (2015b).

Our sensitivity analysis consisted on the evaluation of the QSMs optimal *PatchDiam* value, which gives the most accurate volume estimate among the different *PatchDiam* values tested (1 cm, 2.5 cm, 5 cm, 7.5 cm, 10 cm and 15 cm). For each tree in the sensitivity analysis tree dataset we compared the mean estimated volume (from the 20 QSM realizations per *PatchDiam*) against the tree volume obtained from the destructive measurements. We computed tree volume estimation Root Mean Square Error (RMSE). The optimal *PatchDiam* was chosen as the one that minimized the RMSE.

Once the optimal *PatchDiam* was found, we assessed the stability of the optimization procedure. We replicated the stratified random sampling 1000 times and analysed the frequency of optimal *PatchDiam's* obtained (the one providing the smallest RMSE in each of the 1000 samples) as well as the variability of the RMSE results (range, mean and standard deviation) for all samples with a given optimal *PatchDiam*.

Finally, the optimized PatchDiam was used to run QSM for the independent estimation dataset (20 trees) and to calculate the tree volume following the same procedure described above. We used MATLAB (The MathWorks Inc., 2014) for QSM reconstruction and "R" (R Core Team, 2017) for further calculations.

Tree volume estimation from reference measurements

We used the reference geometric measurements (section 2.2.2) from each harvested tree to determine the tree reference volume. We applied the Smalian formula as in Nogueira et al. (2005) to estimate volume of stem sections and individual branches until 10 cm diameter while for the buttresses we applied a general prism volume formula. Detailed information can be found in Supporting Information (S4). Total tree wood volume was calculated as the sum of volumes of main stem, large branches (> 10 cm), and buttresses.

As in Berger et al. (2014), any misrepresentation of the main stem and branches volumes by the Smalian approximation and any measurement error taken were considered negligible and ignored. Further, the sum of all cylinders was assumed to represent the true tree volume with no error and that the wood volume was measured without error.

Tree AGB estimation from volume models and wood density

We calculated individual tree above-ground biomass by multiplying individual tree wood volume estimates by the specific basic wood density (ρ). Values of ρ were assigned to the finest taxonomic level possible (species, genus, or family) according to the Global Wood Density Database (Zanne et al., 2009; Chave et al., 2009) and tree species identified in the

field. We applied an expansion factor accounting for small branches (≤ 10 cm diameter). The expansion factor related the volume of small branches to the one of large branches (> 10 cm diameter). We calculated an expansion factor of 0.255 using data from biomass destructive sampling of 51 trees in a nearby Peruvian Amazon forest site (Goodman et al., 2013, 2014). We used the same value for Peru and Guyana (0.255) while we calculated the expansion factor for Indonesia (0.28) from our own collected data. The final contribution of small branches to tree volume was 10 %, 14 % and 7 % for Guyana, Peru and Indonesia respectively.

Tree AGB estimation from allometric models

We estimated AGB using 12 allometric models, of which 8 were locally-calibrated and 4 pantropical (See Supporting Information S5). The pantropical allometric models used were developed by Chave et al. (2005), which have been recently improved Chave et al. (2014).

The local allometric models used for the Peruvian trees were developed by Goodman et al. (2014) while allometric models for Indonesian trees were developed by Manuri et al. (2014) and Jaya et al. (2007). No suitable local allometric model could be found for Guyana. The details of the allometric models used to estimate AGB for the harvested trees are described in the Supporting Information.

2.2.4 AGB estimation models accuracies and uncertainty assessment

We used the 20 trees in the dataset reserved for the independent estimation to compare the accuracy of AGB estimates from our TLS-QSM approach (against reference AGB) versus the accuracy obtained from allometric models (against reference AGB). The model error was calculated for each tree and for the mean of the 20 trees using several metrics. The AGB estimation error (Residual, in Mg; Equation 2.1) and Individual tree Relative Error (in %; Equation 2.2) were calculated for each tree while model bias (in %; Equation 2.3) was calculated as the mean of the Estimation Errors divided by the mean of reference AGB.

$$AGB_{\text{estimation error}}(\text{Mg}) = AGB_{\text{model}} - AGB_{\text{ref}} \tag{2.1}$$

$$E_{\text{relative}}(\%) = \left(\frac{AGB_{\text{model}} - AGB_{\text{ref}}}{AGB_{\text{ref}}} \right) \cdot 100 \tag{2.2}$$

$$Model_{\text{bias}}(\%) = \left(\frac{\sum_1^n AGB_{\text{estimation error}} \cdot n^{-1}}{MeanAGB_{\text{ref}}} \right) \cdot 100 \tag{2.3}$$

Where AGB_{model} is the AGB estimated by the model and AGB_{ref} is the AGB observed (AGB calculated from destructive measurements).

As general indicators of model accuracy, RMSE (in m^3 and Mg), Coefficient of Variation of RMSE (CV RMSE, in %) and Mean Relative Error (in percent) were calculated. Slope and Intercept values of orthogonal regression models between AGB modelled and reference values were used to identify departure from the 1:1 line, and the R-squared (hereafter R^2) was used to judge the fitting of these regressions. Finally, the Concordance Correlation Coefficient (CCC) was calculated to compare agreement of AGB model estimates with AGB reference and to previously reported agreement using the QSM method (Calders et al., 2015b).

To assess the uncertainty in the tree AGB estimations, we used the error propagation approach (Equation 2.4) to account for the uncertainties in the models components. We combined them and assumed that the uncertainties were statistically independent (not correlated and with a Gaussian distribution). We used Equation 2.4 expressing model uncertainties in percentage terms:

$$U_{\text{total}} = \sqrt{U_1^2 + U_2^2} \tag{2.4}$$

Where U_{total} is the propagated uncertainty (as percentage) from the model components, U_1 and U_2 are the uncertainties (as percentage) from each component (IPCC, 2006).

For AGB estimations from QSM volume models, the model uncertainty components considered were the wood volume and wood density. The uncertainty in tree wood volume by QSM is provided by the standard deviation of the 20 QSM realizations per tree. For the estimation of wood densities uncertainties, we assumed for all species the same standard deviation of 10 % of the mean as used by Chave et al. (2004). Likewise, to assess the uncertainty in the tree AGB estimation from allometric models, we used the uncertainties reported for each model (See Supporting Information S5). To assess the uncertainty in the tree AGB estimation from reference volume estimates we considered two components: wood density (as described for QSM) and expansion factor. For the expansion factor we assumed an error of 12.5 % as reported in Segura & Kanninen (2005).

2.3 Results

2.3.1 Tree volume estimation with QSM

The results of the tree volume modelling with the TLS-QSM approach are divided in two steps: (i) QSM sensitivity analysis with 9 trees to determine QSM optimal parameters and (ii) an independent assessment of the tree volume estimation accuracy with an independent sample of 20 trees.

Sensitivity analysis of QSM tree volume modelling

The TLS-QSM tree volume estimation error (RMSE) when compared with the reference volume measurements decreased with decreasing PatchDiam (Table 2.3) until it reached a minimum error for *PatchDiam* of 2.5 cm, and then it increased again for smaller *PatchDiam*. This is in line with the results of the sensitivity analysis in Calders et al. (2015b). Therefore, 2.5 cm was considered the optimal *PatchDiam*, and thus selected for the tree volume estimation of the remaining tree dataset.

Table 2.3: QSM volume sensitivity analysis.

PatchDiam (cm)	RMSE (m^3)	CV RMSE (%)	Mean Relative Error (%)
1.0	3.42	27.56	10.31
2.5	2.98	23.92	17.67
5.0	4.60	36.97	31.87
7.5	7.11	57.17	49.42
10.0	9.06	72.81	65.07
15.0	13.32	107.09	98.05

The stability assessment of *PatchDiam* optimization procedure showed that in 75 % of the 1000 random sampling replicates the optimal *PatchDiam* was 2.5 cm . Despite the relatively small sample reserved for the sensitivity analysis (9 out of 29 trees), the optimal *PatchDiam* was relatively stable regardless of the characteristics of the randomly selected trees.

Independent assessment of tree volume estimation from TLS-QSM

To assess the accuracy of the tree wood volume estimation by the TLS-QSM we compared the volume estimates by the TLS-QSM with the reference volume estimates from destructive measurements (Figure 2.3).

The R^2 of the linear model describing the agreement of both datasets (Figure 2.3 blue line) was 0.9. Its slope was 0.93 indicating that the QSMs slightly underestimated the tree volume for the largest trees. The RMSE was 3.29 m^3, compared with the mean tree volume of 15.13 m^3, leading to a CV RMSE of 23.7 %. Figure 2.3 shows that the TLS-QSM performed similarly throughout the three different sites, despite the three study areas contained different tree species, sizes and shapes. Results differ between "small trees" ($D \leq 70$ cm, corresponding approximately with 9 Mg, hereafter *small trees*) and "large tree" ($D > 70$ cm, hereafter *large trees*). For *small trees* -which were mostly part

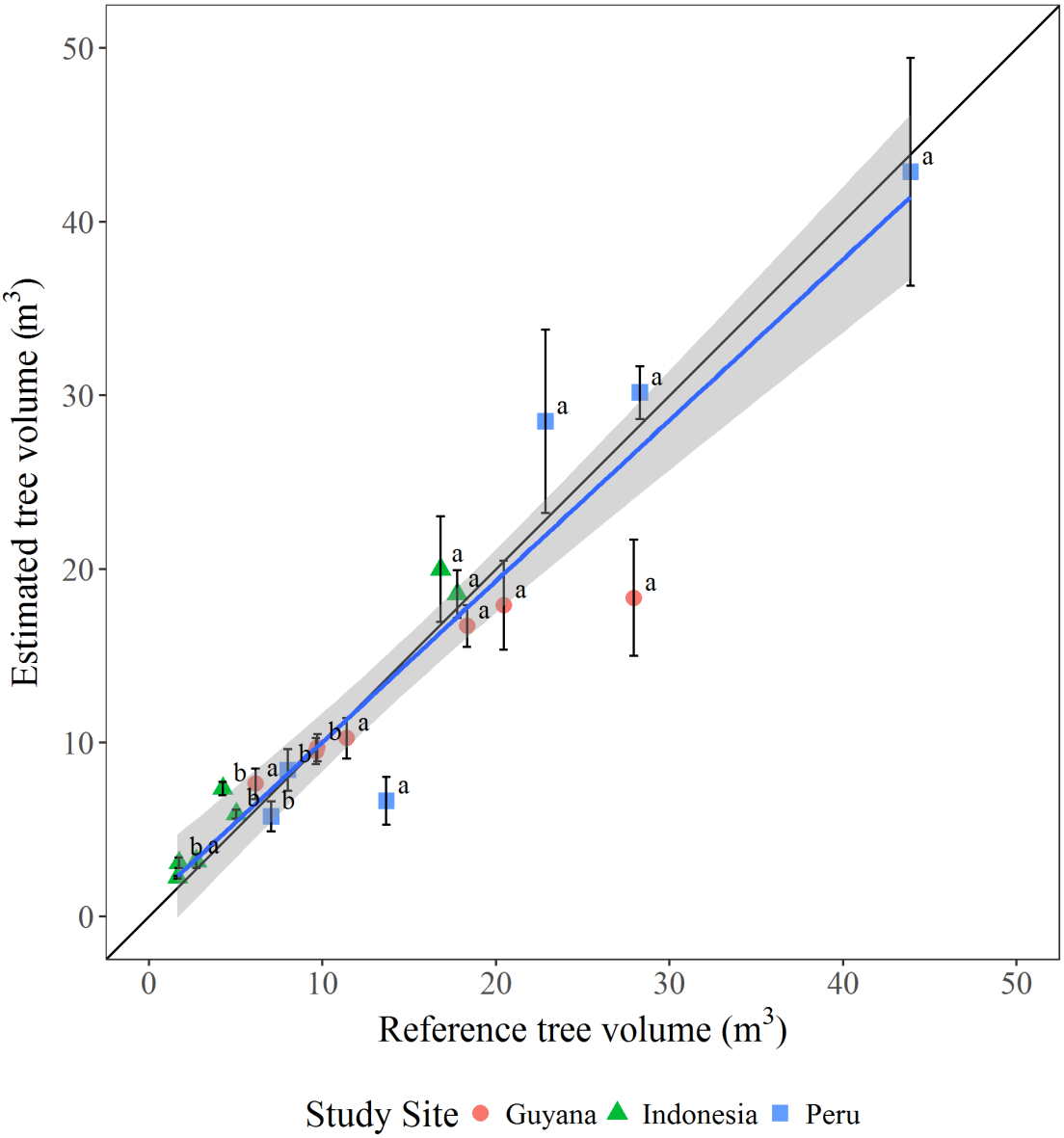

Figure 2.3: Scatterplot of tree volume estimation by TLS-QSM (y axis) against reference measurements (x axis). The solid black line depicts the 1:1 line. Error bars are the standard deviation of the 20 QSM model realizations per tree. Symbols and colours denote values per study site. The blue line depicts the fitted linear regression model between QSM volume estimates and reference volume estimates, and grey bands show the 95 % confidence interval of this regression. Coefficient *a* denotes tree with buttresses and *b* tree with no buttresses.

of the Indonesian dataset- TLS-QSM models showed less uncertainty and less deviation from the reference compared to *large trees*.

On the other hand, the analysis of the residuals (Figure 2.4) reveals that for *small trees* and *large trees* the model did not systematically tend to overestimate nor underestimate

the volume. Despite the larger uncertainty in the volume estimation for large trees, there was no large systematic bias for larger tree size (Figure 2.4).

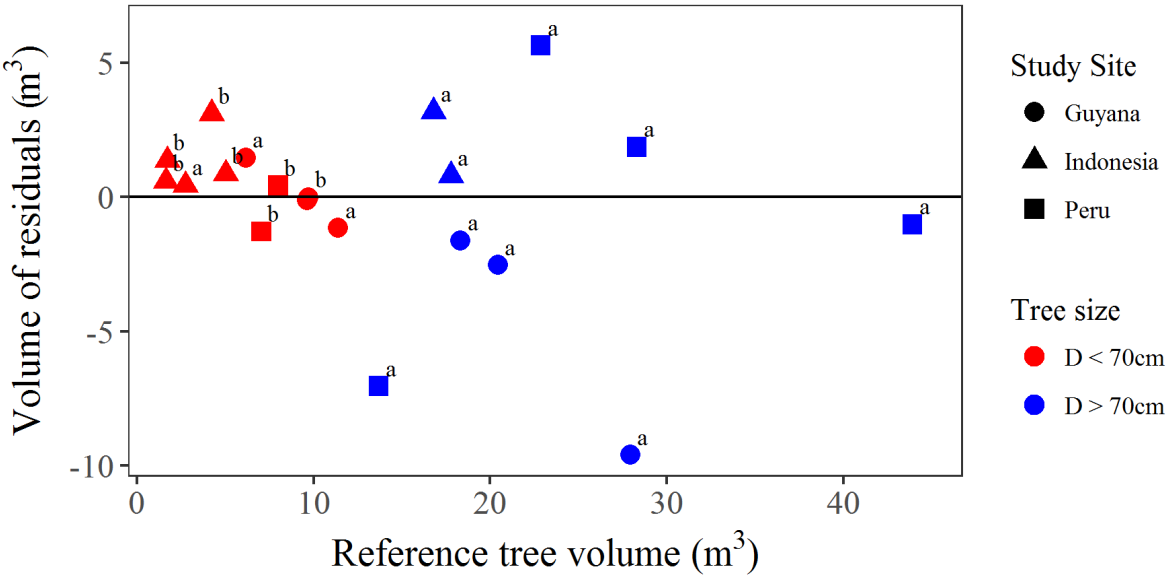

Figure 2.4: Analysis of volume estimation residuals. Trees with $D \leq 70$ cm were classified as small size trees (red colour) and trees with $D > 70$ cm were classified as large trees (blue colour). Coefficient *a* denotes tree with buttresses while coefficient *b* denotes absence of tree buttresses.

Buttresses were predominately absent in *small trees*, which had a better agreement with the reference data than trees with buttresses. Our QSM modelling did not perform a detailed buttress modelling, but a cylinder fitting, which might be the cause of the higher residuals in the trees with buttresses.

2.3.2 Comparison of AGB estimation accuracies: TLS-QSM vs. Allometric models

Overall accuracy across study sites: TLS-QSM vs. Pantropical allometric models

Figure 2.5 shows the agreement between the AGB estimates by TLS-QSM and allometric models (*modelled*) and derived from the destructive measurements (*reference*) for the independent assessment tree dataset. The high level of agreement with the *AGB-reference* provided by the TLS-QSM approach (CCC = 0.95) contrasts with the systematic AGB underestimation of the allometric models for *large trees* (CCC = 0.73 – 0.89).

Table 2.4 shows the statistical indicators of the accuracy of AGB estimations based on the TLS-QSM approach and pantropical allometric models for the mean of the 20 trees in the independent assessment dataset.

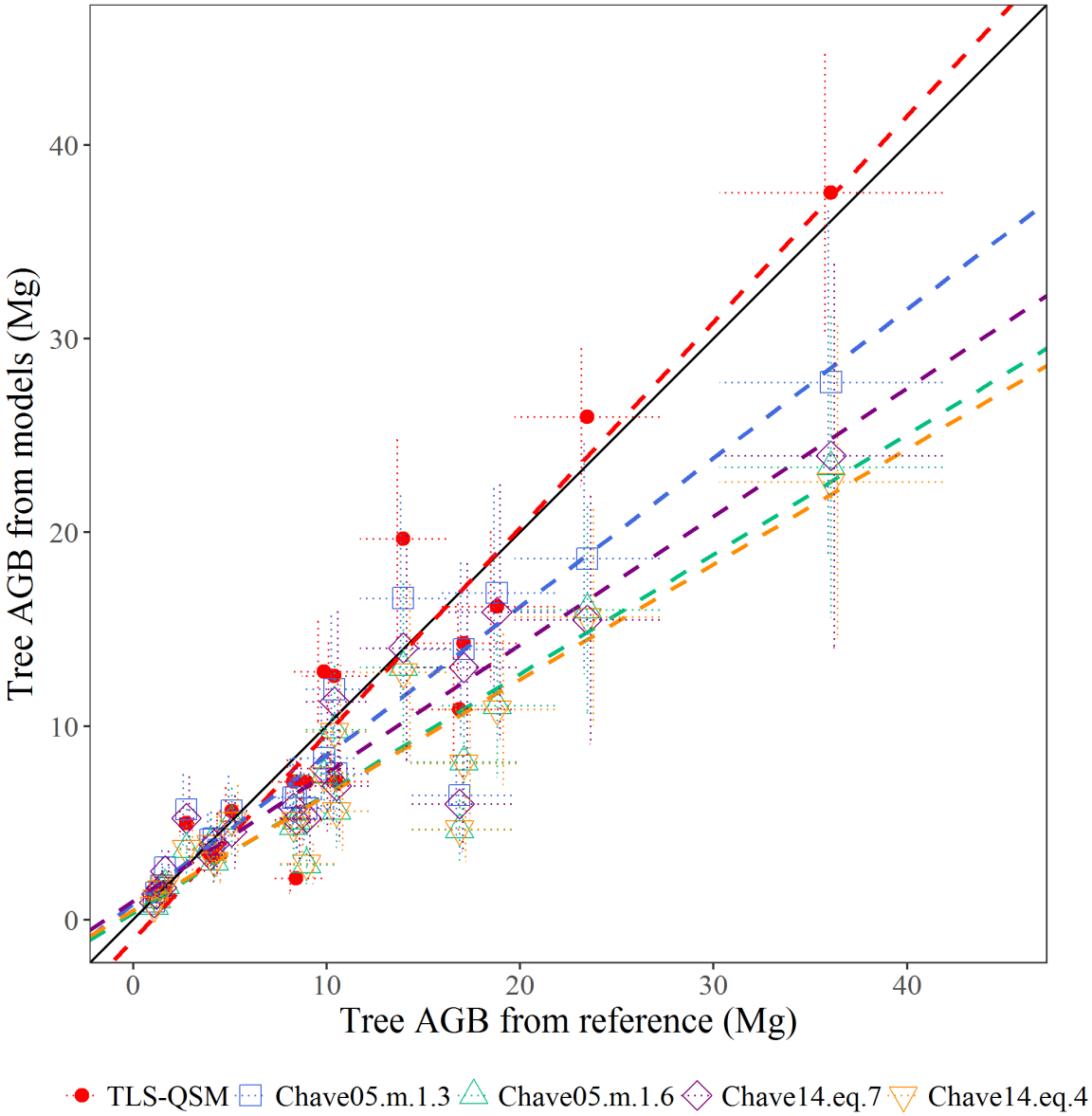

Figure 2.5: Scatterplot of AGB estimates by TLS-QSM approach and pantropical allometric models (Y axis) against the AGB reference values (X axis). The $1:1$ line is depicted as a black solid line. The dashed lines represent the fitted orthogonal models between AGB estimates by TLS-QSM or pantropical allometric models and AGB reference, with colours corresponding the colour used for the model estimates. Vertical bars show the estimated uncertainty (standard deviation) for each model estimate and horizontal bars show the uncertainty for the reference AGB estimates.

The TLS-QSM method had the lowest RMSE, which was respectively 20 % and almost 50 % lower than the most accurate (Chave05.m.1.3) and the least accurate allometric model (Chave14.eq.4). The TLS-QSM approach also had the lowest bias, 75 % and 90 % lower than the most and the least accurate allometric models respectively. The TLS-QSM

Table 2.4: Accuracies of AGB estimations across sites by the TLS-QSM approach and by pantropical allometric models ($n = 20$).

Model	RMSE (Mg)	CV RMSE (%)	Bias (%)	Relative error (%)	R^2	Slope	Intercept (Mg)	CCC
TLS-QSM	2.89	28.37	−3.68	−0.33	0.90	1.06	−1.03	0.95
Chave05.m.1.3[a]	3.63	35.60	−15.22	−0.76	0.88	0.77	0.82	0.89
Chave14.eq.7	4.52	44.35	−24.50	−10.49	0.88	0.66	0.94	0.82
Chave05.m.1.6	5.47	53.65	−34.99	−24.91	0.85	0.62	0.33	0.75
Chave14.eq.4[b]	5.60	54.95	−35.67	−24.41	0.85	0.60	0.49	0.73

[a]most accurate allometric model
[b]least accurate allometric model

AGB estimates also showed the most consistent agreement with the reference AGB (CCC = 0.95) along the range of AGB reference values with no major systematic deviation to the 1:1 line (slope of 1.06), whereas the best allometric model (slope of 0.77) showed a systematic increasing underestimation of AGB for *large trees* and a lower agreement with reference AGB (CCC = 0.89). The trend of systematic increasing underestimation of AGB for larger trees was even more pronounced for less accurate allometric models (slopes ranging from 0.66 to 0.60) showing a lower agreement compared to reference AGB (CCC = 0.73 – 0.82).

Overall accuracy within study sites: TLS-QSM vs. Local allometric models

Figure 2.6 displays the agreement between the *AGB-modelled* based on the TLS-QSM approach and local allometric models (Y axis) against *AGB-reference* (X axis) for the sites where local allometric models were available.

For the Peruvian study area the TLS-QSM approach is the closest to the 1 : 1 line, whereas the deviation from the 1 : 1 line is clearly larger for the three local allometric models tested, which systematically underestimate the AGB of large trees. The TLS-QSM approach showed 10 % and 50 % lower RMSE and 80 % and 85 % lower bias than the most- and least- accurate local allometric model. The agreement between TLS-QSM estimates and reference values expressed as CCC is higher (0.96) compared to the most- and least- accurate allometric model (0.76 to 0.92).

For the Indonesian study area, unlike for the Peruvian site, the local allometric models showed lower RMSE and bias than the TLS-QSM for this particular subset of trees. The best local allometric model had a 44 % smaller RMSE than the TLS-QSM, was closer to the 1:1 line and had a higher agreement with reference values (CCC = 0.96) than our approach (0.92).

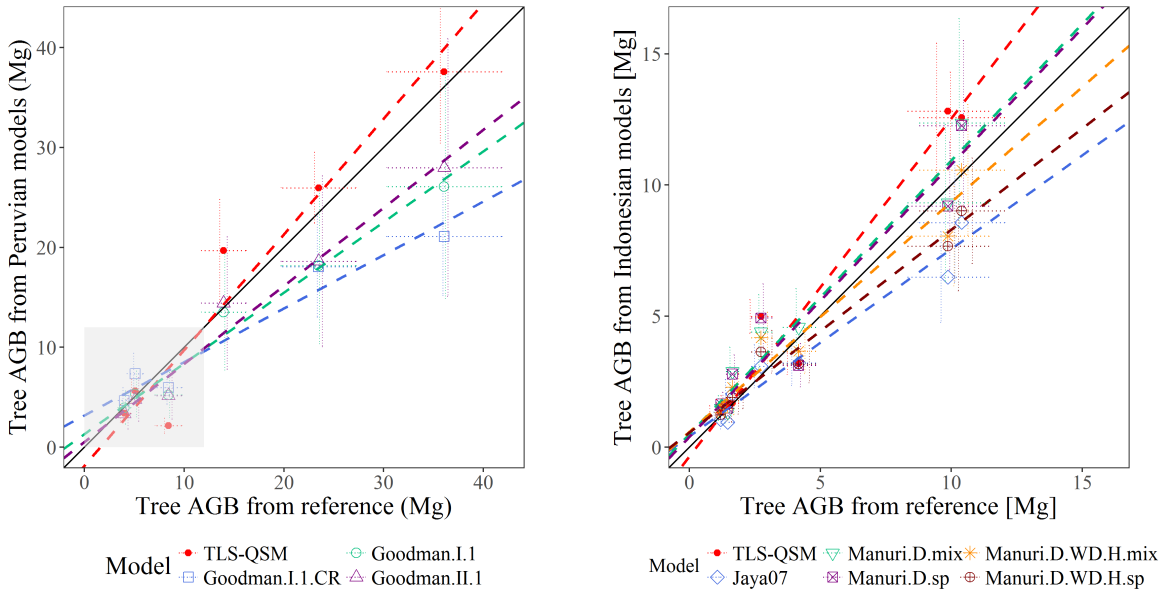

Figure 2.6: Scatterplot of AGB estimates by TLS-QSM approach and local allometric models (Y axis) against the AGB reference values (X axis) for Peruvian study site (left) and Indonesian study site (right). The 1 : 1 line is depicted as a black solid line. The dashed lines represents the fitted orthogonal models between AGB estimates by TLS-QSM or local allometric models and AGB reference, with colours corresponding the colour used for the model estimates. Vertical bars show the estimated uncertainty (standard deviation) for each model estimate and horizontal bars show the uncertainty for the reference AGB estimates. Grey box on the left graph shows where the Indonesian values would fit in the Peruvian Graph

Table 2.5: Accuracies of AGB estimations for Peruvian trees, by the TLS-QSM and by Local allometric models ($n = 6$).

Model	RMSE (Mg)	CV RMSE (%)	Bias (%)	Relative error (%)	R^2	Slope	Intercept (Mg)	CCC
TLS-QSM	3.68	24.27	−3.72	−3.87	0.93	1.16	−1.84	0.96
Goodman.II.1[a]	4.09	26.97	−18.37	−16.87	0.97	0.78	0.54	0.92
Goodman.I.1.CR[b]	7.27	47.98	−26.20	−6.42	0.94	0.54	3.19	0.76

[a]most accurate allometric model
[b]least accurate allometric model

2.4 Discussion

2.4.1 Consistent and accurate AGB estimation of tropical trees from QSMs

We found that the TLS-QSM approach can provide reliable and accurate AGB estimates for large tropical trees ($D > 70\,\text{cm}$), outperforming the accuracy of all the pantropical

Table 2.6: Accuracies of AGB estimations for Indonesian trees, by TLS-QSM approach and by local allometric models ($n = 7$).

Model	RMSE (Mg)	CV RMSE (%)	Bias (%)	Relative error (%)	R^2	Slope	Intercept (Mg)	CCC
TLS-QSM	1.67	37.13	21.36	19.08	0.96	1.29	−0.34	0.92
Manuri.D.WD.H.mix[a]	0.94	20.82	0.63	11.88	0.94	0.88	0.58	0.96
Jaya07[b]	1.52	33.93	−19.33	−12.12	0.95	0.71	0.41	0.89

[a]most accurate allometric model
[b]least accurate allometric model

allometric models tested. To the best of our knowledge, this is the first study assessing the accuracy of tropical trees AGB estimates using QSMs from TLS point clouds of trees across different tropical forest regions. A previous study by Disney et al. (2014) presented a proof of concept for the use of TLS-QSM for tree AGB estimation of tropical trees in Gabon, but in their research no tropical trees were harvested, thus the accuracy of its AGB estimates could not be assessed but only compared to the AGB estimates provided by allometric models. Our study showed that AGB estimations by allometric models often are not a reliable indicator of AGB for large tropical trees. This issue was also addressed by Clark & Kellner (2012), Calders et al. (2015b) and Ploton et al. (2016). Clark & Kellner (2012) and Calders et al. (2015b) both noted that large trees are under-represented in calibration of allometric models, therefore these models may produce large absolute errors for large trees, which is supported by our findings. Ploton et al. (2016) identified an increase in the estimation error of pantropical allometric models with the increase of tree mass. Clark & Kellner (2012) also point out that large trees inherently span a larger range of AGB values for a given D, thus exacerbating this problem of under sampling.

AGB estimations by TLS-QSM vs pantropical allometric models

Across the three sites the TLS-QSM method to estimate AGB was more accurate than the most accurate pantropical allometric model evaluated (Chave05m1.3, in Supporting Information S5), with an absolute improvement of 7.2 % less CV RMSE (Table 2.4). This accuracy improvement, was even more pronounced in terms of bias reduction. Moreover, TLS-QSM showed a higher agreement with reference values (CCC = 0.95) compared to the most accurate pantropical allometric model (CCC = 0.89). Calders et al. (2015b) found a comparable trend of higher accuracy for their TLS-QSM method in relation to allometric models for estimating AGB of eucalyptus trees in Australia. The accuracy of the AGB estimates by TLS-QSM in our study was lower than the accuracy reported by Calders et al. (2015b), and our agreement (CCC = 0.95) was lower than the agreement

found by Calders et al. (2015b) (CCC = 0.98). This is likely due to the greater structural complexity and vegetation occlusion of the tropical very dense forest in our study areas compared to the open eucalyptus forest studied by Calders et al. (2015b). In relation to the updated and widely-used pantropical allometric models of Chave et al. (2004), our method achieved an absolute improvement of 16 % and 27 % lower CV RMSE, which is comparable to the error decrease reported by Calders et al. (2015b).

It should be noted that the models accuracies were estimated by comparing each model AGB estimates with AGB reference estimates derived from destructive geometric measurements, rather than with AGB weighted. The uncertainties introduced in measuring stems, buttresses, and branches volumes were taken into account, but —as in Kankare et al. (2013) and Berger et al. (2014)— the uncertainty due to the use of Smalian formula for estimating true volume was assumed to be negligible. Furthermore, the uncertainty introduced in the correction factor for small branches volume, and in the application of a single species-specific wood density value for each tree instead of discriminating wood density for different woody fractions, both were not measured but taken from literature. Moreover, models uncertainties increasing with tree size indicates heteroscedasticity effects, which should be considered with caution when developing allometric models. This reinforces the need for improved methods for estimating large trees biomass, and for further research with larger datasets to assess the uncertainty on large trees biomass estimation.

AGB estimations by QSM models vs local allometric models in Indonesia and Peru

The TLS-QSM method also produced AGB estimates more accurate than the local allometric models for the Peruvian dataset, with a higher agreement (CCC = 0.96) with reference data than the local allometric models in Peru (CCC = 0.76 to 0.92). However, several local allometric models outperformed our method for the Indonesian dataset, which trees were predominately smaller than 10 Mg. In this case, several local allometric models had better agreement, ranging from 0.89 to 0.96, while TLS-QSM approach had an agreement of 0.92.

For both cases, at pantropical or regional-local level, there are large implications related to the choice of which allometric model one should use for AGB estimation of tropical trees. While some allometric models presented here performed with similar accuracy than our method for some trees; other allometric models proposed for the same region and by the same authors provided significantly larger errors on the same trees.

2.4.2 Reconstructing 3D woody structure of tropical forest trees using QSMs

We showed that the TLS-QSM method can be used to accurately estimate volume from 3D reconstructed structure of large tropical trees from scans in very dense forest with leaf-on conditions. The tree structure reconstructions for these large tropical trees contained larger uncertainty (higher variance on the QSM outcomes) than in previous studies (Calders et al., 2013, 2015b; Raumonen et al., 2015) which evaluated smaller trees and were located in more open forest conditions and less occluded trees. For the smallest trees in our study, the 3D reconstruction uncertainty values were closer to those previously reported by Calders et al. (2015b).

Consistent with previous QSM studies (Calders et al., 2013, 2015b; Raumonen et al., 2015; Disney et al., 2014) we optimized the reconstruction process based on the *PatchDiam* parameter, which was reported to be the most influential parameter (Calders et al., 2013). The main difference compared to Calders et al. (2015b) is in the method for judging the optimal reconstruction.

Our sample of tropical trees was characterized by being among the most challenging conditions for a 3D tree reconstruction method because the target trees were among the tallest trees in each plot and having the largest crown size and complexity. The combination of these limiting factors contributes to increased occlusion, in combination with very dense understory, resulting in under-sampled areas in the tree crowns, and larger uncertainties in the QSM reconstructions. For these low density point cloud areas the QSM's presented some unrealistic branching reconstructions. The low density point cloud issue was also addressed by Raumonen et al. (2011) and Raumonen et al. (2013). They stated that the reconstruction method was quite sensitive to low point cloud density and therefore, reliability of cylinders reconstructing small branches could be very low. Therefore, we discarded all branches with a diameter < 10 cm and applied the expansion factor to account for their volume.

Alternatively, Calders et al. (2015a) recently proposed an automated method for QSM parameterization. This method optimized the *PatchDiam* value based on the maximum match of QSM cylinders diameter with point cloud circle fitting diameter at four different heights along the main trunk. This approach focuses on comparing the reconstructed main trunk, regardless of the quality of the reconstructed tree crown. However, recent studies (Goodman et al., 2014; Ploton et al., 2016) showed the important contribution of the crown biomass to the total tree biomass for large tropical trees. Similarly, for the trees in our study, the crown contribution to the total tree biomass was 50 % on average and even larger for the trees above 10 Mg (60 % of the total tree biomass). Therefore, we decided not to implement the method of Calders et al. (2015b) for our study.

Future research should focus on developing an automated QSM optimization which op-

timizes the reconstruction of the entire tree and does not focus on the tree trunk alone. Automated optimization of this sort might enable to improve even further the accuracy of tree volume and AGB estimates of tropical trees from TLS data at large scale without harvesting trees.

2.5 Conclusions

We present an approach to estimate tree wood volume and AGB for large tropical trees that relies on estimates of tree volume based on 3D data from Terrestrial Laser Scanner (TLS) and basic wood density. We show that tree volume estimation of these large tropical trees based on TLS data and Quantitative Structure Models (QSM) provided a CV RMSE of 23.7 % in comparison to destructive harvest measurements. Tree AGB estimates derived from TLS-QSM provided better agreement with AGB reference data (28.4 % CV RMSE, CCC = 0.95) than AGB estimates based on traditional forest inventory data and pantropical allometric models (33.5 % to 54.9 % CV RMSE, CCC = 0.73 to 0.82). The allometric models considered in this study showed a systematic underestimation for large trees ($D > 70$ cm), increasing with tree size, contrasting with the largely smaller and non-systematic deviation for the TLS-QSM.

This approach can be further used for testing and calibrating new allometric models, since allometric models often have large absolute errors for large trees, which are usually underrepresented in destructive sampling studies. This opens up the opportunity for QSMs derived from TLS measurements to be used in the future for building improved allometric models that might enhance present and past estimates of forest biomass and carbon emissions from tropical forest.

2.6 Acknowledgements

This research is part of CIFOR's Global Comparative Study on REDD$^+$, with financial support from the International Climate Initiative (IKI) of the German Federal Ministry for the Environment and the donors to the CGIAR Fund. This research received further support from a SilvaCarbon research project (14-IG-11132762-350) and the UK NERC National Centre for Earth Observation (NCEO). The authors would like also to thank the scientist and technicians from CIFOR and associated consultants, and the Guyana Forestry Commission for their support and many local villagers who participate in the field work in Peru, Indonesia and Guyana.

Kaieteur National Park, Guyana

Chapter 3

Tropical tree biomass equations from terrestrial LiDAR: A case study in Guyana

This chapter is based on:

Lau, A., Calders, K., Bartholomeus, H., Herold, M., Martius, C., Raumonen, P., Vicari, M., Sukhdeo, H., Singh, J, and Goodman, R. Tropical tree biomass equations from terrestrial LiDAR: A case study in Guyana, 2018, *To be submitted*.

Abstract

Large uncertainties in tree and forest carbon estimates undermine national efforts, such as Guyana's, to accurately estimate aboveground biomass (AGB) for their national monitoring, measurement, reporting and verification system. Although biomass estimates have improved, they still rely on destructive sampling, large trees are under-represented in datasets, crown diameter parameters are not considered, and allometric models cannot be easily transferred between regions. These factors lead to uncertainties and systematic errors in biomass estimations. We developed local allometric models to estimate tree AGB in Guyana based on tree parameters (diameter, height, crown diameter) obtained from terrestrial laser scanning (TLS) point clouds from 72 tropical trees and wood density. We validated our methods and models with data from 26 destructively harvested trees. We found that our best TLS-derived allometric models included crown diameter, provided more accurate AGB estimates ($R^2 = 0.92$ – 0.93) than traditional pantropical models ($R^2 = 0.85$ – 0.89), and were especially accurate for large trees (diameter > 70 cm). The assessed pantropical models underestimated AGB by 4 % to 13 %. Nevertheless, one pantropical model (Chave et al. 2005; without height) consistently performed best among the pantropical models tested ($R^2 = 0.89$) and predicted AGB accurately across all size classes. Our study shows that TLS-derived AGB estimates were unbiased compared to destructively harvested samples. Our methods also demonstrate that tree height is difficult to measure, and the inclusion of height in allometric models consistently worsens AGB estimates. Our TLS approach shows potential to be used as unbiased calibration data to test the suitability of existing allometric models and for remote sensing missions (such as the upcoming GEDI or BIOMASS missions), thereby improving tropical forests biomass estimates.

3.1 Introduction

Guyana is one of the first countries to establish a national REDD+ program (Butt et al., 2015) and has been developing annual REDD+ performance reports based on a nationally agreed reference level since 2010. Guyana's REDD+ activities include the design and implementation of a national monitoring, measurement, reporting and verification (MMRV) system, which should be able to assess and reduce aboveground biomass (AGB) uncertainties within the country's capacities and capabilities (Henry et al., 2015).

AGB is typically estimated with allometric models built from empirical data. The applicability of any allometric model is thus largely dependent on the data used for its development and can produce systematic over- or under-estimations of the true AGB when applied to other regions or areas where no data were included (Alvarez et al., 2012; Goodman et al., 2014; Manuri et al., 2014). Since the performance of a country's MMRV program will be based on the quantification of emission reduction (Gibbs et al., 2007; Manuri et al., 2014), Guyana seeks to test the accuracy of pantropical models and develop a country-specific allometric model.

Current AGB allometric models of tropical forests are commonly based on diameter at breast height (D; which can be measured in the field) and wood density (WD). In recent decades, the inclusion of other parameters such as height (H) and regional attributes (Feldpausch et al., 2012), crown diameter (CD; Goodman et al., 2014), and climate variability (Chave et al., 2014) have been shown to improve prediction of AGB at pantropical level in some cases (Alvarez et al., 2012; Fayolle et al., 2016; Blanchard et al., 2016). However, due to the difficulty of measuring tree heights, the pantropical allometric models developed by Chave et al. (2005) are still widely used because they do not require tree heights (e.g. Fayolle et al., 2016; Sullivan et al., 2018).

Large trees (diameter > 70 cm) are particularly important for both forest biomass and forest biomass estimates. They account for *ca.* 75 % of total forest AGB variations (Slik et al., 2013; Ploton et al., 2016; Meyer et al., 2018) and the error of AGB estimates increases with size (Goodman et al., 2014; Calders et al., 2015b; Gonzalez de Tanago et al., 2017). Despite their relevance, large trees make up only 7 % of available tropical biomass data (as of 2014; Chave et al., 2014), and the lack of inclusion of large tree biomass data in the development of allometric models is increasingly viewed as problematic (Clark & Kellner, 2012; Goodman et al., 2012; Sheil et al., 2017; Disney et al., 2018). AGB error varies greatly with increasing tree size, and pantropical allometric models often underestimated large tree biomass (Goodman et al., 2014; Calders et al., 2015b; Gonzalez de Tanago et al., 2017).

Terrestrial Light Detection And Ranging (LiDAR), also known as terrestrial laser scanning (TLS), has been proven to be a valuable tool to assess the woody structure of trees (Wilkes

et al., 2017; Gonzalez de Tanago et al., 2017; Malhi et al., 2018). Several studies have successfully taken TLS from its original utility —precision surveying applications— to tropical forests (Gonzalez de Tanago et al., 2017; Wilkes et al., 2017; Momo Takoudjou et al., 2018; Rahman et al., 2017; Disney et al., 2018; Paynter et al., 2018; Stovall et al., 2018) and extracted tree parameters such as tree diameter (Calders et al., 2015b), height (Burt et al., 2013; Krooks et al., 2014), and crown width (Holopainen et al., 2011). In combination with quantitative structure modelling —e.g. *TreeQSM* (Raumonen et al., 2013) or *SimpleTree* (Hackenberg et al., 2015a)— 3D tree point clouds were used to infer parameters such as total volume, AGB (Burt et al., 2013; Calders et al., 2015b; Gonzalez de Tanago et al., 2017; Momo Takoudjou et al., 2018; Disney et al., 2018), AGB change (Kaasalainen et al., 2014), and tree species (Åkerblom et al., 2017), as well as ecological questions such as tree mechanics, branching architecture and surface area scaling (Malhi et al., 2018).

This study assesses the potential of TLS and *TreeQSM*-method to develop allometric models to estimate AGB in forest trees of Guyana. We produced a unique tropical tree mass dataset of traditional inventory and TLS scans of 106 tropical trees; 26 of these trees were destructively harvested and weighed to estimate aboveground biomass. The objectives of this study are: (i) to model tree volume and estimate tree AGB from *TreeQSM* models of tree point clouds, (ii) to build allometric models based on TLS parameters for Guyana, and (iii) to evaluate the performance of these TLS-derived data and allometric models against destructively-harvested reference data and estimates from pantropical models.

3.2 Material and methods

Study area

Field work was conducted in January and February 2017 inside an active logging operation company near the Berbice river, in the East Berbice-Corentyne Region of Guyana (Table 3.1).

Table 3.1: Study site description (Muñoz & Grieser, 2006).

Location	4.48 to 4.56 latitude and -58.22 to -58.15 longitude
Forest type	Mixture of white sand forest and mixed forest[a]
Altitude	106 masl
Rainfall	3829 mm yr^{-1}
Temperature	22.5 to 30.5 Celsius
Humidity	86 %

[a]from Guyana Lands and Surveys Commission (2013)

Tree selection and data collection

Tree inventory

An exploratory survey of the area was performed as a guide to sample the species composition of the forest (Appendix 3.B). We grouped our trees into five diameter size classes ($10 \leq D < 30$, $30 \leq D < 50$,..., $D \geq 90$ cm) and inventoried 16 to 23 trees per size class. We measured D and point of measurement (POM), total H, CD, and recorded species, stem damage, and any irregularities. An experienced local taxonomist matched reported local names with scientific names (Appendix 3.B).

TLS data acquisition

All TLS datasets were acquired using a RIEGL VZ-400 3D terrestrial laser scanner (RIEGL Laser Measurement Systems GmbH, Horn, Austria). We scanned at each position with a resolution of 0.04° (Appendix 3.C).

From our full field inventory, 26 trees were destructively sampled trees and removed from the TLS dataset to serve as validation data. We inspected the point clouds of the remaining 80 trees and discarded 8 trees whose point clouds were poor due to occlusion. Thus, 72 trees were used in our TLS database to build allometric models.

Destructive harvesting and fresh mass sampling

Our AGB reference data were selected based on diameter class, species, and wood density to maximize the number of species sampled and avoid biases; all other characteristics were ignored —following Goodman et al. (2014). After felling each tree, we re-measured D and H and weighed each part *in-situ* (Appendix 3.B).

Laboratory analysis

We transported all samples to the laboratory at the Guyana Forestry Commission (Georgetown, Guyana) for species identification, drying, and storage. Samples were oven dried (101 °C to 105 °C until they reached a constant mass; Williamson & Wiemann, 2010) and re-weighed. Wood density was obtained as dry mass per fresh volume, and dry mass fraction (dmf) was the ratio dry to fresh mass (Appendix 3.B).

Tree above-ground biomass estimation from pantropical allometric models

Structural (D and H) and WD data from the 26 harvested trees were used to estimate AGB from pantropical allometric models (Appendix 3.E). We estimated AGB and its error using the most widely used pantropical allometric models (Eqn. Ch05.II.3, Ch05.I.5, Cha14.H and Ch14.E) for moist forests (Chave et al., 2005, 2014) and an updated version of Ch14.E. This revised version (Eqn. Rj17.E) is a direct model fit equation, while the original equation Ch14.E was obtained by merging two equations (Réjou-Méchain et al., 2017).

Tree parameters extraction and biomass estimation from TLS data

Diameter, tree height and crown diameter from TLS data

TLS-derived D was calculated from cross sectional point clouds (6 cm width) taken at every 10 cm on the Z-axis up to 6 m height. Least square circle approach was used to fit circles in each cross sectional point cloud. We automatically determined POM by analysing the angle between two consecutive diameters, starting from the bottom. The first angle within 1° of 90° (*i.e.*, vertical) was considered as the POM. Total height was estimated as the distance between the maximum and the minimum point in the Z-axis from each tree point cloud. Finally, crown diameter was estimated as the average of two horizontal distances between the maximum and the minimum point in the X- and Y-axis from each tree point cloud.

Tree volume and biomass from TLS data

We estimated tree wood volume from 3D quantitative structure models (*TreeQSM* version 2.0; Raumonen et al. 2013; Calders et al. 2015b; Gonzalez de Tanago et al. 2017) from our reconstructed 72 trees. WD values were assigned to each species or genus according to Global Wood Density Database (Zanne et al., 2009; Chave et al., 2009). To obtain tree volume, we had two main components: (i) semi-automatic individual tree extraction

from TLS plots (Fig. 3.1a-c) and (ii) 3D reconstruction of QSMs for individual extracted trees (Fig. 3.1d and Appendix 3.D).

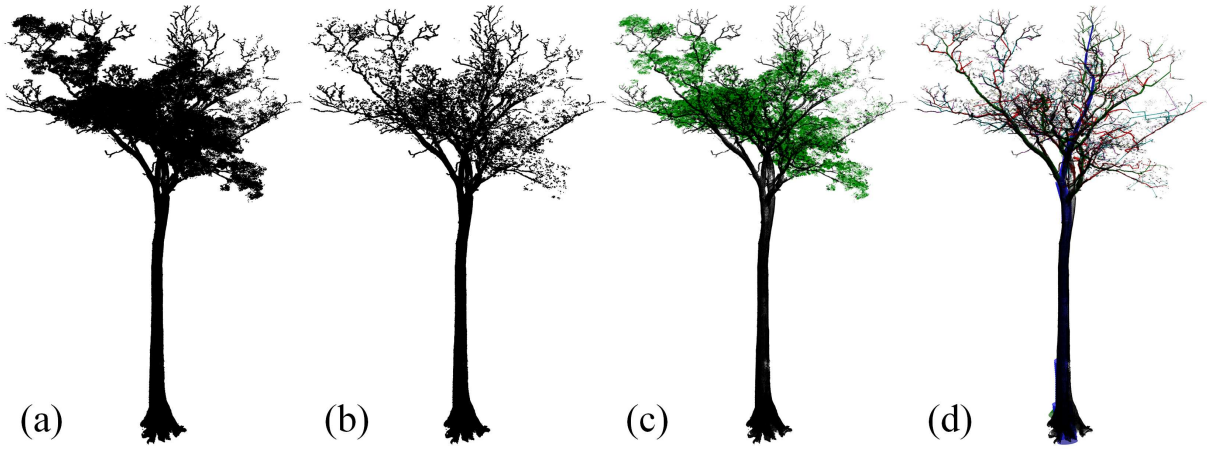

Figure 3.1: (a) *Vitex spp.* tree point cloud, (b) down-sampled tree point cloud, (c) soft tissues (green) and hardwood (black) separated point cloud, and (d) *TreeQSM* modelled after the hardwood point cloud (See details in Appendix 3.D).

Once we extracted the trees, we reconstructed their volume with cylinder features using the automated framework presented in Calders et al. (2015a) to optimize QSMs. We optimized cover patch size (d) by reconstructing the volume using a d range from 0.02 m to 0.09 m with a 0.005 m increment and a minimum number of points per cover patch *nmin* of 4. The optimization process returned the most suitable d for each tree based on least square fit process and 20 models were reconstructed on average. The heuristic decision to accept/reject was taken based on analyst's experience and judgement (Fig. 3.1d; Calders et al., 2015a; Gonzalez de Tanago et al., 2017).

For 43 trees with large buttresses, a triangular mesh was used for the volume modelling in the bottom part of the stem rather than cylinders (Fig. 3.2; see Disney et al. 2018). The volume of the mesh replaced the volume of the cylinders on the total tree volume estimation.

Finally, to estimate AGB, we multiplied the total tree volume with the corresponding wood density. As an indicator of the reconstruction accuracy of the *TreeQSM*, root mean square error (RMSE) was calculated to measure the difference between the reference and modelled AGB; R^2 was used to judge the fit of the *TreeQSM* models; concordance correlation coefficient (CCC) was calculated to compare the agreement of the AGB estimates; and coefficient of variation of RMSE (CV RMSE) was calculate to measure the difference between our TLS-derived AGB and reference AGB (Calders et al., 2015b; Gonzalez de Tanago et al., 2017).

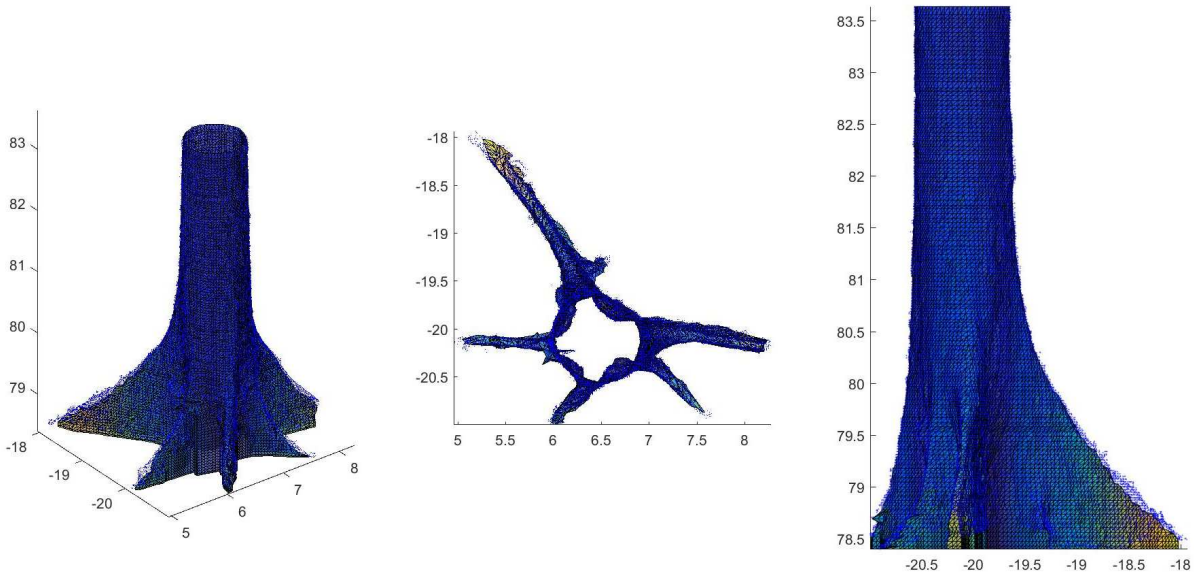

Figure 3.2: Buttresses modelling of a *Hymenolobium flavum* tree. The bottom part of the stem was modelled with a triangular mesh instead of cylinders. The mesh volume replaced the volume of the cylinders.

TLS-derived allometric models

We examined five model forms (Table 3.3) based on previous forms developed by Chave et al. (2005) and Goodman et al. (2014) using TLS-derived parameters (D, H, and CD) and WD to test the relevance of these variables to predict AGB. To build the allometric models, all data were transformed to the natural logarithm to comply with allometric theory and meet the assumptions of linear regression (Appendix 3.F). Moreover, the models were built using multiple regression and the coefficient estimation is based on least squares. Model error (ε) was estimated as the 95 % confidence interval of the regression model.

Model assessment for biomass allometric models

We made two types of assessment. First, we evaluated the log-transformed models based on the fit of the data used to build the models. For that, we evaluated the models by using a penalized likelihood criterion on the number of parameters: adjusted R-square (R^2), corrected Akaike's information criterion (AICc), and the residual standard error (RSE). The best fitted allometric model had highest R^2 and lowest AICc and RSE. To estimate AGB values (in Mg) a correction factor ($CF = exp[RSE^2/2]$) was applied to backtransform predicted values and remove bias from the log-transformed data (Baskerville, 1972).

Second, we assessed the ability of our allometric models to predict AGB (Table 3.3) and

compared them to five pantropical allometric models (Appendix 3.E). We validated these AGB estimates with field-measured reference AGB using the metrics listed below: model error (Eqn. 3.1) and relative error (Eqn. 3.2).

$$AGB_{error}(\text{Mg}) = AGB_{est} - AGB_{ref} \tag{3.1}$$

$$AGB_{relative\,error}(\%) = \frac{AGB_{est} - AGB_{ref}}{AGB_{ref}} \cdot 100 \tag{3.2}$$

where AGB_{est} is AGB predicted by each model, AGB_{ref} is the AGB calculated from our destructive sampling, $mean_{error}$ is the average of AGB_{error} for all 26 trees, and $mean_{ref}$ is the average of AGB_{ref}. We calculated these metrics for our entire harvested tree dataset ($n = 26$) and subsequently split this data into small ($D \leq 70\,\text{cm}$; $n = 17$) and large ($D > 70\,\text{cm}$; $n = 9$) trees. We used both assessments to identify our "best" model(s).

3.3 Results

Tree parameters and estimated biomass

A total of 106 trees were inventoried and scanned across a large range of tree sizes (D 11.20 cm to 149.80 cm). Of these, 26 were destructively sampled and used as test or validation data, 8 were discarded due to low quality point clouds, and the remaining 72 trees were used to build allometric models based on TLS-derived data (Table 3.2 and Appendix 3.G). Six harvested trees had hollow sections in the bole.

Table 3.2: Pre- and post-harvested field measured parameter and TLS-derived parameter ranges for diameter (D), height (H), crown diameter (CD), wood density (WD; from direct measurements for measured trees in reference dataset and from GWDD for all others) and AGB.

Parameters	Allometric model dataset ($n = 72$)		Validation dataset ($n = 26$)	
	Measured^{pre}	TLS-derived	Measured^{post}	TLS-derived
Diameter (cm)	12.9 – 134.0	13.3 – 126.2	16.7 – 128.7	16.7 – 130.2
Tree height (m)	14.0 – 43.0	16.9 – 51.8	16.4 – 51.6	16.6 – 49.1
Crown diameter (m)	4.4 – 42.6	2.5 – 42.9	3.4 – 30.8 ^{pre}	4.6 – 30.2
WD (g cm^{-3})	0.4 – 1.0	0.4 – 1.0	0.4 – 0.9	0.4 – 1.0
AGB (Mg)	NA	0.2 – 28.5	0.9 – 21.8	0.2 – 27.4

Our study found a systematic difference between the three measurements for D in our dataset of 26 validation trees (p-value < 0.05; Table 3.2): mean values were 59.4, 57.7,

and 55.2 cm for pre-harvest, post-harvest, and TLS-derived diameters, respectively. Using post-harvest field measurements as the reference data, we calibrated the TLS-derived D estimate. Neglecting to adjust the systematically lower TLS-derived D would result in a systematic overestimation of the AGB when applying TLS-derived allometric models with field measurements diameters. The other TLS-derived parameters (H, CD, and AGB) were not significantly different from our reference data. However, post-harvest H measurements were significantly taller than H measurements taken on standing trees ($p < 0.05$; 11 %; n=26). WD values from our measurements and the GWDD were similar (our values were 1 % greater; Appendix 3.H). Finally, there was no systematic difference between AGB estimated from QSM and our reference data. AGB estimates from *TreeQSM*, destructive sampling, and the pantropical models had a high level of agreement (CCC = 0.96, R^2=0.92, CV RMSE=33 %), but *TreeQSM* outperformed the pantropical models. Pantropical models showed slightly lower level of agreement (CCC = 0.92–0.94); with a R^2 ranging 0.85–0.89 and CV RMSE ranging 37 %–44 %.

Allometric models using TLS-derived measurements

We created five allometric models using combinations of the TLS-derived parameters D, H and CD and WD from the GWDD (Table 3.3). In the models where the intercept was removed, R^2 was not calculated (Table 3.3). For models using CD (m4 and m5) we found that the residuals were not normally distributed using Anderson-Darling test. Upon further visual inspection of normal quantile-quantile plots, we considered the residuals to be reasonably normally distributed and that these models are reliable (Appendix 3.I). For model forms m2 and m3, models built using field and TLS-derived data were significantly different ($p < 0.05$), thus we applied RDVC to the TLS models (Table 3.3).

Table 3.3: Models description for the TLS-derived above-ground biomass estimations including diameter (D), wood density (WD), height (H), crown diameter (CD), Reference Dummy Variable Corrector ($RDVC$) and associated statistical parameters based on 72 trees.

Model	Type	Form
m1	D	$\ln(AGB) = a + b \cdot \ln(D)$
m2	D.WD	$\ln(AGB) = a + b \cdot \ln(D) + c \cdot \ln(WD) + RDVC$
m3	D.WD.H	$\ln(AGB) = b \cdot \ln(D) + c \cdot \ln(WD) + d \cdot \ln(H) + RDVC$
m4	D.WD.H.CD	$\ln(AGB) = b \cdot \ln(D) + c \cdot \ln(WD) + d \cdot \ln(H) + e \cdot \ln(CD)$
m5	D.WD.CD	$\ln(AGB) = a + b \cdot \ln(D) + c \cdot \ln(WD) + e \cdot \ln(CD)$

Notes: df are degrees of freedom of the model, RSE is residual standard error of estimates, R^2 is adjusted R^2, AICc is the corrected Akaike's information criterion and NA is not applicable.

Table 3.3: *(continued).*

Model	a	b	c	d	e	$RDVC$	df	RSE	adj-R^2	AICc
m1	0.6788	1.9337	...	...	...	...	70	0.360	0.90	61.52
m2	0.6765	2.0246	1.0932	...	...	−0.1968	69	0.274	0.94	23.61
m3	...	1.9091	1.0978	0.3224	...	−0.2138	69	0.266	NA	19.48
m4	...	1.7282	0.2603	1.1522	0.3698	...	68	0.240	NA	6.23
m5	0.5366	1.8124	1.1512	...	0.3878	...	68	0.246	0.96	9.28

Evaluation of allometric models

We assessed how well the five TLS-derived allometric models developed in this study and five pantropical allometric models estimate AGB of our destructively-harvested reference data on the original scale (in Mg; Fig. 3.3 and Table 3.4). Results were similar to the assessment done on the log-transformed scale, and our models including CD estimated AGB better than all other models. On the original scale (Table 3.4), AGB estimates from TLS-derived allometric models were slightly better (R^2 0.87–0.93; CCC 0.89–0.96) than the pantropical models assessed (R^2 0.85–0.89; CCC 0.92–0.94).

Table 3.4: Summary of AGB estimates from TLS-derived and pantropical allometric models —R^2, RMSE, CCC, sum of errors (sum, mean, standard deviation [SD]), mean percent error and relative error ($n = 26$). Models are arranged based on the statistical parameters from the best model to the worst model.

Model	Type	R^2	RMSE	CCC	Error (Mg)			Relative error (%)	
					Sum	Mean	SD	Mean	SD
m5	D.WD.CD	0.93	1.91	0.96	1.03	0.04	1.95	28.25	61.35
m4	D.WD.H.CD	0.92	1.99	0.96	1.36	0.05	2.03	28.33	57.91
Ch05.II.3	WD.D.D^2.D^3	0.89	2.32	0.94	−7.49	−0.29	2.35	5.54	48.26
Ch05.I.5	D^2.WD.H	0.85	2.75	0.92	−9.86	−0.38	2.78	7.35	41.98
Ch14.H	(D^2.WD.H)	0.85	2.67	0.92	−11.89	−0.46	2.69	9.59	43.31
m1	D	0.87	2.52	0.93	13.65	0.53	2.51	68.01	105.95
Rj17.E	D.WD.E	0.88	2.43	0.93	−19.28	−0.74	2.36	−1.62	44.04
Ch14.E	D.WD.E	0.88	2.49	0.93	−21.56	−0.83	2.39	−3.62	43.52
m3	D.WD.H	0.88	2.92	0.89	−32.11	−1.23	2.69	14.80	60.97
m2	D.WD	0.89	2.96	0.92	32.21	1.24	2.74	73.80	98.95

Our TLS-derived allometric models with CD performed better than all other models in terms of producing the lowest absolute errors (Table 3.4 and Fig. 3.3). The pantropical models tended to underestimate AGB but had lower relative errors (Table 3.4 and Fig. 3.3). In contrast to the model evaluation with the 72 TLS-trees on the logarithmic scale, m5 (without H) performed slightly better than m4 (with H). By several metrics, model m2 and m3 performed the worst of all models evaluated. Adding WD and H to the model did not definitely improve estimates over m1 with only D. In fact, adding these parameters increased overall error. However, adding CD to models with WD and H improved estimates by all metrics. Adding H to models did not improve their accuracy. In both cases, models m5 vs. m4 and m3 vs m2, the model without H performed better than the counterpart model with H.

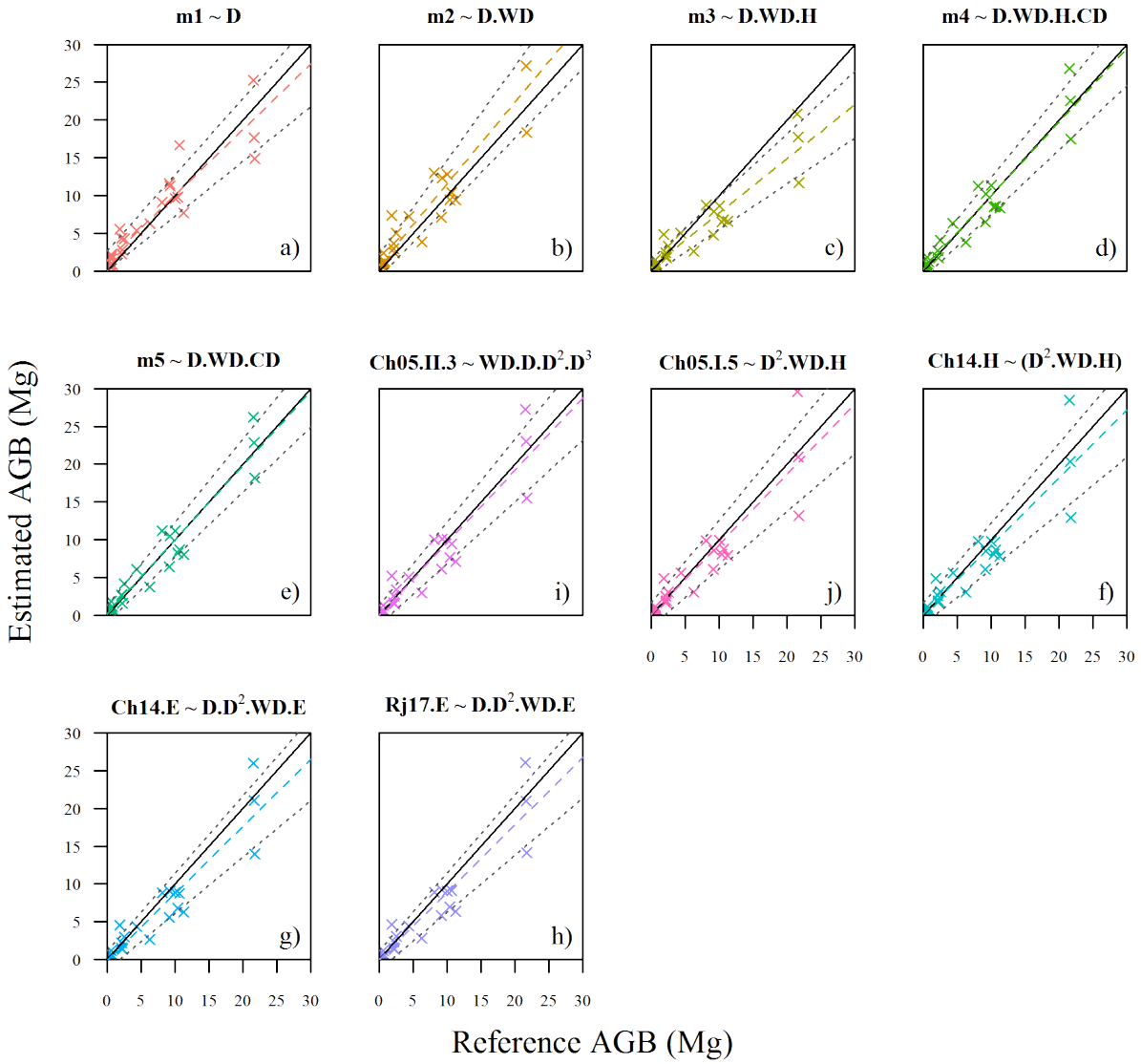

Figure 3.3: Relationship between reference AGB (harvested trees; $n = 26$) and AGB estimated by TLS-derived and pantropical allometric models. Black solid line is 1:1 relationship, dashed coloured lines depicts linear fit, and dotted grey lines indicate 95 % confidence interval for the linear fit.

Among the pantropical models, Ch05.II.3, with just D and WD, had the highest R^2, CCC and the lowest RMSE, but slightly underestimated AGB (Table 3.4 and Fig. 3.3). The two models including the "environmental stress" (E) parameter (Ch14.E and Rj17.E) produced the largest underestimates of AGB in absolute terms but lowest relative error (Appendix 3.K). Models including H (Ch05.I.5 and Ch14.H) also underestimated AGB and were, by several metrics, the least accurate among all models evaluated (lowest R^2, lowest CCC, highest RMSE).

Because allometric models often over- or under-estimate AGB differently systematically

with tree size, we also assessed the performance of the TLS-derived and pantropical models for small trees ($D \leq 70\,\text{cm}$; $n = 17$) and large trees ($D > 70\,\text{cm}$; $n = 9$) separately (Appendix 3.J and 3.K). The inclusion of CD in the models reduced error in AGB estimates for both size classes, but the effect was much more substantial in large trees. The mean error of TLS-derived models m4 and m5 is very close to zero for both small and large trees, but mean relative error is very high for small trees (44 %). The inclusion of H in TLS-derived models improved AGB estimations for small trees but reduced the accuracy of AGB estimates for large trees when compared to their counterpart model without H. All pantropical models underestimated AGB, and the underestimation is greater for large trees (Appendix 3.K).

For the most accurate AGB estimates in Guyanese forests, we recommend model m5 (Equation 3.3), especially for large trees. AGB is measured in kg dry mass, D in cm, H and CD in m and WD in $\text{g}\,\text{cm}^{-3}$. The back-transformation correction factor has been incorporated:

$$AGB = \exp[0.5669 + 1.8124 \cdot \ln(D) + 1.1512 \cdot \ln(WD) + 0.3877 \cdot \ln(CD)] \tag{3.3}$$

3.4 Discussion

This study presents the first assessment of the potential of TLS and *TreeQSM* to develop TLS-derived allometric models to estimate AGB for trees in Guyana and takes Guyana one step closer to its aim of developing a national MMRV system. In a similar assessment, Stovall et al. (2018) reconstructed 329 trees in Virginia, USA and found that TLS-derived allometric models predicted AGB better than the equivalent national models. Our results showed better results for TLS-derived allometric models that include CD compared to the pantropical models from Chave et al. (2005, 2014) and Réjou-Méchain et al. (2017), which included trees from the same region (French Guiana, $n \approx 390$ trees). In the absence of CD data, the oldest and simplest of the pantropical models (Ch05.II.3) provides the most accurate AGB estimates in this region. This is one of the first studies to have explicitly used TLS-derived parameters and wood density to develop allometric models to estimate AGB of tropical trees. A similar study, by Momo Takoudjou et al. (2018), calibrated an allometric model from Chave et al. (2014) using TLS tree point clouds from a semi-deciduous forest in Cameroon and yielded a good fit ($R^2 = 0.95$).

Recent studies have highlighted the relevance of including crown dimension in allometric models (Goodman et al., 2014; Jucker et al., 2017; Ploton et al., 2016). Models including CD had the highest R^2 in Goodman et al. (2014); Jucker et al. (2017) and lower bias ($-4.5\,\%$) in Jucker et al. (2017). These authors had independently agreed that CD improves tropical tree biomass estimates, especially for large trees ($D >$ *ca.* 100 cm in

Goodman et al. 2014; Ploton et al. 2016; and $\geq 10\,\mathrm{Mg}$ for Jucker et al. 2017). From our results we can assure that allometric models using CD provides better AGB estimates for trees in Guyana especially for large D size classes (Appendix 3.J). However, obtaining crown diameter is time-consuming, and hence often avoided during fieldwork.

Our study reveals that AGB estimates from allometric models with H general performed worse than their counterparts without H, for both TLS-derived and pantropical allometric models. Goodman et al. (2014) also found that models including H underestimated AGB and suggested the inclusion of CD instead of H in allometric models. Our results contrast those of Feldpausch et al. (2012), in which their models with H performed better estimating AGB than models without H, and agree with Goodman et al. (2014), which found that pantropical models that include H tend to be systematically inaccurate when applied to other locations.

We found significant differences in the pre-, post-harvest and TLS-derived D and H values, demonstrating the difficulty and ambiguity of measuring the diameter and height of tropical trees. Although it is nearly impossible to say what "true" and repeatable diameter above buttresses and total H are, TLS offers new insights. For example, even with rigorous protocols determining the top of buttresses is a judgement call, and our data show variation in measurements on standing and felled trees. Pre-harvest D measurements were significantly higher, reflecting the difficulty of measuring high above the ground; and post-harvest measurements were much more conservative. Our novel methods of determining D from TLS point clouds to the point where taper reduced 4 % on average was perhaps too conservative but probably more repeatable. It is important to note that conservative D measurements yield conservative AGB estimates from allometric equations, but the opposite is true when building allometric models. Measuring tree height in tropical forests is notoriously difficult, especially for trees above forest canopy. The precision of repeated height measurements from the ground ranged from 3 % to 20 % of the total height, leading up to 16 % mean error for AGB estimates Hunter et al. (2013). In our study we did not record repeated measurements, but our pre-harvest height measurements were on average 10 % lower and TLS-derived measurements were on average only 2 % lower than our reference (post-harvest) heights. Pre-harvest measurements had a greater variation and greater underestimation than our TLS-derived height. Our data show that H measurements are smallest on standing trees measured with a laser rangefinder (probably because either the highest point is not visible and/or the laser did not hit the highest point), highest on harvested trees (perhaps because trees stretch or break during the fall), and intermediate from TLS scans of standing trees. Thus, it is quite possible that TLS provides the most accurate H measurements.

We also estimated AGB for our trees using five well-known pantropical models (Appendix 3.E) showing that all five models underestimated AGB. Our results contrasts with some studies and support others. In Colombia, Alvarez et al. (2012) found that using Chave

et al. (2005) moist pantropical equations (with and without H) all overestimated AGB (with relative errors up to 52.8 %); while Gonzalez de Tanago et al. (2017) found that AGB was underestimated 15.2 % to 35.7 % when compared to estimated AGB from *TreeQSM* models in Guyana, Indonesia and Peru. As in Alvarez et al. (2012), Kuyah et al. (2012) found that AGB in Kenya was overestimated in 22 % using Chave et al. (2005) moist forest equation (with H) and suggested that overestimations were due to the dominance of small trees ($D < 10\,\text{cm}$) and lack of larger trees in their plots. We theorized that with more trees scanned, we could understand the reasons for these differences. When disaggregating by diameter size, we found that pantropical models tended to overestimate small trees and underestimate large trees (Appendix 3.J). This contrasts Chave et al. (2005), whose models tended to underestimate small trees. Our results are more aligned with Chave et al. (2014), insofar as their models tended to overestimate small trees, be fairly accurate with medium size trees, and underestimate larger trees.

Scanning tropical trees *in-situ* remains challenging, not only because of the harsh environment but also because the novel sampling design we developed for this study (Appendix 3.C). In our study, we increased the scanning resolution from 0.06° to 0.04° (Appendix 3.C) as suggested by Wilkes et al. (2017) to balance trade-off between accuracy and scanning time requirements. Gonzalez de Tanago et al. (2017) pointed out that low-density point clouds created unrealistic branching reconstructions. Still, we discarded 8 tree point clouds due to under-story occlusion. Because a detailed analysis of quality of tree point clouds is usually done after the fieldwork, we suggest increasing the number of scanned trees by 10 % over the desired sample size in case some trees need to be removed due to poor quality.

Tropical countries seeking to participate in REDD+ that do not possess own tree biomass database might find our TLS-driven methodology a resourceful alternative. They can test and develop national allometric models based on TLS-derived parameters and some destructively harvested reference data. Our methodology provided unbiased AGB estimates regardless of tree structure, even with partially hollow and irregular stems. However, we suggest that this outcome is further tested with destructively harvested data from other forests. For Guyana, developing a national monitoring system based on the now known most appropriate pantropical model or their own national model could contribute to more accurate biomass estimates for REDD+ MMRV. Our results demonstrated that TLS-derived AGB estimates can be used as a decision-making tool in MMRV selection of an adequate pantropical allometric model, and in case TLS-derived allometric models using CD are out of scope, Ch05.II.3 would be an adequate model (on average conservative and reasonably accurate).

Being able to obtain TLS-derived AGB estimates without destructively harvesting trees is relevant also environmentally desirable. We are able to quantify AGB for trees that would be illegal, expensive, impractical, or simply unnecessary to harvest. We are aware that our

methods and analyses require expensive equipment and expert knowledge, but the process is much faster, less labour intensive, and environmentally sustainable than destructive harvesting, especially for large trees. Research has already begun to semi-automatize the modelling processes by separating individual trees (Raumonen et al., 2015) and splitting hardwood from soft tissues (Disney et al., 2018).

With the advances on tree segmentation algorithms (Burt, 2017; Calders et al., 2018), the modelling of trees is being semi-automatized. Tree segmentation algorithms would allow us to segment and estimate AGB using *TreeQSM* for entire TLS scanned forest plots. As mentioned before, the estimation of AGB from tropical trees is being biased by underestimation from the pantropical allometric models, TLS can remove this bias.

Although this is a case study of creating site-specific allometric models for Guyana, we showed that TLS-derived allometric models (including CD) can be an unbiased estimator of AGB, even in a logged forest where we would expect a high proportion of damaged and hollow trees remaining. Our method's potential to rapidly produce large, unbiased calibration tree datasets is of great significance to remote sensing missions, which rely on field data for their calibration, thereby improving tropical forests biomass estimates. We strongly encourage other studies to expand upon our findings to determine whether TLS always provides unbiased AGB estimates and could replace destructive sampling in the future.

3.5 Conclusions

We advanced TLS methods to estimate tree metrics and explored the accuracy of field and TLS-derived methods to develop local allometric models for Guyana. We showed that TLS-derived allometric models can be built from TLS-derived tree volume and wood density without destructive harvesting, even with the occurrence of hollow and irregular stems. We demonstrated that tree AGB estimates from TLS-derived allometric models including crown diameter (models m4 and m5) provide better agreement with reference data (mean error 0.04 Mg to 0.05 Mg) than AGB estimates from pantropical allometric models (mean error -0.83 Mg to -0.29 Mg), especially for large trees (D $>$ 70 cm). AGB estimates from TLS-derived allometric models and pantropical models including height provided poor agreement with reference data when compared to their counterpart without height (m2 and m5 respectively). The simplest pantropical model (Chave et al. 2005, with only D and WD) provided very good estimates of our data. Our results are based on 72 TLS scanned trees, a small number of trees compared to other studies. Nonetheless, our new approach can be further applied for developing allometric models without the need to harvest vast numbers of trees. This new approach can be used to test and choose existing allometric models calibration remote sensing metrics to forest biomass, and improve the future estimates of forest biomass from tropical forest.

3.6 Acknowledgements

This research is part of CIFOR's Global Comparative Study on REDD$^+$, with financial support from the International Climate Initiative (IKI) of the German Federal Ministry for the Environment and the donors to the CGIAR Fund. This research received further support from SilvaCarbon research project 14-IG-11132762-350; ERA-GAS NWO-3DforMod project 5160957540; BELSPO STEREO III programme — project 3D-FOREST (SR/02/355) and CNPq (National Council of Technological and Scientific Development — Brazil) through the programme Science Without Borders (Process number 233849/2014-9). Our field data was acquired through collaboration between Wageningen University and Research and Guyana Forestry Commission.

3.A Appendix

3.B Biomass sampling design

3.B.1 Field protocol summary

1. Measure preharvest
    - Mark coordinates, label tree
    - Measure: diameter (paint location), total height (H_{tot}), crown radius
    - Note: crown quality, structural damage, stem irregularities
2. Post-felling measurements
    - Remeasure tree size
        - Re-measure: diameter (same location), total height (H_{tot}), crown radius
        - Measure: H_{tot}, stump height (H_{stump}), commercial height (H_{com}), height of first major branch ($\geq$5 cm; H_{FMB})
    - Separate and weigh
        - Small branches ($<$10 cm diameter)
        - Large branches ($\geq$10 cm diameter)
        - Commercial bole
        - Non-commercial bole
        - Stump
    - Take wood samples
        - Label each sample and measure fresh mass
            * Small branches (Bs)
            * Large branches (BL)
            * Trunk (T)
            * Stump (St)
        - Measure volume as soon as possible
        - Store samples in the sun, if possible

– Transport samples to laboratory, dry, and weigh

3.B.2 Tree inventory

All individuals fitting the diameter classes were included in the selection regardless of commercial value, structural irregularities, health, or wood defects. We measured each position using the average of 1000 GPS measurements (WGS84 Geographic coordinate system). We measured diameter at 1.3 m or above buttress with a diameter tape and recorded the point of measurement (POM). Total height, height of first branch, and crown width were measured with a Nikon Forestry-Pro hypsometer (precision of 0.2 m). We noted any structural damage or irregularities, and an experienced local taxonomist matched reported local names with scientific names.

3.B.3 Pre-harvest tree measurements

We will measure DBH, total height, height of the commercial bole, depth and diameter of the canopy, angle of the branches, and extract a wood sample with an increment borer.

1. Tree information
    - Mark coordinates with GPS
    - Label tree with spray paint.
2. Diameter at Reference Height (DRH; from the RAINFOR field manual for plot establishment and remeasurement).
    - Mark POM on tree (with marker or paint)
    - Make note of POM
3. Height: It is optional to measure height on standing trees. Height can be measured with a laser rangefinder as per the "Measuring tree height in tropical forest trees" manual (Chave, 2005):
    - Rangefinder: Only for trees > 10 m in height can be measured this way.
4. Height of snapped crown
    - Measured by the same methods to account for crown damage (Chambers et al., 2001)
5. Crown measurement

- Take crown radius as the distance from the trunk to the projected edge in 4-8 compass directions (Kitajima et al., 2004). For each tree, crown radius will determined as the mean the above 4-8 measurements (Kitajima et al., 2004).
- Crown area can be measured as an ellipse, measuring the diameter at the longest and shortest widths

6. Classification of canopy quality, as Jiménez-Rojas et al. (2002).
   - good (symmetrical and vigorous)
   - average (some defects with respect to the symmetry and density of the foliage)
   - poor (not vigorous, substantial portions of the limbs without foliage or branching, markedly asymmetrical)
7. Alive status
   - According to the manual RAINFOR field work database codes for trees as in Phillips et al. (2005).
8. Structural damage
   - Take note of any loss of large branches, stem damage, etc
9. Stem irregularity
   - Take note of buttresses, fluted trunks, etc.

3.B.4 Post-harvest tree measurements

1. Felling
   - Ask chainsaw operator to saw off trunk as close to ground level as possible
   - Ask chainsaw operator to remove as many large branches as they would normally
2. Labelling
   - If the trunk is cut into multiple pieces, label (spray paint) each section with its ID number plus *a*, *b*, *c*, etc (going from base to crown).
   - Record the total number of sections per trunk.
3. Heights: Measured on felled trees with a measuring tape
   - Total height: Measure to top leaf
   - Height of commercial bole (Hc): The point of measurement will be identified by experienced loggers

- A main branch is defined as one > 5 cm diameter, with leaves
- Height of first living branch: this will identify crown depth:
  - Crown depth will be defined as "the distance between the crown apex and the lowest foliated branch" (Kitajima et al., 2004)
  - Measured on the ground as $Crown\ depth =$ $(Total\ height)$ – $(Height\ to\ the\ first\ living\ branch)$
  - Branch height will be measured at the base

4. DRH:
   - Re-measure trunk diameter (at the same point)
5. Stem taper
   - Diameter will be measured every 1 m from the base of the tree (0 m) to the top of the bole.
   - Potential problems and how they will be handled:
     - Climbers will be removed prior to measurement
     - Fluted and all irregular stems: "diameter" will be measured regardless of irregularity (though, the type and extent of irregularity will be noted)
     - Resprouts and multiple stems: diameter will be measured and recorded separately for up to 3 stems (any more will be considered the canopy).
     - Sloped trees (i.e., the base of the tree is not perpendicular to the rest of the trunk): we will take measurements starting (0 m) at the uphill side of the tree.
6. Each tree will be separated into the following parts:
   - main stem
   - large branches (≥ 10 cm)
   - small branches (< 10 cm) and leaves
7. Fresh mass of each tree part will be measured in the field
   - Tarps will be used to catch as much material as possible (e.g., saw dust and leaves)
   - Large branches will be sawed into manageable sizes
   - Small samples will be weighed near the felled tree with the 250 kg scale (attached to a nearby tree)

- Trunks will be left until the company can drag them to a logging deck. They will be weighed with the use of a front loader whenever the machinery is possible.

8. For all trees, we will take at least one cross-sectional slice of the bole. Trees will only be cut according to the forestry concession's standard practices. This will include cuts at the base and top of commercial bole. In the case of very large (> 6 t) trees or other circumstances, there may be intermediate cuts. We will ask for a 3 cm disk at the point of every cutting.

9. If it is absolutely not possible to weigh a tree, the volume will be calculated from a series of diameter and length measurements and converted to dry mass
   - Diameter should be measured every 1 m
   - At least 2 disks or wedges (3 cm cm thick) will need to be obtained from different points along the stem
   - Measure fresh mass of disk in the field.
   - In the case of semi-direct measurements, these methods will need to be compared to a subsample of direct measurements.
10. Sub-samples to be taken to laboratory:
    - Wood disks from stem: as described above
    - Wood disks from large branches – check lateral variability
    - Small branches

3.B.5 Laboratory work

1. Label samples. In field, label all pieces of the wood samples. Bark may fall off while air drying, so label the bark as well and/or put in a labelled paper bag.
2. Volume of samples.
   - We separated and weighed each tree into the following parts: small branches (< 10 cm diameter, including leaves), large branches (≥ 10 cm diameter), bole (stump to first branch), and stump.
   - Fresh mass was measured directly in field with a 300-kg capacity digital scale with 0.1 kg precision. All irregular boles and boles of D < 70 cm were weighed directly. Larger and non-irregular stems and very large branches were measured

through volume estimation (diameter every 1 m). We measured length, top diameter, and bottom diameter of any hollow sections.

- Measure by displacement: "Accurate water displacement requires immersion of the wood sample into a beaker of water loaded on a top-loading electronic balance. The wood sample is pressed below the water surface with the aid of a "volumeless" needle or insect pin. The volume of the wood is read accurately on the balance as the mass of the displaced water. Older methods of volume displacement in graduated cylinders or beakers where water levels are read by sight are much less accurate and increase variance in volume measurements" (Williamson & Wiemann, 2010).

3. Oven dry samples.
    - Wood samples at 101 °C to 105 °C.
    - Foliar, fruit, and flowers at 60 °C to 70 °C (Williamson & Wiemann, 2010).
    - Dry to constant mass
4. Dry Weight.
    - Remove samples from oven
    - Cool in box with desiccant
5. Save samples.
    - Dry sub-samples will be prepared and stored for analysis of carbon concentration. Sampling will depend on variability of carbon contents, time, and financial resources.

We calculated tree dry mass by two methods: (i) for tree parts which had been directly measured, we calculated dry mass by multiplying fresh mass by dmf; and (ii) for tree parts which had been measured by volume, dry mass was calculated by multiplying volume (minus hollow sections) by WD. We added the estimates from both methods for each tree part and then the complete tree.

3.C TLS data acquisition and Plot sampling design

3.C.1 TLS data acquisition

This LiDAR scanner is a discrete multiple-return laser scanner and its specifications are detailed in the following table. We set up two (virtual) rings around each tree to be

scanned: an inner ring at 6 m from the trunk and an outer ring at 14 m from the trunk. We set up 8 to 10 scan positions between the inner ring and outer ring.

Terrestrial laser scanning RIEGL VZ-400 specifications for wavelength, beam divergence scan range and scan resolution.

Wavelength	1550 nm
Beam divergence	0.35 mrad
Scan range	360° in azimuth
	100° in zenith
Scan resolution	0.04 degree

3.C.2 TLS acquisition protocol

1. Plot delineation.
    - Find tree, label tree.
2. Plot set up
    - Set up inner and outer ring of 8 scan positions.
    - Set up reflector sets + 3 reflectors for tilt.
    - Clean up area low vegetation occluding reflectors view (1 m to 2 m height along the view lines from scan positions to reflectors).
    - Note on field sheet data.
3. GPS
    - Turn on GPS.
    - Save name of position in GPS and field sheet.
    - Save averaged measurements (leave it running, save it at the end before going to new scan position).
4. TLS scanning
    - Set up tripod where the scan position was determined.
    - Set up TLS and plug battery.
    - Find north and orient TLS in Y-axis towards the target tree.
    - Fill field sheet (orientation, position number, tripod height, GPS code).
    - Turn on TLS.

- Scan on upright position.
- Scan on tilt position.
- Turn off TLS.
- Remove TLS from tripod and take it to next scan position.

5. Start again from point 2.
6. Download and backup TLS data
   - Connect TLS to power and to laptop.
   - Copy data to two 2 external hard drives.
   - Delete scans from TLS.

3.C.3 Plot set up and scanning progression within the plot

Once we found the tree, we label the tree (see Figure 3.A1). We set up a total of eight scan positions, four in an inner ring at 6 m from the tree and the other four at 14 m from the tree. We cleared the surrounding vegetation and check that the tree can be clearly seen (specially the crown) at every position.

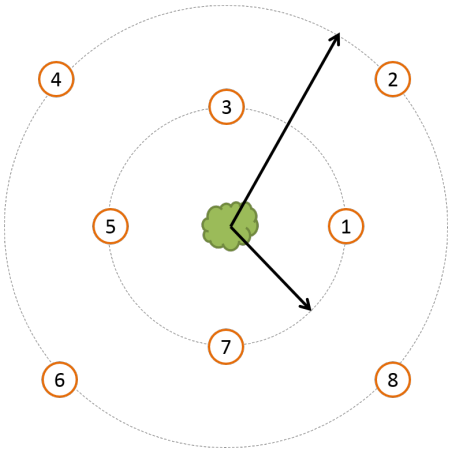

Figure 3.A1

This is the direction that we will follow from the tree (see Figure 3.A2). Choose one point and scan counter-clockwise.

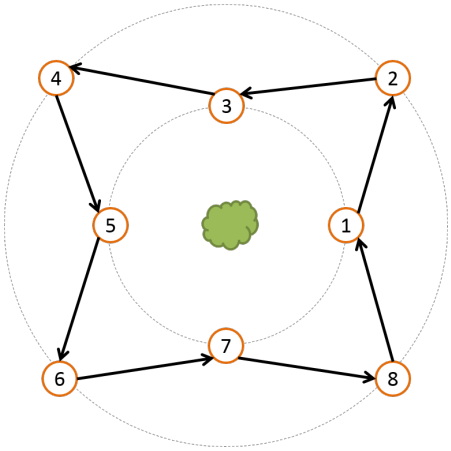

Figure 3.A2

For the first scan, we set up three sets of reflectors: A, B and C (Figure 3.A3, left). We must be careful enough that each set of reflectors is being seen by the other scan position. For example, Set of reflector A has to be seen from scan position 1 and 2. Once the scan finished, we moved to scan position 2 (Figure 3.A3, right). We set up reflector set D and can this position. Then, we move to scan position 3 (Figure 3.A4, left) and move reflector set A and E. We continue following this pattern until we finished the plot (Figure 3.A5 and 3.A6).

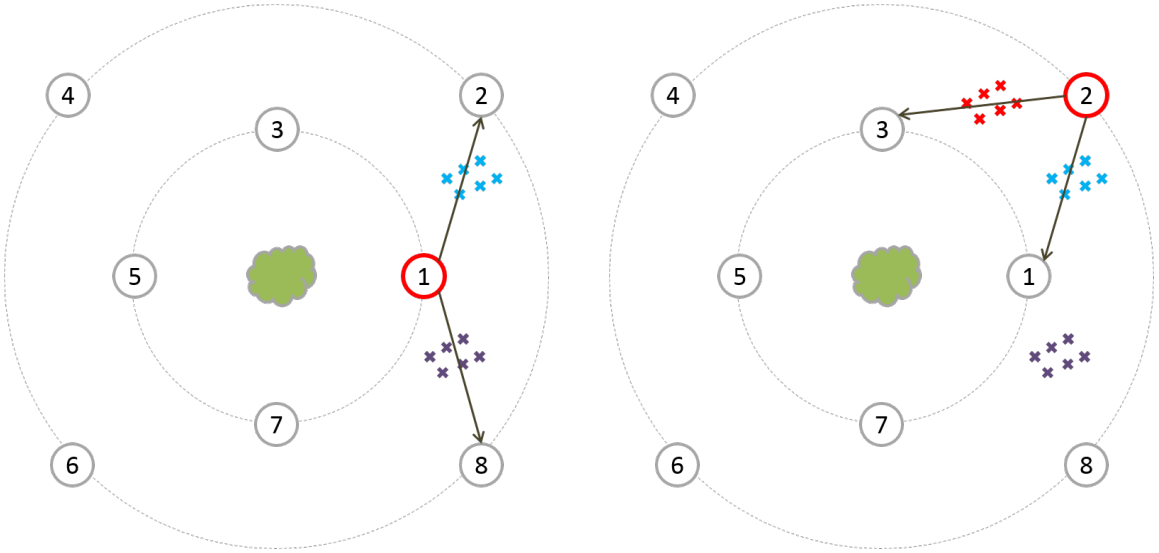

Figure 3.A3

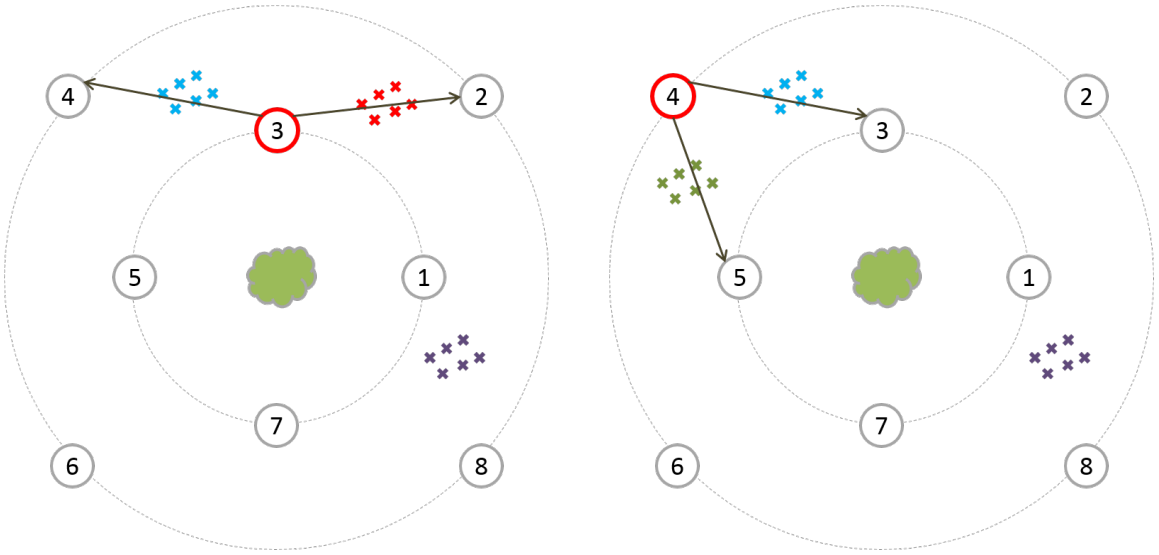

Figure 3.A4

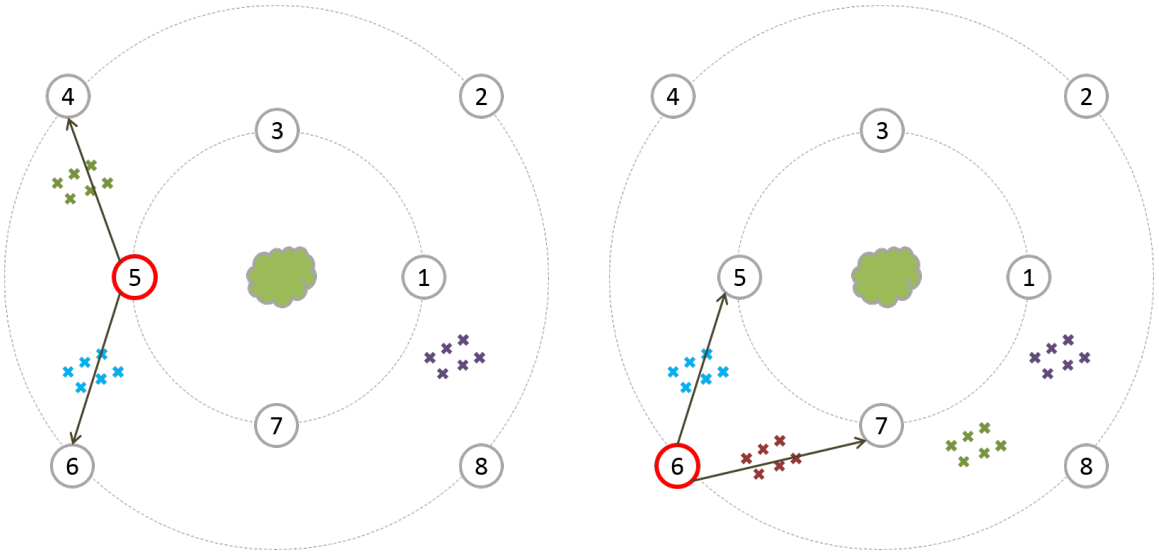

Figure 3.A5

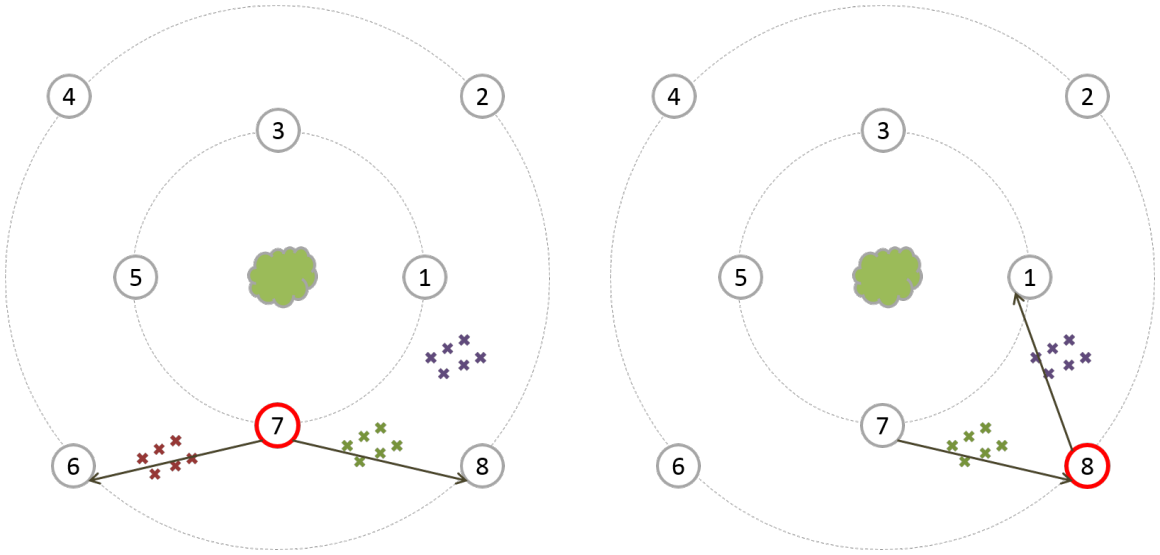

Figure 3.A6

3.C.4 Download data and backup

For each tree, create a folder with the treeID and we copy the number of scans (minimum 16 scans).
Transcribe the field sheet into a word file with the same name of the tree.
Download the GPS data and save it with the treeID.
Download camera pictures and save them in a folder.
After downloading, create copies in external hard drives.

3.D Semi-automated extraction of individual trees from TLS plots

A framework was designed to semi-automated extract individual tree from TLS plots:

a) We co-registered each scan using RiScan Pro Software [RIEGL Laser Measurement Systems GmbH, Horn, Austria, `www.riegl.com`, version 2.5.1] with a registration accuracy below 1 cm (Wilkes et al., 2017). We kept the co-registration files and the individual files as input for the algorithm.

b) For each tree, we extracted a small cross-sectional point cloud. This cross section specifies the location of the tree to the algorithm.

c) The algorithm locates the tree from the ring and creates a point cloud subset which contained the potential tree.

d) We manually cleaned the tree point cloud subset from other features present (such as lianas, stems and canopies from other trees). In addition, we ensure that no branches or canopy parts are missing in the subset. If parts were missing, we manually extracted them from the initial point cloud.

e) Individual trees are down-sampled to a minimum of 1 point per 26 mm^3 to create a uniform point density throughout the whole tree.

f) Finally, material separation algorithm separated hardwood (stem and branches) from soft tissues (leaves) on our down-sampled trees (Vicari, 2017).

3.E Pantropical allometric models

Pantropical models from Chave et al. (2005, 2014) and Réjou-Méchain et al. (2017) included diameter at breast height (D, in cm), specie-specific wood density values according to the GWDD (WD, in $\mathrm{g\,cm^{-3}}$ or $\mathrm{kg\,m^{-3}}$), total height (H, in m), the environmental stress (E, calculated from the GPS average location of each tree (`http://chave.ups-tlse.fr/pantropical_allometry.htm`) to estimate aboveground biomass (AGB, in kg dry mass) and ε is the model error.

Model	Form $AGB =$
Ch05.II.3	$WD \cdot \exp[-1.499 + 2.1481 \cdot \log(D) + 0.207 \cdot \log(D)^2 - 0.0281 \cdot \log(D)^3] + \varepsilon$
Ch05.I.5	$0.0509 \cdot WD \cdot D^2 \cdot H + \varepsilon$
Ch14.H	$0.0673 \cdot (WD \cdot D^2 \cdot H \cdot)^{0.976} + \varepsilon$
Ch14.E	$\exp[-1.803 - 0.976 \cdot E + 0.976 \cdot \log(WD) + 2.673 \cdot \log(D) - 0.0299 \cdot \log(D^2)] + \varepsilon$
Rj17.E	$\exp[-2.024 - 0.896 \cdot E + 0.920 \cdot \log(WD) + 2.795 \cdot \log(D) - 0.0461 \cdot \log(D^2)] + \varepsilon$

3.F TLS-derived allometric model assumptions

We used a t-paired test to analyse whether the TLS-derived parameters had a significant difference compared to our post-harvested field measurements. If TLS and field-based measurements differed significantly, a calibration factor was applied to the input parameter.

We also tested whether there were significant differences between models built using field measurements or TLS-derived data. We built models using both sets of data with data source as a dummy variable. When the dummy variable was significant, we applied its parameter estimate (Reference Dummy Variable Corrector; RDVC) to the corresponding model form to modify the TLS built models.

We removed insignificant parameters using backwards stepwise regression to produce a minimum adequate model. We tested assumptions of the final models. We tested for normal distribution of the residuals using Q-Q plots and Anderson-Darling test, Durbin-Watson test to assess independence, and plots of residuals against fitted values to assess homogeneous variance and linearity.

3.G Tree point cloud dataset

Tree point clouds of the TLS dataset by diameter size class and coloured by height. Tree dataset comprises 72 TLS scanned trees and 26 harvested trees from 48 different species in 24 different families with diameter ranging from 12.9 cm to 149.8 cm and heights ranging from 6.33 m to 49.2 m.

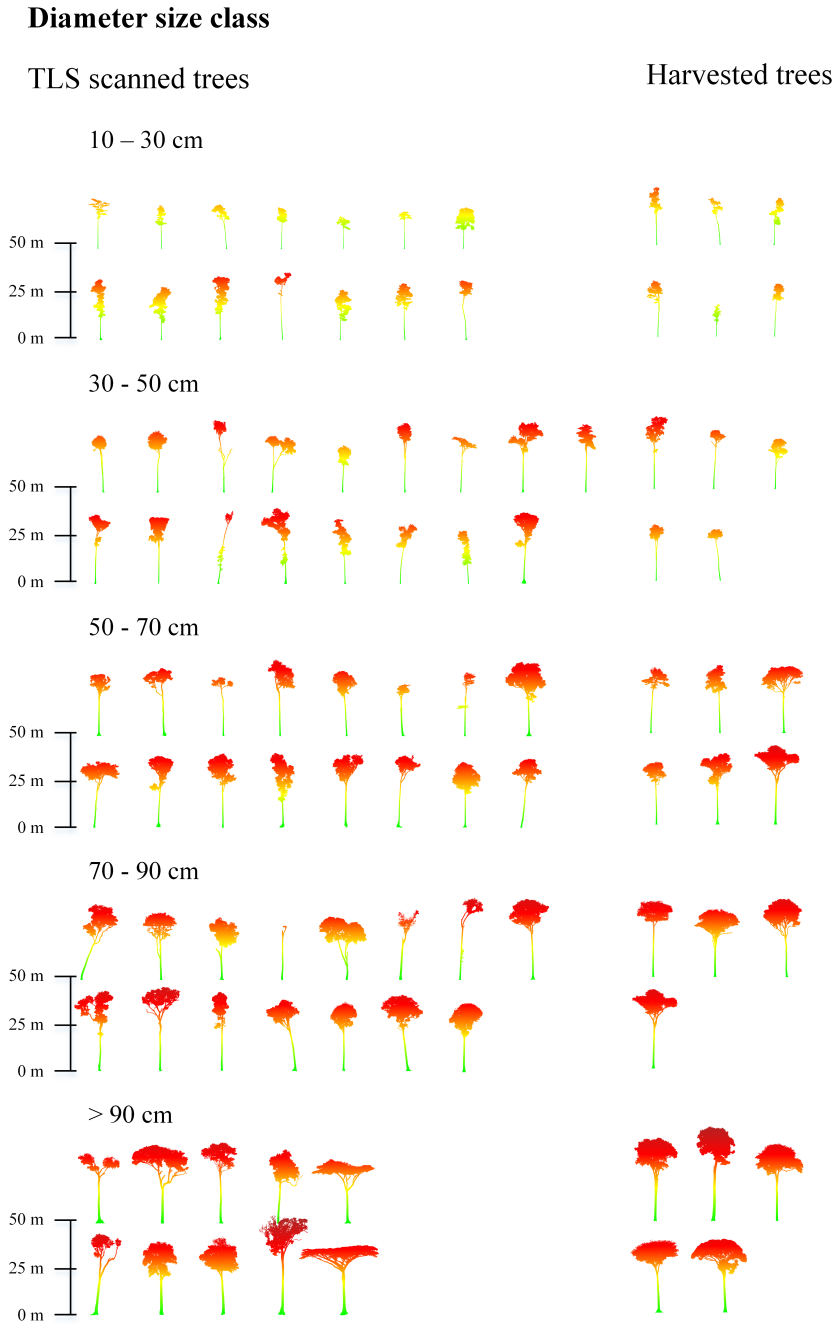

3.H Wood density values for field inventory and destructive sampling

Wood density from field inventory (GWDD) and destructive sampling (weighted) from 72 and 26 trees respectively.

Diameter class (cm)	Field inventory ($n = 72$)				Destructive sampling ($n = 26$)			
	n	min	max	mean	n	min	max	mean
$10 \leq$ DBH < 30	14	0.520	0.971	0.756	6	0.561	0.836	0.711
$30 \leq$ DBH < 50	17	0.378	0.971	0.777	5	0.384	0.908	0.634
$50 \leq$ DBH < 70	16	0.484	0.971	0.760	6	0.421	0.857	0.713
$70 \leq$ DBH < 90	15	0.524	0.862	0.733	4	0.627	0.852	0.706
DBH ≥ 90	10	0.390	0.862	0.627	5	0.408	0.808	0.635

3.I Residuals vs fitted and Q-Q plots for models m4 and m5

TLS-derived allometric model m4 (top) and m5 (bottom) residual vs fitted (left) and Q-Q plots (right) graphs.

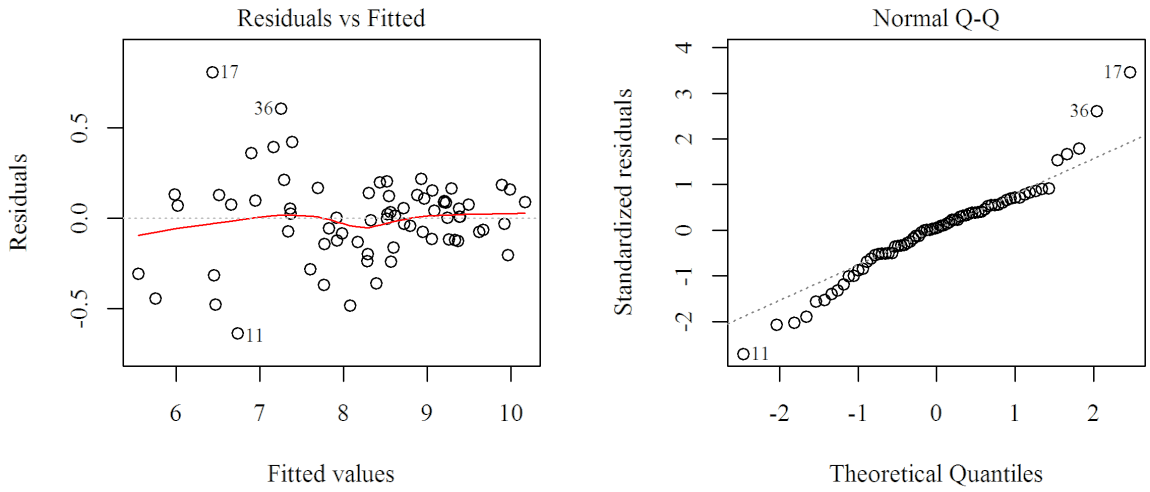

Figure a: Model m4

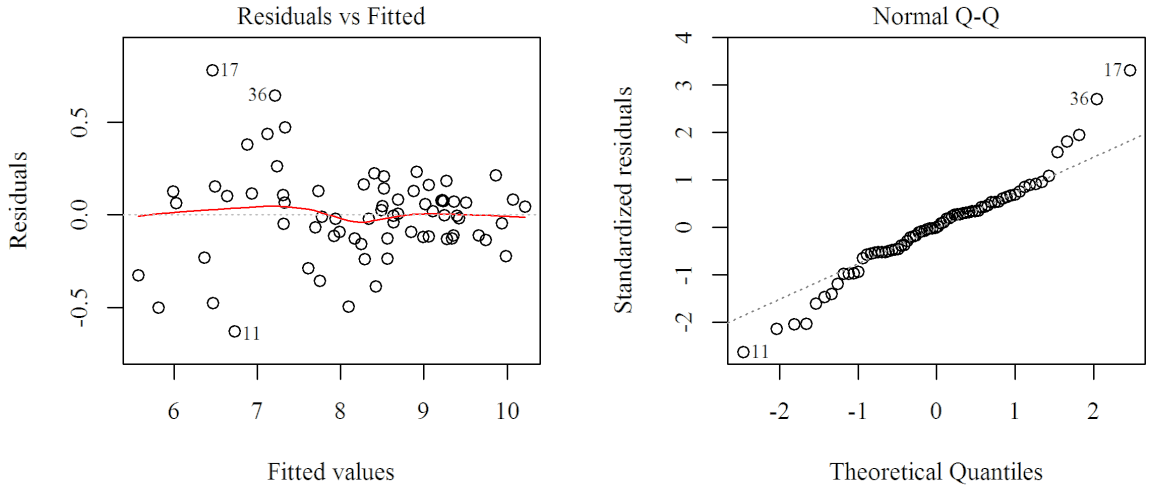

Figure b: Model m5

3.J Summary of statistics for small and large trees

Table 3.A1: Summary of AGB estimates from TLS-derived and pantropical allometric models —R^2, RMSE, CCC, sum of errors (sum, mean, standard deviation [SD]), mean percent error and relative error ($n = 26$) separated in small trees (D $\leq$ 70 cm) and large trees (D $>$ 70 cm). Models are arranged based on the statistical parameters from the best model to the worst model.

Model	Type	R^2		RMSE		CCC		Sum Error (Mg)	
		small	large	small	large	small	large	small	large
m5	D.WD.CD	0.83	0.84	1.27	2.69	0.87	0.90	0.50	0.53
m4	D.WD.H.CD	0.83	0.81	1.22	2.89	0.89	0.89	1.23	0.13
Ch05.II.3	WD.D.D^2.D^3	0.70	0.78	1.57	3.30	0.79	0.86	−3.61	−3.88
Ch05.I.5	D^2.WD.H	0.76	0.67	1.40	4.25	0.84	0.79	−1.95	−7.91
Ch14.H	(D^2.WD.H)	0.75	0.67	1.41	4.11	0.84	0.79	−1.45	−10.44
m1	D	0.74	0.59	1.55	3.71	0.81	0.76	10.81	2.84
Rj17.E	D.D^2.WD.E	0.70	0.77	1.65	3.45	0.75	0.85	−6.72	−12.55
Ch14.E	D.D^2.WD.E	0.70	0.77	1.68	3.55	0.74	0.84	−7.45	−14.11
m3	D.WD.H	0.67	0.74	1.67	4.39	0.75	0.72	−2.66	−29.45
m2	D.WD	0.64	0.77	1.90	4.30	0.76	0.81	14.30	17.91

Table 3.A1: *(continued).*

Model	Mean error (Mg)		SD error (Mg)		Mean rel. error (%)		SD. rel. erro (%)	
	small	large	small	large	small	large	small	large
m5	0.03	0.06	1.31	2.86	44.08	0.11	70.75	22.73
m4	0.08	0.01	1.26	3.07	44.29	−0.04	65.74	23.30
Ch05.II.3	−0.21	−0.43	1.60	3.47	10.71	−4.22	57.51	22.36
Ch05.I.5	−0.11	−0.88	1.44	4.42	15.26	−7.57	47.45	24.95
Ch14.H	−0.09	−1.16	1.45	4.19	19.54	−9.21	48.42	23.74
m1	0.64	0.32	1.46	3.92	99.92	7.74	118.63	26.22
Rj17.E	−0.40	−1.39	1.65	3.34	3.61	−11.50	52.33	20.40
Ch14.E	−0.44	−1.57	1.67	3.37	1.39	−13.08	51.60	20.94
m3	−0.16	−3.27	1.71	3.11	35.20	−23.72	65.90	19.41
m2	0.84	1.99	1.75	4.04	105.06	14.74	109.05	28.47

3.K Mean error estimates for allometric models in Mg

Mean error in estimates (estimated AGB minus reference AGB in Mg) by DBH size class: small trees (D $\leq$ 70 cm; $n = 17$) and large trees (D $>$ 70 cm; $n = 9$) for the TLS-derived allometric models and pantropical models.

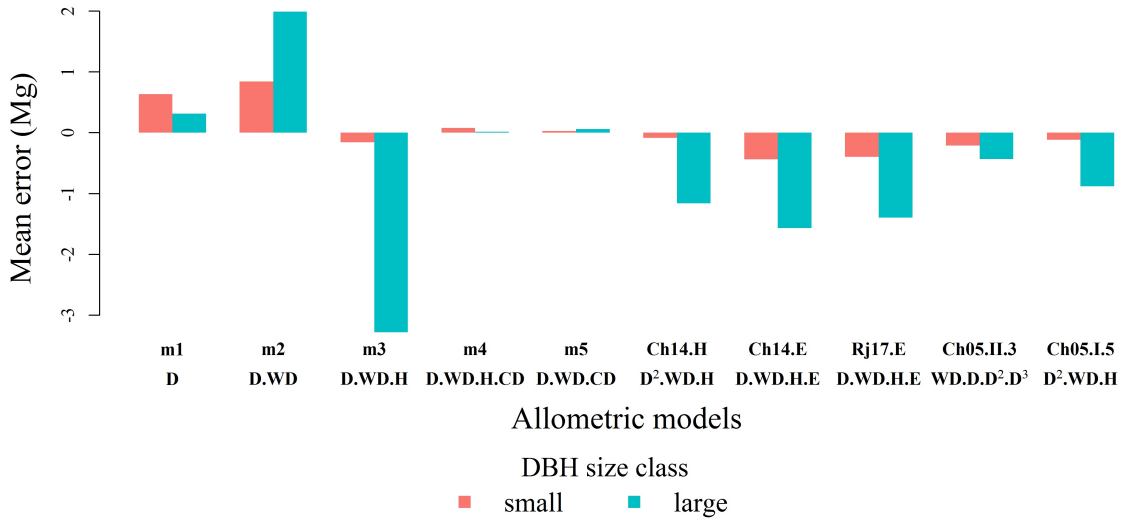

East Berbice-Corentyne, Guyana

Chapter 4

Quantifying branch architecture of tropical trees using terrestrial LiDAR and 3D modelling

This chapter is based on:

Lau, A., Bentley, L.P., Martius, C., Shenkin, A., Bartholomeus, H., Raumonen, P., Malhi, Y., Jackson, T. and Herold, M. (2018). Quantifying branch architecture of tropical trees using terrestrial LiDAR and 3D modelling. *Trees*. 2018, 1-12. DOI: 10.1007/s00468-018-1704-1

Supplementary materials to this chapter can be found in the online publication.

Abstract

Tree architecture is the three-dimensional arrangement of aboveground parts of a tree. Ecologists hypothesize that the topology of tree branches represents optimized adaptations to tree's environment. Thus, an accurate description of tree architecture leads to a better understanding of how form is driven by function. Terrestrial laser scanning (TLS) has demonstrated its potential to characterize woody tree structure. However, most current TLS methods do not describe tree architecture. Here, we examined nine trees from a Guyanese tropical rainforest to evaluate the utility of TLS for measuring tree architecture. First, we scanned the trees and extracted individual tree point clouds. *TreeQSM* was used to reconstruct woody structure through 3D quantitative structure models (QSMs). From these QSMs, we calculated: 1) length and diameter of branches > 10 cm diameter, 2) branching order and 3) tree volume. To validate our method, we destructively harvested the trees and manually measured all branches over 10 cm (279). *TreeQSM* found and reconstructed 95 % of the branches thicker than 30 cm. Comparing field and QSM data, QSM overestimated branch lengths thicker than 50 cm by 1 % and underestimated diameter of branches between 20 cm and 60 cm by 8 %. *TreeQSM* assigned the correct branching order in 99 % of all cases and reconstructed 87 % of branch lengths and 97 % of tree volume. Although these results are based on nine trees, they validate a method that is an important step forward towards using tree architectural traits based on TLS and open up new possibilities to use QSMs for tree architecture.

4.1 Introduction

Tree architecture can be defined as the three-dimensional arrangement of the organs of a tree. This arrangement includes the size and spatial arrangement of branches, leaves and flowers (Reinhardt & Kuhlemeier, 2002) and can be defined by specific morphological traits (Rosati et al., 2013). Tree architecture is a consequence of genetics and chance. Genetics encode an adaptation of tree form and function to its surroundings with respect to both biotic and abiotic factors such as competition for space, differential resource distribution (e.g., light), and support and safety against mechanical forces (e.g. gravity or wind) (Chéné et al., 2012; Dassot et al., 2010). Chance includes stochastic processes such as wind damage and damage to neighbours. Tree architecture directly influences biophysical processes, such as photosynthesis and evapotranspiration (Rosell et al., 2009; Van der Zande et al., 2006), ultimately leading to changes in carbon and water storage. The West, Brown and Enquist (WBE) model (West et al., 1997; West, 1999a) uses the fractal-like architecture of branching networks as a building block to predict how metabolism scales with body size and structure in a simplified and generalized way (West et al., 1997; West, 1999a). Within the context of the WBE theory, tree architectural traits can be used to understand and explore specific links among, for example, tree height, biomass, diameter, growth and mortality (Bentley et al., 2013; Kempes et al., 2011; West, 1999b; West et al., 2009). Thus, an accurate description of the architecture of trees can play a key role in understanding tree-level and plot-level processes (Kempes et al., 2011; Rosati et al., 2013).

Previous studies have described the architecture of tropical trees (Hallé et al., 1978; Hallé & Oldeman, 1970) with the goal of qualitatively classifying tree forms. Standardized structural assessment of forest canopies or individual trees have been developed, but these assessments are based on subjective methods that do not allow a quantitative comparison (Van der Zande et al., 2006) and generate a limited number of attributes that can be readily obtained with non-destructive methods (Henning & Radtke, 2006). Studies have quantitatively described tree architectural traits, but are limited due to the intensity of manual labour needed to sample large numbers of trees with enough detail (Bentley et al., 2013; Dassot et al., 2010). In light of these limitations, here we propose another way forward to characterize tree architecture: terrestrial LiDAR (light detection and ranging; Dassot et al., 2012) combined with a 3D quantitative structure model (*TreeQSM*; Raumonen et al., 2013).

Terrestrial LiDAR, also known as terrestrial laser scanning (TLS), is a valuable tool to assess the woody structure of trees (Holopainen et al., 2011; Calders et al., 2015b; Gonzalez de Tanago et al., 2017). In the field, a forest plot is scanned from multiple locations, which are later co-registered into a point cloud to which 3D tree models can be fitted (Raumonen et al., 2013; Hackenberg et al., 2014) and from which structural parameters can then

be extracted in an objective and consistent way (Calders et al., 2015b; Pueschel et al., 2013). A tree point cloud is an uninterpreted collection of data and the actual structural information cannot be directly extracted (Bremer et al., 2013). To derive the structural parameters from tree point clouds, several approaches have been developed (Pfeifer et al., 2004; Thies et al., 2004; Dassot et al., 2012; Raumonen et al., 2013; Hackenberg et al., 2014). Among these, *TreeQSM* - a 3D quantitative structure model (QSM) reconstruction method - has been recognized as a promising tool for topological and structural assessment of individual trees (Raumonen et al., 2013; Calders et al., 2015b; Gonzalez de Tanago et al., 2017). *TreeQSM* splits the tree point cloud into segments and then reconstructs the whole tree topological structure by fitting cylinders to each segment (Raumonen et al., 2013; Gonzalez de Tanago et al., 2017). From each segment, we are able to calculate surface and volume (Gonzalez de Tanago et al., 2017) and reconstruct topology. The output, a QSM, is a hierarchical collection of cylinder which closely resemble the tree point cloud in shape. More details regarding the mechanics of *TreeQSM* can be found in Åkerblom (2017); Calders et al. (2015b); and Gonzalez de Tanago et al. (2017).

TLS, in combination with *TreeQSM*, has proven to be an accurate method to estimate direct tree parameters such as tree height (Burt et al., 2013; Krooks et al., 2014), diameter at breast height (D), trunk and branch volumes (Burt et al., 2013); and even indirect and complex parameters such as biomass (Calders et al., 2015b) and changes in tree biomass (Kaasalainen et al., 2014). Tree structure modelling with *TreeQSM* was also successfully employed for automatic species recognition as in Åkerblom et al. (2017). However, most studies so far have focused on measuring total tree volume as the only validation method for this approach (Burt et al., 2013; Calders et al., 2015b; Gonzalez de Tanago et al., 2017). Moreover, previous studies using TLS have mostly focused on temperate trees in their leafless condition and with a comparatively low canopy height (Burt et al., 2013; Dassot et al., 2010; Hackenberg et al., 2014; Holopainen et al., 2011; Kaasalainen et al., 2014; Krooks et al., 2014; Pueschel et al., 2013; Seidel et al., 2012) (but see Wilkes et al. (2017); Gonzalez de Tanago et al. (2017); and Momo Takoudjou et al. (2018) for tropical forests). Scanning tropical trees is more difficult due to the complex forest layers with evergreen species which lead to occlusion in the under story, frequently changing weather conditions and logistical challenges (such as scanner settings, hardware requirements, distance to plot, plot area; Wilkes et al., 2017).

Because quantitative measurements of tree architecture in the tropics are needed, this paper assessed whether tree architecture can be reconstructed using TLS and *TreeQSM*. Specifically, we aimed to: (i) reconstruct tree architecture scanned with TLS using *TreeQSM*, (ii) validate individual branch lengths, branch diameters and branching orders with field reference measurements taken manually, and (iii) provide guidelines for future studies endeavouring to reconstruct tree architecture using TLS and QSMs.

4.2 Material and methods

4.2.1 Study area and plot design

Field data were collected in Vaitarna Holding's forest concession in the tropical forest of central Guyana during November 2014. Nine plots were established in a lowland tropical moist forest located between 6°2′2.4″N 58°41′56.4″W and 6°2′20.4″N 58°41′38.4″W. The field study had a mean elevation of 117 meters above sea level and mean precipitation of 2195 mm yr^{-1} (Muñoz & Grieser, 2006). Tree selection was based on its harvestable diameter and its suitability for harvesting. We located nine suitable trees for harvesting. A local experienced taxonomist identified the trees, and the local names were later matched with scientific names (Miller & Détienne, 2001). A total of seven *Eperua grandiflora*, one *Ormosia coutinhoi* and one *Eperua falcata* were harvested.

In each plot, the selected tree was located and a 30 x40 m grid subplot (Online Resource 1 and Figure OR1.1) was established around it. The origin of the local coordinate system was located at bottom left corner of the plot (bottom left red sun cross in Figure OR1.1). The selected tree was located at 15 m East and 5 m North from the origin and a total of thirteen scan locations were set up in the plot (sun crosses in Figure OR1.1), whereas the y-axis was parallel to the expected felling direction. Each plot was scanned with TLS and then the focal tree was felled and detailed measurements were taken.

4.2.2 TLS data acquisition

TLS data were acquired using a RIEGL VZ-400 V-Line 3D© terrestrial laser scanner [RIEGL Laser Measurement Systems GmbH, Horn, Austria, <www.riegl.com>]. The RIEGL VZ-400 is a discretized multiple-return LiDAR with a 1550 nm wavelength and a beam divergence of 0.35 mrad (Wilkes et al., 2017; Gonzalez de Tanago et al., 2017). The beam scan range is 360° in the azimuth and 100° in the zenith direction. In this study an angular resolution of 0.06° was used. To co-register each scan, 5-cm cylindrical reflecting targets (tie-points) were distributed throughout the plot, in such a way that they were scanned from several positions. In total, thirteen scan locations were set up in each plot using 60 reflectors. The average distance between scan locations was 17.5 m. These tie-points were later used to register multiple individual point clouds into one unified point cloud (Gonzalez de Tanago et al., 2017; Wilkes et al., 2017).

4.2.3 Manual measurements from harvested trees

After each tree was harvested, the geometrical structure of the main stem and branches with a diameter of > 10 cm was manually measured with a 1 cm precision forestry tape.

Buttresses were assumed to be cylindrical in order to enable comparison with 3D models. To homogenize the measurement process on the harvested trees (Figure 4.1), we defined a "branch node" as the furcation point over a tree segment where another tree segment originates. From an ecological point of view, a "branch" is referred to the lateral axis from the axillary meristems which begin in the axils of the leaves (Reinhardt & Kuhlemeier, 2002). In this study, we referred to "branch" as the tree segment which originates from a furcation point and terminates either:

- when the tree segment begins to widen into another furcation point (specially noticed on the main stem),
- when the tree segment reaches 10 cm diameter, or
- when the tree segment ends or is broken.

For each branch, we measured two parameters: length and diameter. We defined "branch length" as the distance between the base furcation point and the termination point of the branch, and "branch diameter" as the average of the diameter taken over the base furcation point and the diameter taken below the termination point of the branch. In addition, a unique BranchID was labelled to each measured branch for identification. For "branching order", we adapted a similar coding strategy as used in Gaaliche et al. (2016). We determined the relative branching order centrifugally as shown in Figure 4.1, beginning from the tree main stem. The main stem was considered as "first branching order", then the branches originated from the first furcation were considered as "second branching order", then the branches originated from this second furcation were considered as "third branching order" and continuing by adding another branching order on each furcation as in Figure 4.1. More details on how we determined branching order for this study can be found in Online Resource 2. Finally, the "parent branch" was defined as the tree segment on which another tree segment was originated and shared the same branch node as shown in Figure 4.1. We recorded the branch length, branch diameter, branching order and parent branch relative to each branch until they reached 10 cm diameter.

4.2.4 Tree architecture reconstruction

Our reconstruction procedure had three components: (i) manual tree extraction from the registered point cloud, (ii) 3D reconstruction of individual tree point clouds using *TreeQSM*, and (iii) individual analysis of QSM branches via manual branch-by-branch pairing. First, to manually extract an individual tree from the point cloud of the entire plot, a framework was designed:

1. Individual point cloud scans were co-registered into a plot point cloud using RiScan Pro software [RIEGL Laser Measurement Systems GmbH, Horn, Austria, `<www.riegl.com>`, version 2.0]. The achieved accuracy of our co-registration process was

below an average of 1 cm per plot.

2. The main stem and canopy of each harvested tree were located in the registered point cloud.

3. From a top view, a bounding box which enclosed the harvested tree was created. The bounding box limits were defined by the area of the canopy.

4. The point cloud containing the harvested tree inside the bounding box was extracted.

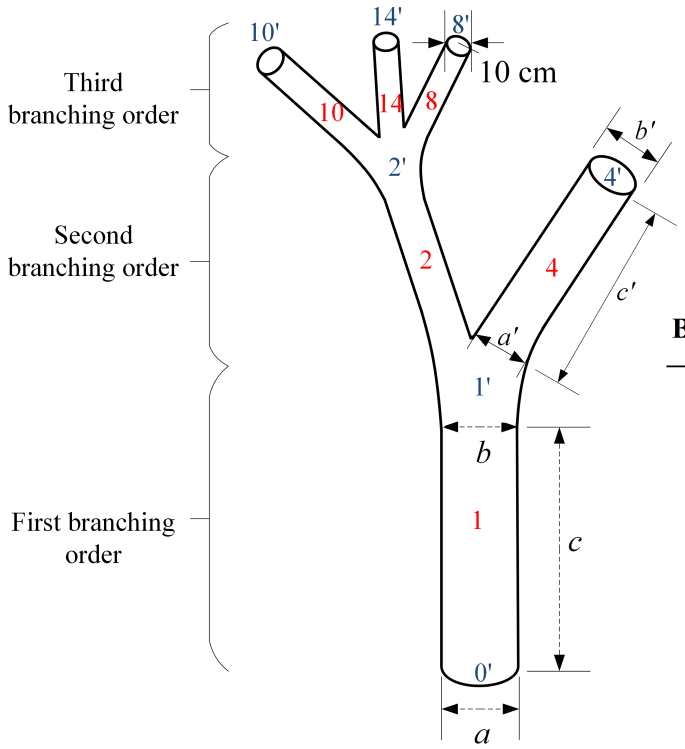

BranchID	Node	Parent branch	Branching order
1	0'	0	1
2	1'	1	2
4	1'	1	2
8	2'	2	3
10	2'	2	3
14	2'	2	3

Figure 4.1: Diagram of manual measurements from a harvested tree. A "branch node" is the furcation point over a tree segment where another tree segment originates (0', 1', 2'). Then, we defined a "branch" as the tree segment which originates from a furcation point and terminates either: when the tree segment begins to widen into another furcation point (1'), when the tree segment reaches 10 cm diameter (8'), or when the tree segment ends or is broken (4', 10', 14'). "Branch length" was defined as the distance between the base furcation point and the termination point of the branch (*c* and *c'*) and "branch diameter" as the average of the diameter taken over the base furcation point (*a* and *a'*) and the diameter taken below the termination point of the branch (*b* and *b'*). In addition, a unique BranchID was labelled to each branch for identification. We labelled each parent branch, i.e. BranchID 2 and BranchID 4 had the same parent branch (BranchID 1), while BranchID 8, BranchID 10 and BranchID 14 shared the same parent branch (BranchID 2). The branching order was determined relative to the main stem and given centrifugally by the furcations originated on each branch.

5. Features that were not related to the harvested tree, such as lianas, stems and canopies from other trees were manually removed.

6. In addition, visual inspection was performed to ensure that no branches or canopy parts were missing in the subset. Missing parts were manually copied from the entire plot point cloud and merged with the individual tree point cloud.

Once the individual tree point clouds were extracted, cylindrical models were fitted to those point clouds using *TreeQSM* (Raumonen et al., 2013; Calders et al., 2015b; Gonzalez de Tanago et al., 2017). In this paper, *TreeQSM* version 2.2.1 was used (a later version is available and functions in a similar way). Reconstructing trees using *TreeQSM* is semi-automatic and requires the input of a few parameters. *TreeQSM* partitions the point cloud into small connected surface patches and then uses them to reconstruct each segment of the tree. Then, cylinders are fitted to the segments and geometric and topological features are obtained (Raumonen et al., 2013). The most important input parameter is the diameter (d) that defines the size of the surface patches. Furthermore, the partition into patches is random and thus repeating the reconstruction always results slightly different QSMs, even if all inputs are the same. To assess the robustness of the d parameter, previous works (Calders et al., 2015b; Gonzalez de Tanago et al., 2017) have focused on optimizing total volume and not the detailed structure of tree branches. They produced several models for each case and calculate the mean and standard deviation from these repetitions. To choose the most robust value of d we:

1. Fitted 10 QSMs of three random trees using values for the d parameter ranging from 0.05 to 0.5 at a 0.05 increment.

2. Visually inspected each QSM for each d value, as described in Calders et al. (2015b). The best d value was heuristically determined based on the visual inspection.

Based on the visual inspection, *TreeQSM* produced the most visually accurate models for tree architecture when d was set to 0.1. Nevertheless, we decided that quantitative measures of fit were necessary. Once the point clouds had been transformed into cylindrical models, we continued to the final step of analysing individual QSM branches as follows:

1. Each TLS tree point cloud was reconstructed 20 times using d set to 0.1.

2. The *TreeQSM* simplification algorithm was performed to obtain simplified QSMs outputs (Tobias Jackson, personal communication, May 17, 2017). This simplification method is also available with the latest version of *TreeQSM*. This simplification algorithm specifies that:

    - QSMs cylinders with a diameter $< 10\,\text{cm}$ are removed to be comparable with our manual measurements dataset and to minimize the possibility of including lianas.

- QSMs cylinders with a radius less than or equal to 1/3 of its parent radius are removed to eliminate very small artefact cylinders.

3. Each QSM branch was split at each branch node, since the original *TreeQSM* did not split QSM branches at each branch node (See Online Resource 2 and Figure OR2.1).
4. The branching order of the QSMs was arranged to add a level at every branch node (See Online Resource 2 and Figure OR2.1).
5. All 20 repetitions were ranked using a quantitative scale based on visual inspection (Online Resource 3) and the seven most accurate models were saved for further analyses.

Finally, the geometrical structure and branching order from the QSMs were reconstructed following the measurements from the harvested trees (Figure 4.2). A QSM branch node was defined as a QSM cylinder from which two or more cylinders are originated. This cylinder defined the termination of a QSM branch and the following cylinders are the origin of new QSM branches. Then, we defined a QSM branch as a collection of consecutive QSM cylinders which originate from a QSM branch node and terminates either:

- on another QSM branch node,
- when a QSM cylinder reaches 10 cm diameter, or
- when the QSM branch ends

The QSM branch length was estimated as the sum of the length of all cylinders belonging to the QSM branch and the QSM branch diameter was estimated as the average of the first and last cylinder belonging to the QSM branch.

4.2.5 Visual branch-by-branch pairing

The manually measured tree and QSM tree were visually paired branch-by-branch. The architecture of the manually measured tree was followed and each individual manually measured branch was located and identified. Then, we visually paired the measured branch with a QSM branch following the architecture of the QSM tree. Manually measured branches which did not have a QSM pair at all were excluded for further analysis. In the case that a manually measured branch was a suitable pair to two or more QSM branches, the similarity of each QSM branch with their manually measured counterpart was analysed. The length and diameter of each QSM branch were the parameters used to analyse quantitatively the similarity of branches. Because length and diameter had different orders of magnitude (one order of magnitude difference in length parameter is a hundred order of magnitude difference in branch diameter), we could not compare them using Euclidian distance. To overcome this, a special type of Euclidian distance,

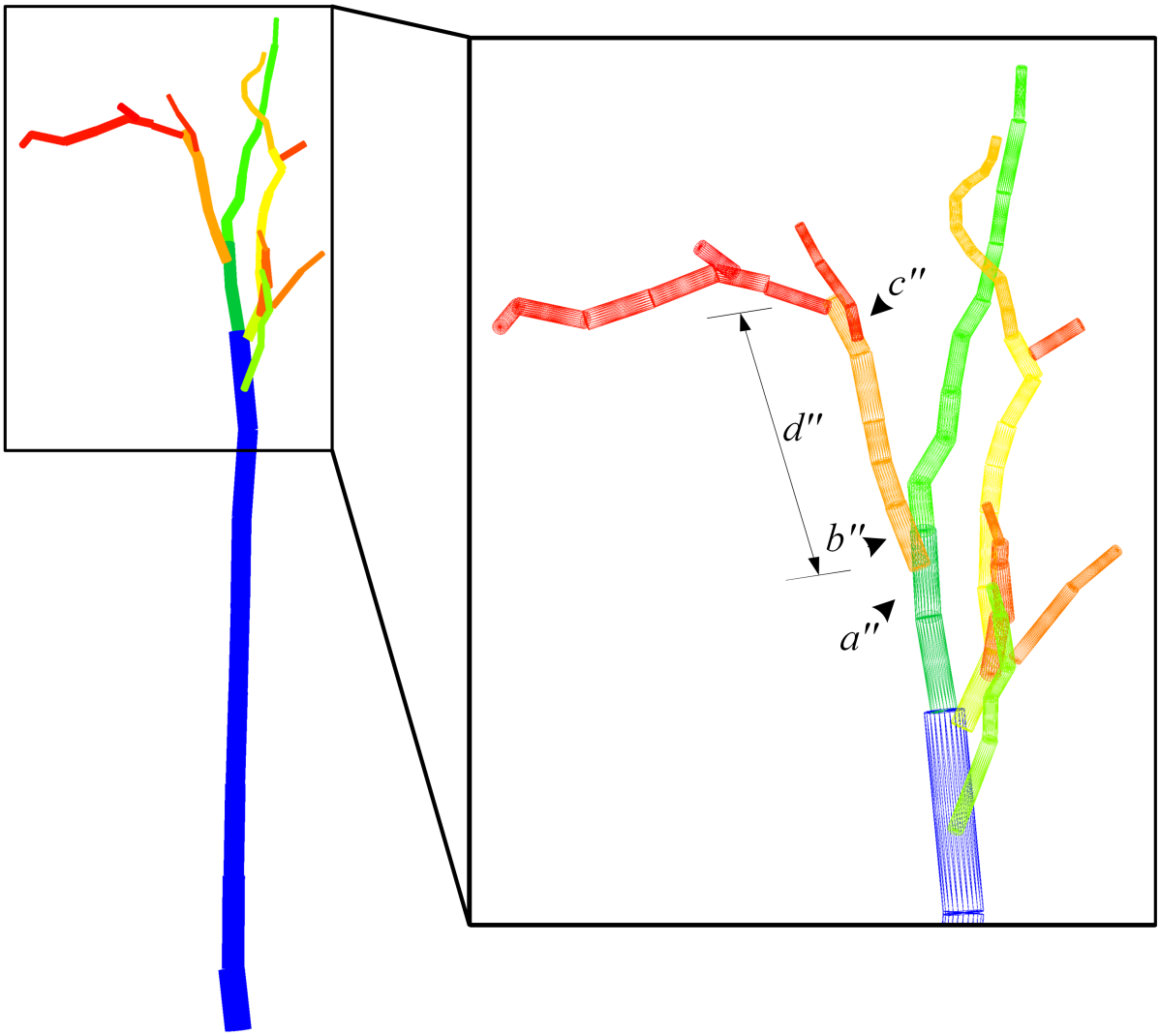

Figure 4.2: Diagram of QSM reconstruction. QSMs cylinders with a diameter $< 10\,\text{cm}$ were removed. Different colours depict different QSM branches. A branch node is a QSM cylinder from which two or more cylinders are originated (dark green *a"* cylinder and orange *c"* cylinder). These cylinders are also the termination of their respective QSM branches. An orange QSM branch started from *b"* cylinder and terminated on *c"* cylinder. The QSM branch length *d"* was calculated as the sum of the length of the consecutive cylinders from the orange QSM branch and the QSM branch diameter was calculated as the average of the first cylinder (*b"*) and the last cylinder (*c"*) diameters. Please refer to the digital version for colour image.

the Diagonal-norm approach (Bezdek, 1981) was applied. The diagonal-norm approach computed standardized values for both parameters and allowed us to compare them quantitatively in the same order of magnitude. Then, the QSM branch most similar to the manually measured branch in standardized length and standardized diameter was chosen as the best fitted pair.

4.2.6 Tree metrics assessment

We examined the absolute and relative error to evaluate branch length and diameter accuracy per individual paired branch. A confusion matrix was used to validate the accuracy of our branching order method when compared to our manual measured dataset. Finally, the relative error was used to compare the cumulative length and the cumulative branch volume of total branches (as the aggregation of all paired branches) and separated by diameter classes. The cumulative branch length was calculated as the sum of branches' length per cumulated diameter class. Likewise, the cumulative branch volume was calculated as the total sum of branches' volume per cumulated diameter class. The length and mean diameter values of each branch were used to calculate branch volume.

4.3 Results

4.3.1 Manual measurements from trees

The D of the nine trees harvested ranged from 61.3 cm up to 97 cm and the total tree height ranged from 18.8 m up to 29.9 m. We collected and manually measured 279 branches up to diameter > 10 cm and the highest branching order recorded was 8 (Table 4.1).

Table 4.1: Local name, scientific name, D, tree height, number of branches measured and branching order for the nine trees harvested in this study.

Tree	Local name	Scientific name	Tree diameter (cm)	Tree height (m)	Measured branches	Branching order
1	Wallaba ituri	*E. grandiflora*	89.3	25.4	39	8
2	Wallaba ituri	*E. grandiflora*	61.3	18.8	23	6
3	Wallaba ituri	*E. grandiflora*	66.0	22.2	23	5
4	Wallaba ituri	*E. grandiflora*	68.7	29.6	30	6
5	Wallaba ituri	*E. grandiflora*	72.7	28.8	26	5
6	Wallaba ituri	*E. grandiflora*	97.0	29.2	32	7
7	Wallaba ituri	*E. grandiflora*	82.6	27.0	20	6
8	Korokororo	*O. coutinhoi*	76.0	29.8	54	7
9	Wallaba soft	*E. falcata*	65.5	29.9	32	8

4.3.2 Pairing individual QSM branches with manually measured branches

We needed to pair one measured tree with the seven most accurate QSMs. To cope with this, we compared seven times the measured branches with the seven most accurate QSMs. Thus, a total of 279 manually measured branches were compared seven times (a total of 1953 branches were compared) and expected to pair with QSM branches. *TreeQSM* was able to find all measured branches at least once within the seven repetitions. However, only 1149 QSM branches paired, a 59 % success rate (Table 4.2). *TreeQSM* was able to reconstruct more than 95 % of the branches thicker than 30 cm. These branches were mostly the main stem and big branches. However, the reconstruction accuracy decreased for thinner branches (which usually have also lower point cloud density). *TreeQSM* reconstructed less than 56 % of the branches with diameter measured between 10 cm to 30 cm.

Table 4.2: Manually measured branches and the average and standard deviation of the most accurate QSM branches with *TreeQSM* (7 repetitions) by diameter classes. Accuracy shows the percentage of manually measured branches successfully reconstructed by *TreeQSM*. Our analysis was based only using QSM branches that could be paired with a manually measured branch.

Diameter class (cm)	Measured branches	Average of QSM branches	Accuracy (%)
10–20	160	72.29 ± 13.03	45
20–30	67	44.86 ± 7.27	67
30–40	26	21.86 ± 9.14	84
40–50	11	10.14 ± 3.93	92
50–60	7	7	100
60–70	5	5	100
≥ 70	3	3	100

4.3.3 Branch length from QSMs

We analysed the performance of *TreeQSM* by comparing the length of QSMs branches against the length of our manually measured branches and calculating the absolute error difference between diameter classes (Table 4.3 and Figure 4.3a). For average length values per classes, refer to Table OR4.1 in Online Resource 4. For branches greater than 50 cm diameter, the length of QSMs branches was overestimated by 1 % (0.21 m larger on average than the manually measured branches). *TreeQSM* had lower accuracy reconstructing length for branches smaller than 50 cm diameter. The length of QSM branches was

underestimated by 20 % (0.58 m shorter on average) when compared to its measured counterpart.

Table 4.3: Average absolute error and average relative error for QSM branches by diameter classes. Our analysis was based on the QSM branches which paired a manually measured branch. Negative values indicated a model underestimation while positive values indicate a model overestimation compared to the manually measured branches.

Diameter	Absolute error and SD		Relative error	
class (cm)	Length (m)	Diameter (cm)	Length (%)	Diameter (%)
10–20	-1.03 ± 1.81	5.14 ± 5.50	12	40
20–30	-0.67 ± 1.50	-0.65 ± 4.76	10	−2
30–40	-0.42 ± 2.19	-5.33 ± 5.26	37	−15
40–50	-0.21 ± 1.37	-4.23 ± 7.83	19	−9
50–60	-0.10 ± 0.76	-3.61 ± 8.98	−1	−7
60–70	0.34 ± 0.40	-5.33 ± 5.68	3	−9
≥ 70	0.39 ± 0.30	-1.54 ± 0.80	2	−2

4.3.4 Branch diameter from QSMs

For branches greater than 60 cm in diameter, the diameter of QSMs branches was underestimated by 6 % (3.44 cm thinner on average than that of the measured branches) as seen in Table 4.3 and Figure 4.3b. For average diameter values per classes, refer to Table OR4.1 in Online Resource 4. For branches with a diameter between 20 cm to 60 cm, *TreeQSM* underestimated the diameter by 8 % (3.46 cm thinner on average than measured branches). Also *TreeQSM* did not perform well for branches between 10 cm to 20 cm. For these branches, QSMs diameters were overestimated by 40 % (5.14 cm thicker on average).

4.3.5 Branching order from paired QSMs

The confusion matrix revealed that our method was very accurate in assigning the correct branching order when compared to the branching order of our manually measured paired dataset (Table OR5.1 in Online Resource 5). Our method correctly assigned 1143 QSM paired branches with an overall accuracy of 99 % and an overall kappa coefficient of 0.99. Only 6 QSM branches were assigned incorrectly, and all of these were assigned to higher branching orders.

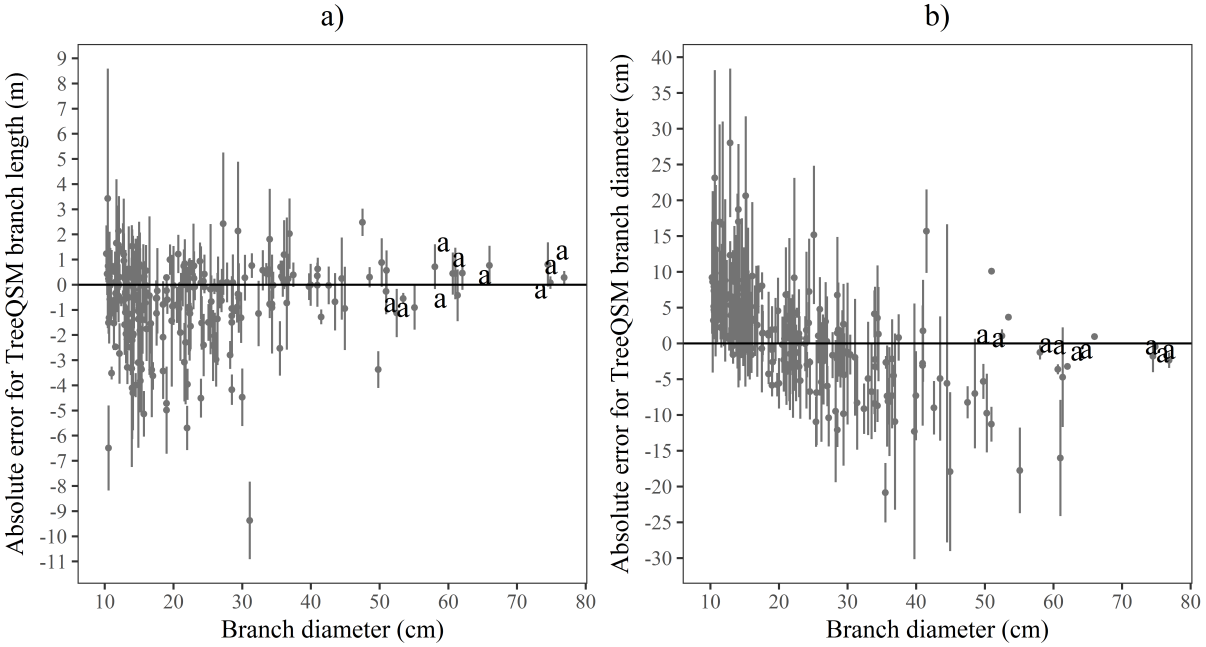

Figure 4.3: Absolute error for length for each unique QSM branch (a) and diameter (b). The solid black horizontal line depicts a perfect match (absolute error of 0 m). Vertical lines depict the range of values of the seven reconstructions of the QSM per tree and the dot depicts the average value from the seven repetitions. Coefficient *a* denotes each tree main stem.

4.3.6 Absolute and cumulative branch length and branch volume from QSMs

The absolute length and absolute volume of *TreeQSM* matched branches were compared with the absolute length and absolute volume of manually measured matched branches by diameter classes (Table 4.4). When analysing by diameter classes, for branches between 10 cm to 20 cm, *TreeQSM* underestimated the absolute branch length by 30 %. For thicker branches, with diameter between 20 cm to 50 cm, absolute branch length is underestimated by 17 % and for branches thicker than 50 cm, is slightly overestimated by 1 %. On the other hand, *TreeQSM* greatly overestimated the absolute branch volume for branches between 10 cm to 20 cm (40 %). However, for the branches with diameter between 20 cm to 50 cm, *TreeQSM* underestimated the absolute branch volume by 29 %. For thicker branches ($>$ 50 cm), the absolute volume is slightly underestimated by 0.4 % (Table 4.4).

The cumulative branch length and cumulative branch volume of each *TreeQSM* tree were compared to the same parameters of each manually measured tree (Table 4.5). When analysing all measured branches, *TreeQSM* underestimated the length by 13 %. *Tree-*

Table 4.4: Absolute values for manually measured branches and absolute values and relative error for QSM branches for the absolute branch length and absolute branch volume separated by 10 cm diameter classes. Values shown are the average values and standard deviation from the seven models.

Diameter class (cm)	Absolute branch length (m)			Absolute branch volume (m3)		
	Measured branches	QSM branches	Relative error (%)	Measured branches	QSM branches	Relative error (%)
10–20	25.50 ± 8.21	17.82 ± 6.49	−30	0.44 ± 0.15	0.61 ± 0.34	40
20–30	13.51 ± 4.86	9.78 ± 4.62	−28	0.66 ± 0.23	0.47 ± 0.24	−29
30–40	6.61 ± 5.49	5.61 ± 3.53	−15	0.60 ± 0.45	0.42 ± 0.28	−30
40–50	4.16 ± 2.16	3.80 ± 1.60	−8	0.66 ± 0.38	0.49 ± 0.22	−26
50–60	14.88 ± 6.77	14.88 ± 6.85	−1	3.39 ± 1.74	3.62 ± 2.05	7
60–70	11.22 ± 7.65	11.56 ± 7.94	3	3.47 ± 2.38	3.28 ± 2.42	−5
≥ 70	21.23 ± 4.57	21.62 ± 4.79	2	9.51 ± 2.19	9.25 ± 2.02	−3

QSM only slightly overestimated below 1 % the length of branches thicker than 40 cm compared to the manual measurements. When summing branches up to 20 cm diameter, the accuracy decreased and the cumulative length was underestimated by 6 %. Similarly, *TreeQSM* tended to underestimate the cumulative volume when compared to manual measurements (Table 4.5). When analysing all measured branches, *TreeQSM* underestimated the volume by 3 %. For branches thicker than 50 cm, the volume of QSM branches was overestimated by 1 % and the cumulative accuracy decreased when summing thinner branches. For branches thicker than 30 cm, *TreeQSM* underestimated volume by 3 %.

4.4 Discussion

Our TLS and the *TreeQSM* method correctly identified and reconstructed 95 % of the measured branches thicker than 30 cm diameter, 67 % of the measured branches with diameter between 20 cm and 30 cm and 45 % of the measured branches thinner than 20 cm diameter. Our method was exceptionally accurate assigning branching order (Figure 4.4). However, we identified limitations with this method for reconstructing the length of measured branches less than 50 cm and the diameter of measured branches thinner than 20 cm. In a similar study on non-tropical trees, Hackenberg et al. (2015b) found that branches with diameter thicker than 10 cm were reconstructed accurately, but with smaller branches, especially twigs with diameter thinner than 4 cm, models overestimated branch volume. In a study by Kaasalainen et al. (2014) branches with diameter thinner than 5 cm were hardly visible in the point cloud and therefore were mostly left out of the model.

Table 4.5: Cumulative values and relative error (%) for cumulative branch length and branch volume for manual measurements and *TreeQSM* models. Negative values show underestimation while positive values show overestimation. Values are average values from the seven models.

Cumulated branch diameter (cm)	Cumulative branch length (m)			Cumulative branch volume (m^3)		
	Measured branches	QSM branches	Relative error (%)	Measured branches	QSM branches	Relative error (%)
≥ 70	21.23	21.62	2.0	9.51	9.25	−3
≥ 60	32.45	33.18	2.0	12.98	12.52	−3
≥ 50	47.33	47.92	1.0	16.36	16.15	−1
≥ 40	51.49	51.71	0.4	17.02	16.64	−2
≥ 30	58.10	57.33	−1.0	17.63	17.05	−3
≥ 20	71.61	67.11	−6.0	18.29	17.52	−4
Measured tree	97.11	84.93	−13	18.73	18.14	−3

Our method underestimated absolute measured branch cumulative length on average by 13 %. When analysing by cumulative diameter classes, our method slightly overestimated less than 1 % the length of cumulative measured branches thicker than 40 cm. When including thinner measured branches (up to 20 cm), the absolute measured length was underestimated by 6 %. Dassot et al. (2012) found that reconstructed stem length agreed well with destructive measurements while reconstructed length of thinner branches did not.

Moreover, our method tended to slightly overestimate the length of thicker branches and underestimate the length of thinner branches (Table 4.4). This pattern was also observed in the relative error of the cumulated branches (Table 4.5). The relative error of the absolute branch length was greater as branches got thinner (Table 4.4). However, the cumulative branch length did not reflect this pattern, due to the small influence of the length of smaller branches when compared to the absolute length of our measured branches.

Similarly, our method underestimated the absolute branch volume by 3 %. When analysing by cumulated diameter classes, our method slightly underestimated the estimated volume of branches thicker than 50 cm by 1 %. When including thinner branches (below 20 cm), cumulative branch volume underestimation increased up to 4 %. This systematic underestimation of tree volume regardless of species or absolute volume was also reported by Dassot et al. (2012); Calders et al. (2015b); and Gonzalez de Tanago et al. (2017). Similar studies also described similar accuracy values, Gonzalez de Tanago et al. (2017) showed an overall underestimation of 4 % and Hackenberg et al. (2015a) described a absolute relative error of 8 % compared to volume reference data. Although our method

greatly underestimated the volume of thinner measured branches (Table 4.4), these did not contribute significantly to the cumulative branch volume, as seen in Table 4.5.

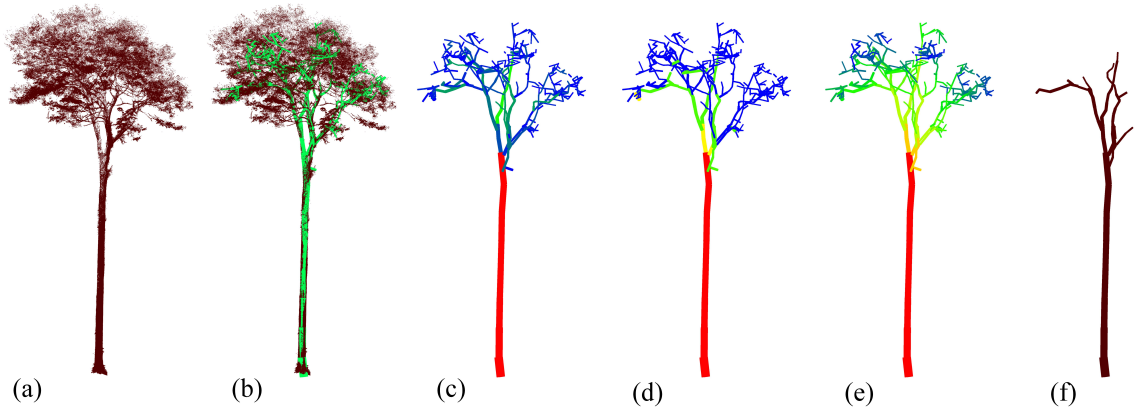

Figure 4.4: (**a**) *E. grandiflora* tree point cloud, (**b**) *TreeQSM* with branches > 10 cm diameter reconstructed from the tree point cloud. (**c**) QSM branches classified by length, (**d**) by branch diameter, and (**e**) by branching order. (**f**) QSM branches which were paired with manually measured branches. Please refer to the digital version for colour image.

A conceptual difference where the main stem terminated was found between the manual measurements and the tree reconstruction. In the manual measurements, the length of the main stem stopped where the stem began to widen, before the point of furcation (Figure 4.1); while in our method (Figure 4.2), the length of the main stem terminated where the actual furcation was. The point of the manual measurement was up to several meters below where the measured branch split occurred and where the *TreeQSM* reconstructed a new branch. Thus, we took new measurements using the tree point cloud. The new measurements lowered the absolute error from 4.6 m to 0.7 m. Based on our results, we recommend for future research to explicitly define a measured branch starting from the base of a branch. An ambiguous branch definition might lead to higher uncertainty in the length of the QSM branch. In addition, we observed that some big branches were destroyed during tree felling and could not be manually measured afterwards. Luckily, these branches had been scanned before felling, and thus appeared in the point cloud and were reconstructed by *TreeQSM*. As such, in the future, we suggest that the destroyed branches should be taken into account during the reconstruction process, because a missing branch might confuse the branching order and misclassify the QSM branch.

While our tree reconstruction method helped us to understand the architecture of the branches, it also constrained representing the architectural complexity. In this study, we enforced a simple cylinder-fractal structure of trees and lost details of the complex nature of the architecture of trees. Figure 4.1 shows that branch daughters exactly originated from a single branch node. However, two branches might originate from different branches nodes which are very close to each other and they might be confused as one branch node. While in this study we did not find this case, future studies should take into account the

exact point of furcation as the origin of the branches. Enforcing a cylindrical structure also impacted the buttresses modelling. In this study, the presence of buttresses did not impact our branches analysis. Moreover, the *TreeQSM* version used for this analysis was not able to render buttresses, thus we assumed them as cylinders. Recent work done by Gonzalez de Tanago et al. (2017) suggested that the modelling of buttresses has an impact on decreasing uncertainty on total tree volume and encouraged further studies to analyse buttresses in depth. In addition, we applied a simplification algorithm to reduce the number of output cylinders. This step reduced the number of cylinders by, either removing specific cylinders (based on our threshold), or merging two or three cylinders into a larger one. Nevertheless, this simplification indirectly added uncertainty in the reconstruction. Figure 4.2 shows three cylinders originating from the blue branch. While two cylinders originated from a very close furcation point, the first cylinder originated below this furcation point. However, the simplification process of our method created a single cylinder and simplified the output model.

The quality of any *TreeQSM* output is a reflection of the quality of the point cloud on which it was based and the accuracy assessed for reconstruction. Several studies proved that *TreeQSM* was able to reconstruct smaller branches with high accuracy when these branches had sufficient point density for an proper reconstruction (Raumonen et al., 2013; Calders et al., 2015b; Åkerblom et al., 2017). In our study, we scanned the trees in dense tropical environments, which made it difficult to scan properly the smaller branches inside the crown. The quality of the point cloud is directly influenced by several factors such as: the distance between the TLS scanner and the scanned tree, the scanning parameters and the environment surrounding the tree. The distance from the instrument to the tree canopy was especially noticed, which is the farthest path from the TLS scanner, surrounded by under story and (very often) lianas. The presence of lianas did not help us in the reconstruction process; however, in this study we are not modelling tree volume, and so the effects were not considered important. Even though our results showed that *TreeQSM* could not reconstruct thinner branches (it found 56 % of branches between 10 cm to 30 cm diameter), the deviations of the *TreeQSM* matched branches from the real data measured in the field are relatively small. Moreover, we scanned with an angular resolution of 0.06°, which had proven to be a good trade-off between accuracy and time requirements for estimating other tree parameters (Calders et al., 2015b; Gonzalez de Tanago et al., 2017; Wilkes et al., 2017), but might not be the most adequate parameter for inside canopy measurements. Wilkes et al. (2017) suggested that an angular resolution of 0.01° might be a better choice when scanning branches in high detail. By decreasing the resolution to 0.01°, we would be increasing the point density at larger distances, capturing more details of branches at higher heights. However, by increasing the angular resolution, we are also exponentially increasing the time scanning. Moreover, we are also increasing the chance that we capture the branches being swayed by the wind, creating a ghosting effect in the point cloud (Wilkes et al., 2017).

Occlusion (the hiding of some structural elements by others) is a big issue for scanning in the tropics, thus to avoid occlusion and capture branches in detail within the canopy, the scanner should be located within a gap in the understory or in flexible positions. Implementing a radial sampling design with flexible locations around the tree could potentially produce a more evenly distributed point density along the tree (Wilkes et al., 2017) and avoid occlusion by the surroundings. Our study employed 9 fixed position and only 4 flexible positions (set up arbitrarily within canopy gaps to capture the tree canopy) for TLS scanning per plot (Online Resource 1). We suggest that further studies should increase the number of flexible scan positions. The inclusion of more flexible scan positions might increase the point density at plot level. Moreover, when scanning, one should take into account wind, which swayed the medium to small branches and introduced noise in the point cloud. Seidel et al. (2012) have recommended to avoid wind with speed greater than 5 m/s.

Although our sample size is small and dominated by one tree species, our methodology can be applied to most tree species. We suggest that future research can apply our methodology on trees with different architecture and compare the accuracy. Equally important, one should be aware of the presence of non-hardwood components (leaves), branches from other trees and lianas. Tree architecture relies mostly on hardwood measurements and the presence of leaves, foreign branches and lianas introduces uncertainty in the branch reconstruction at canopy level. Lianas are very difficult to distinguish within the canopy and manually removing them creates extra work. In this paper, we systematically deleted all cylinders with diameter less than 10 cm to remove lianas. Future research on branch architecture in the tropics should aim to incorporate new algorithms for leaves and lianas removal.

The branching order is a very sensitive parameter. *TreeQSM* will reconstruct foreign cylinders from a point cloud which has not been properly cleaned (with lianas or branches from other trees). The presence of these foreign branches will add several levels to the branching order, especially if those foreign branches are attached to the main stem, changing the order drastically. Even though the branching order was highly accurate with our paired branches, some branches were misclassified in higher branching orders.

We excluded branches thinner than 10 cm from our analysis. The low point density (due to the scanner angular resolution used in this paper), the plot design (Online Resource 1) and the high occlusion (due to lianas and the same branches) inside the crown made the reconstruction of branches within the crown unreliable. Moreover, our field data collected only measurements of branches > 10 cm. While removal of branches below 10 cm facilitated branch reconstruction in this study, it also reduces the applicability of this method for further studies. Despite that, it does not complete discard it; future research could adopt this methodology for smaller branches and still have comparable results.

Our paper relied on visual inspection in several steps of this paper (sections 4.2.4 and 4.2.5). Even though visual inspection is subjective, it was done heuristically based on the expertise of the authors. Other studies relied on other parameters to optimize *TreeQSM*, e.g. Gonzalez de Tanago et al. (2017) used the absolute volume to estimate an optimal *d*. We could not apply the same optimization method as in Gonzalez de Tanago et al. (2017), since their method was optimized upon estimating biomass and their sample size was bigger than ours. Future research should focus on an automated *TreeQSM* optimization method, as proposed by Calders et al. (2015b).

4.5 Conclusions

Our study assessed the accuracy of using TLS and *TreeQSM* to reconstruct tree architecture parameters (branch length, branch diameter, branching order, absolute and cumulative measured tree length and absolute and cumulative estimated tree volume) from tropical tree point clouds. Our method is able to reconstruct accurately big branches (> 40 cm diameter), while for smaller branches the accuracy decreased. A series of limitations were discussed which could improve the constraints encountered in this study and improved the modelling of smaller branches. We encourage future studies to optimize the plot and sampling design to obtain a more optimal point cloud density for branches inside the canopy and to take other factors into account while scanning, such as wind and disturbance from sampling activities (Wilkes et al., 2017). Even though our results perform worse at the tree level, our approach still represents a significant step forward into studies of tree architecture based on TLS and *TreeQSM* which could accelerate and improve our understanding of tree architecture and how it may influence ecological (Kempes et al., 2011; Rosati et al., 2013) and metabolic processes (West, 1999b; Bentley et al., 2013) or, in turn, be shaped by those processes.

4.6 Acknowledgements

This research is supported by CIFOR's Global Comparative Study on REDD+, ERA-GAS NWO-3DforMod project 5160957540, ERC Advanced Investigator Award (GEM-TRAITS, 321131) and NERC grant NE/P012337/1. The authors acknowledge the collaboration of Guyana Forestry Commission for their support in Guyana and Cornelis Valk for his aid in the QSM visualization.

Chapter 5

Estimating architecture-based metabolic scaling exponents of tropical trees using terrestrial LiDAR and 3D modelling

This chapter is based on:

Lau, A., Martius, C., Bartholomeus, H., Shenkin, A., Malhi, Y., Jackson, T., Herold, M., and Bentley, L., 2018, Estimating architecture-based metabolic scaling exponents of tropical trees using terrestrial LiDAR and 3D modelling, *To be submitted*.

Abstract

Tree architecture influences physical and ecological processes within the tree. Prior work suggested the existence of general principles which govern these processes. Among these, the West, Brown and Enquist (WBE) theory is prominent; it holds that biological function has its origin in a tree's idealized branching system network; from which scaling exponents can be estimated. The scaling exponents of the WBE theory (branch radius scaling ratio, α and branch length scaling ratio β) can be derived from branch parameters and from these, metabolic scaling rate (θ) can be derived. Until now, branch parameter values are taken from direct measurements, either from standing trees or from harvested trees. Such measurements are time-consuming, labour intensive and susceptible to subjective errors. Terrestrial LiDAR (TLS) is a promising alternative, being both less biased to error, scalable, and being able to collect large quantities of data without the need of destructive sampling the trees. In this thesis we estimated scaling exponents and derived metabolic rate from TLS and quantitative structure models (*TreeQSM*) models from nine trees in a tropical forest in Guyana. To validate these TLS-derived scaling exponents, we compared them with scaling exponents and derived metabolic rate from field measurements at three levels: branch-level, tree-level and plot-level. For that, we destructive sampled the scanned trees and measured all branches $> 10\,\text{cm}$. Our results show that, with some limitations, radius, length scaling exponents and architecture-based metabolic rate can be derived from 3D data of tree point clouds. However, we found that only θ converged between our *TreeQSM* modelled and manually measured dataset at both, the branch-level (0.59 and 0.50 for *TreeQSM* and manually measured exponent, respectively) and at the tree-level (0.56 and 0.51). Our results did not support the same conclusion for α nor β - neither at the branch-level nor at the tree-level. The α diverged between *TreeQSM* and manually measured dataset at the branch-level (0.45 and 0.63) and at the tree-level (0.46 and 0.64). The β was the exponent which most deviated between *TreeQSM* and manually measured dataset at the branch-level (0.42 and 0.07) and at the tree-level (0.41 and 0.05). At the tree-level, we found that all estimated averaged exponents deviated significantly from metabolic scaling theory predictions (α=1/2 , β=1/3 , and θ=3/4). Our study provides an alternative method to estimate scaling exponents variation at both the branch- and tree-level in tropical forest trees without the need for destructive sampling. Although this approach is based on a limited sample of nine trees in Guyana, can be implemented for large-scale plant scaling assessments. These new data might improve our current understanding of metabolic scaling without harvesting trees.

5.1 Introduction

Tropical forests are structurally complex ecosystems. This complexity is due to the distribution of woody stems and the three-dimensional arrangement of the aboveground elements (such as leaves, branches, trunk) from the bottom to the top of the canopy (Saatchi et al., 2011). The architectural form of the tree is the results of a combination of both its genetic programme and its adaptive response to the surroundings (Malhi et al., 2018) and influences physical (such as growth, water movement and nutrient allocation) and ecological processes (such as photosynthesis, CO_2 sequestration and evapotranspiration) (Rosell et al., 2009). Previous studies found similarities in the relationships between these physical and ecological processes that suggest the existence of general underlying principles which govern these processes (Savage et al., 2010; Sperry et al., 2012; Tredennick et al., 2013).

Several "universal" theories, including the Geometric Similarity Model (McMahon & Kronauer, 1976), Stress Similarity model (Niklas, 1994) and the West, Brown and Enquist (WBE) model (West et al., 1997; West, 1999a) have been developed to understand these principles with reproducible theoretical predictions (Tredennick et al., 2013). Among these theories, the WBE model (West et al., 1997; West, 1999a) has best stood the test of time. The WBE theory holds that the scaling of metabolic rate and other biological functions has its origin in a (theoretical) optimal branching system network at both internal (vascular) and external (branching) components (West et al., 1997; West, 1999a; see Appendix 5.A for more information regarding WBE theory). In terms of the WBE model, the external structure assumes an idealized branching network which must be symmetrical, self-similar and hierarchical (Appendix 5.A). From this branching network, three key parameters (branching ratio, branch radius scaling and length scaling ratio) can be extracted and used to estimate the scaling exponents (Fig. 5.1 top and Malhi et al., 2018). Nevertheless, real trees do rarely conform to idealized branching. To understand the basis of this theory, an accurate quantification of the branching architecture of trees is needed.

Detailed description of branching architecture can be traced back to Leonardo Da Vinci in the 15^{th} century; however, it was not until the work of Francis Halle in the late 70's that tree form was qualitatively classified (Hallé et al., 1978). From there, only few studies have quantitatively assessed branch architecture at branch-level or tree-level and used them as a base for plant scaling models (Nygren & Pallardy, 2008; Bentley et al., 2013; Tredennick et al., 2013); using either destructive harvesting or direct measurements with *xyz*-local coordinates. The intensity of manual labour to sample large quantities of trees with enough detail (Bentley et al., 2013) and the uncertainty of subjective errors in the measurements are the biggest limitations for quantifying branches in an objective way. An accurate estimation and quantification of the branching architecture is key to understand

the ecological processes of plant metabolism.

Terrestrial Light Detection and Ranging (LiDAR) or terrestrial laser scanning (TLS) is a valuable tool to capture the three-dimensional structure of trees and, in combination with specialized algorithms, to assess the woody structure in a repeatable, non-invasive and objective way (Wilkes et al., 2017; Malhi et al., 2018). This active remote sensing technique is based on the emission and reception of tens to hundreds of thousands of monospectral laser beam pulses (Grau et al., 2017) which are propagated into the surroundings of the instrument up to hundreds of metres (Malhi et al., 2018). When these pulses hit an object they are reflected back to the instrument. The reflected pulse's return time is used to create an accurate and highly detailed spatial three-dimensional representation of the surface of the objects surrounding the scanner. With the use of specialized software, a highly detailed 3D point cloud of the scanned area is created (Wilkes et al., 2017).

TLS has rapidly been developed to extract various attributes (at plot-level and tree-level) from scanned forest environments. Studies initially focused on extracting plot-level attributes (Côté et al., 2012; van Leeuwen et al., 2011; Dassot et al., 2011; Newnham et al., 2015; Xi et al., 2016; Wilkes et al., 2017; Grau et al., 2017), mostly because of the manual labour identifying and extracting individual trees from the massive point cloud. The development of tree segmentation algorithms (Raumonen et al., 2015; Ayrey et al., 2017) may assist in a semi-automated extraction of individual trees. From individual tree point clouds we can directly estimate branch diameter (Tansey et al., 2009; Huang et al., 2011), tree height (Burt et al., 2013; Krooks et al., 2014; Brede et al., 2017), and crown diameter and area (Zhao et al., 2012; Srinivasan et al., 2015), among other tree parameters.

The development of quantitative models to reconstruct the fine structure of trees (e.g. *TreeQSM*; Raumonen et al., 2013 and *Simple Tree*; Hackenberg et al., 2015a) made a new approach available to derive indirect parameters. Several studies focused on the potential of these reconstruction algorithms to estimate tree volume, and indirectly, aboveground biomass (Calders et al., 2015b; Gonzalez de Tanago et al., 2017; Momo Takoudjou et al., 2018; Saarinen et al., 2017; Stovall et al., 2017). Further, from these estimations, Olagoke et al. (2016) was able to construct allometric models. Other studies focused on other characteristics of trees, such as root modelling (Smith et al., 2014a; Paynter et al., 2016) and species recognition (Åkerblom et al., 2017). TLS scanning of the same area at different periods allowed Olivier et al. (2017) to observe canopy change and Kaasalainen et al. (2014) to observe aboveground biomass change. The reconstruction of tree structure in fine detail allows not only to quantify tree productivity, as mentioned above, but also to assess tree structure from an ecological point of view. Malhi et al. (2018) detailed the potential application of TLS and quantitative structure models to understand the ecological challenges regarding branching architecture, surface area scaling, tree respiration, seed dispersal and tree mechanics.

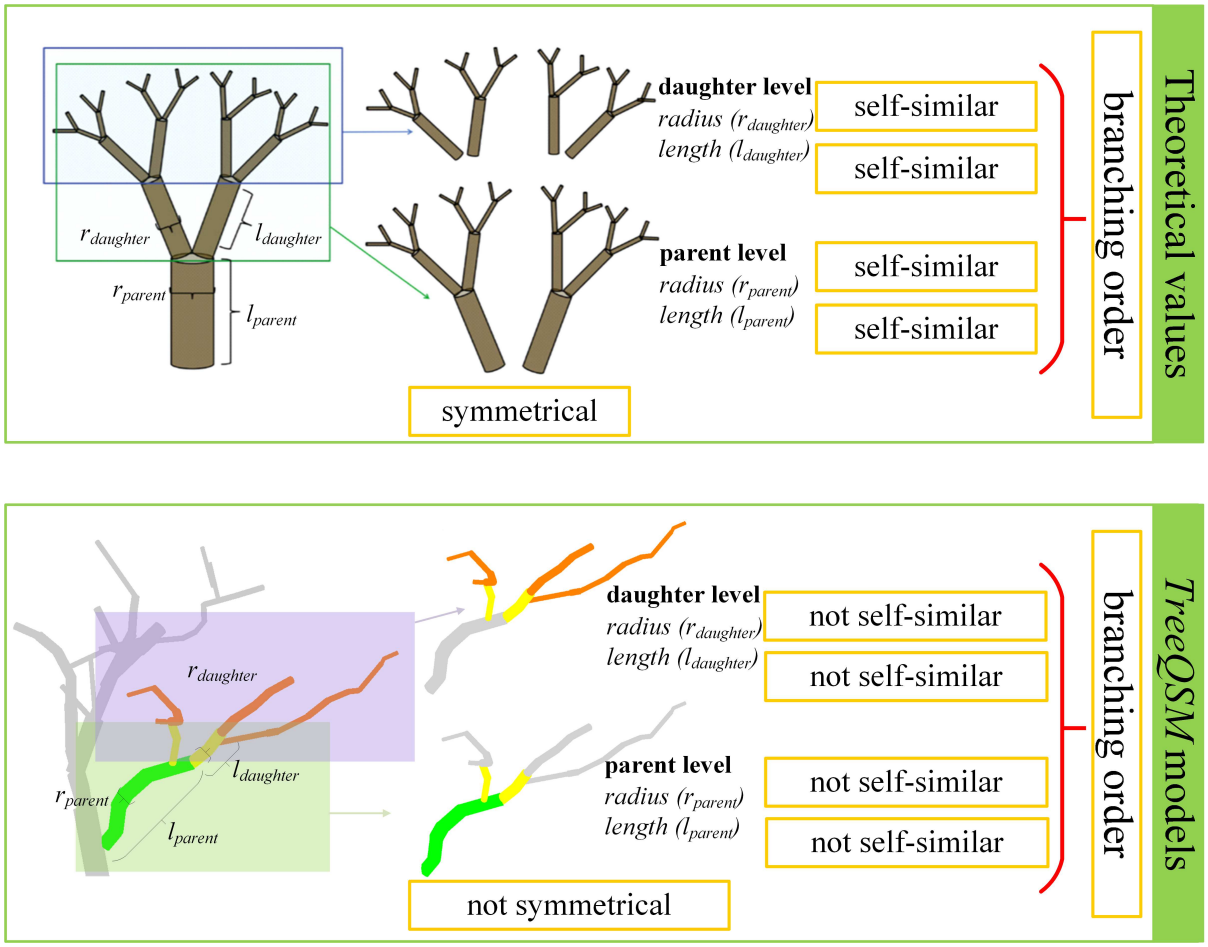

Figure 5.1: Branch scaling ratios for idealized symmetrical trees (top) and for trees modelled with *TreeQSM* (bottom) based on branch radius (r), length (l), and branching ratio (n). The branching ratio is the number of daughter branches per parent branch. The branch radius scaling parameter is $\frac{r_{\text{daughter}}}{r_{\text{parent}}}$ and the length scaling parameter is $\frac{l_{\text{daughter}}}{l_{\text{parent}}}$. Based on Fig. 3 from Malhi et al. (2018). Refer to digital version for colour image.

This study aims to provide a better basis for understanding metabolic scaling through an approach to estimate scaling exponents using TLS and *TreeQSM* (Fig. 5.1). We do not try to improve the understanding of metabolic scaling, but to offer an approach that does not rely on destructive sampling and can increase data collection with better data in shorter time than traditional methods. We aim to: (i) estimate WBE-based metabolic scaling exponents from TLS point clouds and *TreeQSM*, (ii) validate these exponent estimates from the *TreeQSM* with manually measured exponents estimates and, (iii) assess whether theoretical metabolic scaling predictions are included within our estimations.

5.2 Material and methods

We used the data collected in Chapter 4. A total of nine trees in Guyana were scanned, destructively harvested and all of their branches measured down to 10 cm diameter. We used the tree parameters (branch diameter, length and branching order) from Chapter 4 to assess the architecture-based metabolic scaling exponents in this study.

Study area

Field data were acquired from Vaitarna Holding's concession, central Guyana, during November 2014. The area is a lowland tropical moist forest with an elevation of 117 m above sea level and a mean rainfall of 2195 mm yr^{-1}. Seven *Eperua grandiflora*, one *Ormosia coutinhoi*, and one *Eperua falcata* were selected based on their diameter and timber suitability (Fig. 5.A1 in Appendix). The diameter at breast height (DBH) ranged from 61.3 cm to 97.0 cm and the height ranged from 18.8 m to 29.9 m. A 30 x 40 m plot was set up around each selected tree on the expected felling direction. We scanned each plot with TLS, harvested the tree and took detailed geometrical measurements. Plot details can be found in Gonzalez de Tanago et al. (2017) and Wilkes et al. (2017).

TLS acquisition and plot design

All TLS datasets were acquired using a RIEGL VZ-400 V-Line 3D© terrestrial laser scanner (RIEGL Laser Measurement Systems GmbH, Horn, Austria, www.riegl.com). The instrument used in this study is a discretized multiple-return LiDAR scanner with a 1550 nm wavelength and a 0.35 mrad beam divergence (Gonzalez de Tanago et al., 2017; Wilkes et al., 2017). This TLS has a scan range of 360° in the azimuth, 100° in the zenith and the angular resolution used in this study was 0.06°. In each plot, 9 to 16 scan positions were set up and 80 to 100 5-cm-diameter cylindrical reflecting targets (tie-points) were distributed evenly in the plot. The tie-points were placed in such a way that each of them could be scanned from several positions. These tie-points were later used to co-register the individual points clouds into a unified point cloud as in Gonzalez de Tanago et al. (2017), Wilkes et al. (2017) and in Chapter 4.

Manual measurements of branches

The manual measurements of the nine harvested trees were analysed in Chapter 4. Here, we give a summary of the methodology employed. We measured a total of 279 individual branches up to 10 cm diameter with 1 cm-resolution forestry tape. We took two measurements of each branch: length (m) and diameter (cm). The length was defined as

the distance between the base and the termination of the branch and the diameter was defined as the average of two diameter measurements, one taken at the base, and the other, at the termination of the branch (See Fig. 1 in Chapter 4). Finally, we defined the branching order and hierarchy. The branching order was established "centrifugally", starting from the main stem and adding an order at every branch node. The branch hierarchy was defined as the branch correspondence between a parent branch and daughter branch. A daughter branch is any branch with originates from a parent branch and the parent branch was recorded for each individual branch.

Branching reconstruction

The branching reconstruction of the digital trees was performed in Chapter 4 and had three components: (i) manual tree extraction from the point cloud (Fig. 5.2a), (ii) 3D reconstruction of individual tree point clouds using *TreeQSM* (Figs. 5.2b-5.2c), and (iii) individual analysis of *TreeQSM* branches against manually measured branches (Fig. 5.2d). All individual TLS scans were co-registered into a plot point cloud, in which the harvested trees were located and extracted. For quality control, visual inspection was performed on each tree point cloud to ensure that no parts of the tree were missing. Then, individual tree point clouds were reconstructed using quantitative structure modelling *TreeQSM* (Raumonen et al., 2013 and see Fig. 2 in Chapter 4). A series of steps was performed to ensure that the seven best-fitted *TreeQSM* models were obtained (Chapter 4).

We visually paired each manually measured branch with a QSM modelled branch following the structure of the modelled tree. If a measured branch did not have a modelled branch, the measured branch was not paired and excluded from further analysis. If a measured branch corresponded to two or more modelled branches, we quantitatively analysed the similarity of these branches using their length and diameter. We used a diagonal-norm approach to standardize both parameters and analysed their similarities. The modelled branch most similar to the measured branch was chosen as the best-fitted pair.

The geometrical structure was determined as follows: *TreeQSM* branch length was the sum of the length of all cylinders of the same branch, *TreeQSM* branch diameter was the average of the first and last cylinder of the same branch, and branching order was estimated starting from the main stem and adding a new level at each branch node.

Tree metrics

The tree architecture of these trees was analysed in Chapter 4 and a summary of tree metrics for this dataset can be seen in Table 5.1. Chapter 4 validated the reconstruction accuracy of branches lengths, branches diameters and branching orders of 279 modelled

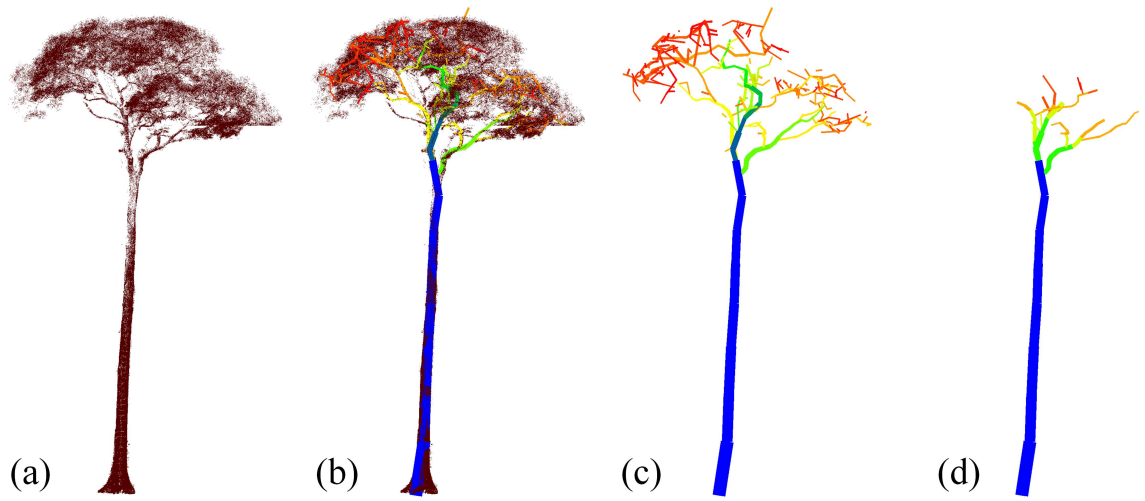

Figure 5.2: (**a**) *Ormosia coutinhoi* tree point cloud, (**b**) *TreeQSM* with branches > 10 cm diameter reconstructed along with the tree point cloud, (**c**) QSM branches classified by branching order and (**d**) QSM branches which were paired with manually measured branches. Refer to digital version for colour image.

branches compared with manually measured branches. Their method found and reconstructed 95 % of branches thicker than 30 cm diameter. The accuracy of the length and diameter of the modelled branches varied among diameter classes. For branches smaller than 50 cm in diameter, the length of the modelled branches was underestimated by 20 %.

For branches greater than 50 cm in diameter, the length of the modelled branches was overestimated by 1 %. For branches between 10 cm and 20 cm in diameter, the modelled branch diameters were overestimated by 40 %. For branches with a diameter between 20 cm and 60 cm, diameter was underestimated by 8 %; if the branch diameter was greater than 60 cm, diameter was underestimated by 6 %. In this study, the branching order was correctly assigned with an overall accuracy of 99 %.

Table 5.1: Tree metrics from *TreeQSM* branches and manually measured branches from the Vaitarna dataset. From Chapter 4.

Diameter class (cm)	Measured branches	Reconstruction Accuracy (%)	Absolute error		Relative error	
			Length (m)	Diameter (cm)	Length (%)	Diameter (%)
10–20	160	45	-1.03 ± 1.81	5.14 ± 5.50	12	40
20–30	67	67	-0.67 ± 1.50	-0.65 ± 4.76	10	−2
30–40	26	84	-0.42 ± 2.19	-5.33 ± 5.26	37	−15
40–50	11	92	-0.21 ± 1.37	-4.23 ± 7.83	19	−9
50–60	7	100	-0.10 ± 0.76	-3.61 ± 8.98	−1	−7
60–70	5	100	0.34 ± 0.40	-5.33 ± 5.68	3	−9
≥ 70	3	100	0.39 ± 0.30	-1.54 ± 0.80	2	−2

Finally, we used the information of branch length, diameter and hierarchy provided in Chapter 4 to estimate architecture-based metabolic scaling exponents from modelled trees and compare them with architecture-based metabolic scaling rates from manually measured branches.

Estimation of WBE scaling exponents

Based on previous work by Savage et al. (2010) and Bentley et al. (2013), the scaling exponents from the WBE model for idealized trees can be described using three key parameters (West, 1999a; Malhi et al., 2018): branch radius scaling ratios (α), branch length scaling ratios (β), and branching ratios (n, ratio between number of daughter branches per parent branch). From these branch-level attributes, the scaling of architecture-based metabolic rate (θ) can be further predicted (Table 5.2). Within the WBE model, constant values are given to these parameters when idealized trees are estimated ($\alpha = 1/2$, $\beta = 1/3$, and $\theta = 3/4$; Savage et al., 2008; Malhi et al., 2018).

Table 5.2: Scaling exponents α_{branch} and β_{branch} were calculated at branch-level and definitions are as follows: r = branch radius, n = number of branches, and l = branch length, while the θ_{branch} was derived from α_{branch} and β_{branch}.

Exponent	Equation
α - Radius scaling	$\alpha_{\text{node}} = -\frac{\ln \delta_{\text{node}}}{n_{\text{node}}}$ where: $\delta_{\text{node}} = \frac{r_{\text{daughter}}}{r_{\text{parent}}}; n_{\text{node}} = \frac{n_{\text{daughter}}}{n_{\text{parent}}}$
β - Length scaling	$\beta_{\text{node}} = -\frac{\ln \gamma_{\text{node}}}{n_{\text{node}}}$ where: $\gamma_{\text{node}} = \frac{l_{\text{daughter}}}{l_{\text{parent}}}; n_{\text{node}} = \frac{n_{\text{daughter}}}{n_{\text{parent}}}$
θ - Estimated metabolic rate	$\theta_{\text{node}} = \frac{1}{2\alpha_{\text{node}} + \beta_{\text{node}}}$

Assessment of WBE scaling exponents

The scaling exponents α, β and θ were assessed at three different levels:

- *Branch–level:* scaling exponents at branch-level are shown as the distribution of the exponents, calculated from all branch nodes as in Table 5.2 and Fig. 5.1 for all the

nine trees in this study. We also estimated the median values and 95 % confidence interval (CI) of all the branch nodes.

- *Tree–level:* scaling exponents at tree level are shown as the median values and 95 % CI of all the branch nodes within a tree.
- *Plot–level:* scaling exponents at plot-level are shown as the range between the trees in this study.

Median values were used instead of the arithmetic mean because we did not want to assume unimodal and symmetrical distributions and could not use the geometric mean due to negative numbers (Bentley et al., 2013). We analysed the normality of the distribution of values, and in the case of a non-normal distribution, a non-parametric approach (Wilcoxon Test) would be used to calculate the (pseudo)median with 95 % confidence interval. We included the theoretical predictions and analysed whether the theoretical predictions fall within the CI of our estimations in all three levels.

5.3 Results

Scaling exponents at branch-level

The scaling exponent distributions at branch-level of branch radius scaling ratio (α_{branch}), branch length scaling ratio (β_{branch}) and architecture-based metabolic rate (θ_{branch}) for both, *TreeQSM* and manually measured branches were statistically significant (*p-value* $<$ 0.05; Table 5.A1 in Appendix) and did not follow a normal distribution (Fig. 5.3).

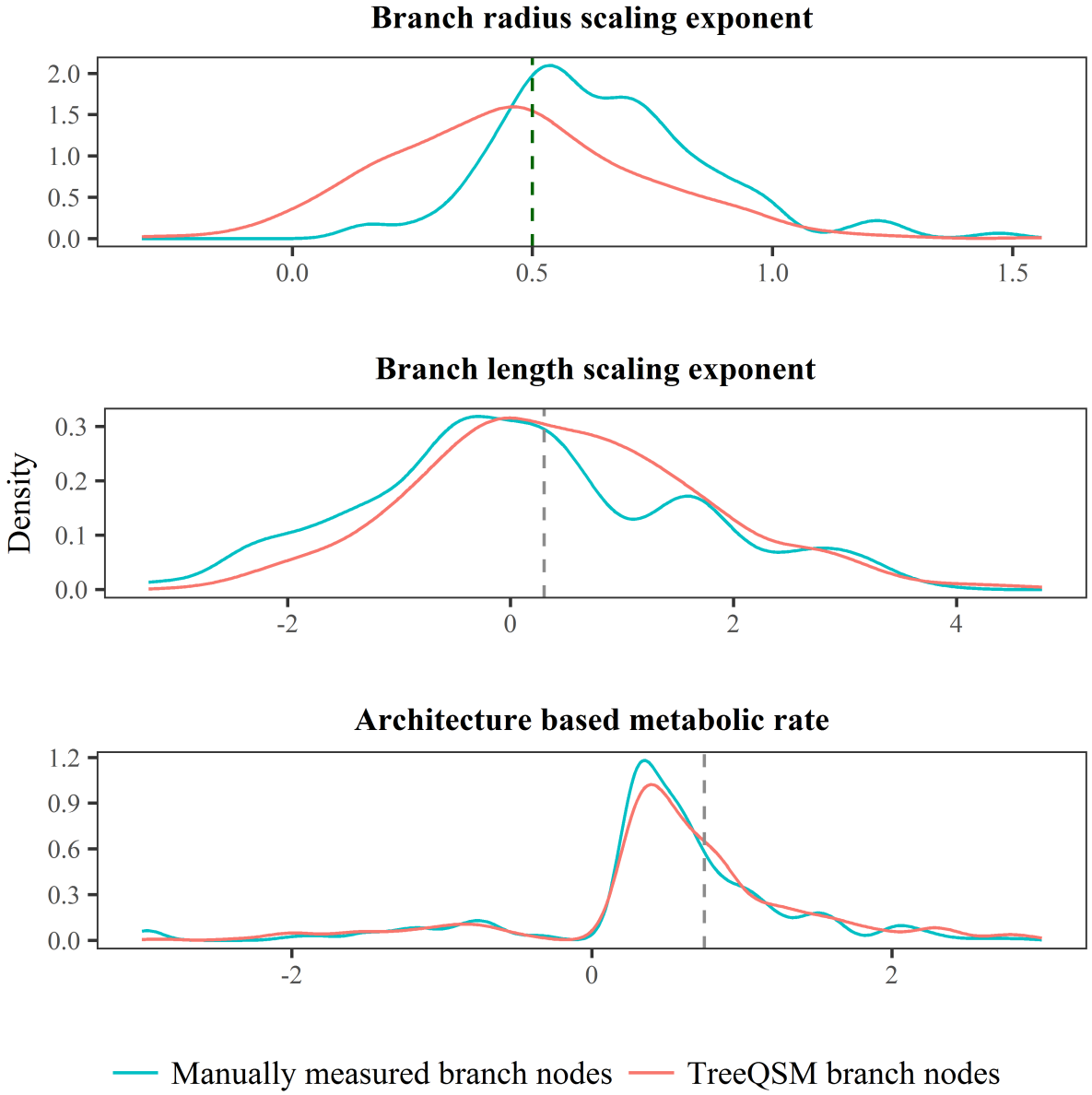

Figure 5.3: Distribution of individual branches for radius scaling exponent (top), length scaling exponent (middle) and architecture-based metabolic rate (bottom) exponents as density function (y-axis), for *TreeQSM* and manually measured estimated scaling exponents. Vertical dashed line indicates WBE idealized predictions for $\alpha = 1/2$, $\beta = 1/3$, and $\theta = 3/4$ Refer to digital version for colour image.

The pseudo(median) values and 95 % CI for scaling exponent distributions at branch-level are displayed in Table 5.3. The *TreeQSM* α_{branch} showed a slightly lower pseudo(median) than its manually measured counterpart and the *TreeQSM* θ_{branch} showed a slightly higher pseudo(median) than its manually measured counterpart. Nevertheless, the *TreeQSM* β_{branch} showed great disparity compared to its manually measured value. We found that α_{branch} and θ_{branch} had a relative narrow CI range. On the contrary, β_{branch} had a relative

larger CI range. This trend was found for both *TreeQSM* and manually measured branches scaling exponent values.

Table 5.3: Scaling exponents of branch radius scaling ratio (α_{branch}), branch length scaling ratio (β_{branch}) and architecture-based metabolic rate (θ_{branch}) of the *TreeQSM* and manually measured branches at branch-level. Values shown as (pseudo)median with 95 % CI (low and high in parenthesis) for the branch-level distribution and values are shown as average values for plot-level.

Scaling exponents	Theoretical value	Branch-level			
		TreeQSM		Measured	
Branch radius scaling ratio - α	$1/2$	0.45	0.43 – 0.48	0.63	0.62 – 0.65
Branch length scaling ratio - β	$1/3$	0.42	0.31 – 0.54	0.07	−0.06 – 0.20
Architecture-based metabolic rate - θ	$3/4$	0.59	0.53 – 0.65	0.50	0.40 – 0.56

Branch scaling exponents per cumulative branching order at branch-level

We also analysed the representation of the scaling exponents for cumulative branching orders for both, *TreeQSM* and manually measured branches up to the 8^{th} branch order (Fig. 5.4 and Table 5.A2 in Appendix). The *TreeQSM* and manually measured scaling exponents followed the same pattern in each cumulative scaling exponent. Moreover, in the cumulative branch radius scaling exponent, the *TreeQSM* exponents had slightly higher exponents than the manually measured exponents from the second branch order onwards. While for the cumulative branch length scaling exponent and cumulative estimated metabolic rate, the *TreeQSM* exponents had higher values than the measured ones. The confidence interval of the radius scaling exponent and the architecture-based metabolic rate showed a narrow range, while the CI of the length scaling exponent showed a wider range across the cumulative branching orders for both *TreeQSM* and manually measured branches.

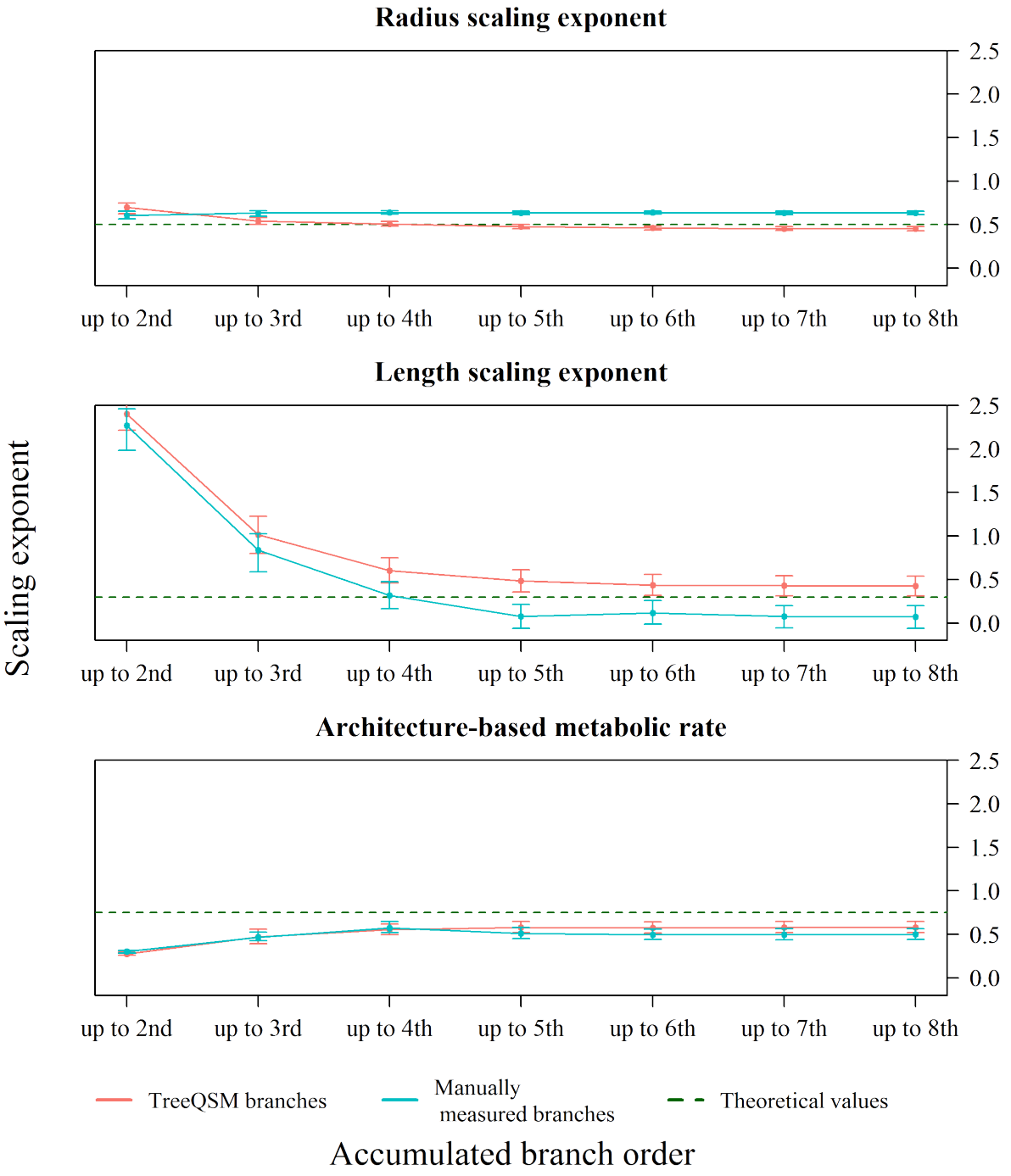

Figure 5.4: Cumulative (pseudo)median and 95 % CI for radius scaling exponent (top), length scaling exponent (middle) and architecture-based metabolic rate (bottom) exponents for *TreeQSM* and manually measured branches up to cumulative 8^{th} branch order. The 95 % CIs are shown as vertical lines on the (pseudo)medians. Horizontal dashed line indicates WBE idealized predictions for $\alpha_{\text{branch}}=1/2$, $\beta_{\text{branch}}=1/3$, and $\theta_{\text{branch}}=3/4$ Refer to digital version for colour image.

Branch radius scaling exponents showed no significant variation for branching order higher than 6th order (Fig. 5.4 and Table 5.A2 in Appendix). On the other hand, branch length scaling exponents showed high (pseudo)medians on the 2nd and 3rd branch order (2.4 and 2.27 up to 2nd branch order for *TreeQSM* and manually measured branches respectively) and displayed no significant variation after 6th branch order. The architecture-based metabolic rate showed a different pattern, both with *TreeQSM* and manually measured branches. The metabolic rate started with lower (pseudo)medians and no significant difference after the 5th branch order for *TreeQSM* and manually measured branches, respectively.

Scaling exponents at tree-level and plot-level

Table 5.4 shows the pseudo(median) values for each tree and 95 % CI from each exponent distribution at tree-level. The average pseudo(median) values for the estimated scaling exponent α_{tree} was 0.46 and 0.64; for the β_{tree} was 0.41 and 0.05; and for the θ_{tree} was 0.56 and 0.51 for the *TreeQSM* and manually measured values, respectively.

Table 5.4: Branch radius scaling ratio (α_{tree}), branch length scaling ratio (β_{tree}) and architecture-based metabolic rate (θ_{tree}) pseudo(median) values, 95 % CI per individual tree and plot-level ranges between trees. *Continued on the following page.*

Trees	Branch radius - α			
	TreeQSM		Measured	
GUY01	0.49	0.44 – 0.54	0.66	0.61 – 0.70
GUY03	0.45	0.36 – 0.52	0.62	0.60 – 0.69
GUY04	0.43	0.37 – 0.49	0.69	0.65 – 0.76
GUY05	0.44	0.32 – 0.56	0.68	0.65 – 0.75
GUY06	0.47	0.41 – 0.51	0.62	0.54 – 0.67
GUY07	0.50	0.40 – 0.60	0.65	0.62 – 0.68
GUY08	0.50	0.41 – 0.61	0.66	0.60 – 0.73
GUY09	0.52	0.46 – 0.59	0.62	0.56 – 0.66
GUY10	0.33	0.28 – 0.38	0.53	0.46 – 0.59
plot-level	0.33 – 0.52		0.53 – 0.69	

When comparing *TreeQSM* with manually measured trees estimated radius ratio scaling exponent (α_{tree}) and metabolic rate (θ_{tree}), both showed the same trend. As with the scaling exponents at branch-level, *TreeQSM* α_{tree} also showed slightly lower value compared to manually measured α_{tree}. This trend was also found in θ values, where *TreeQSM* θ_{tree} showed slightly higher values compared to manually measured θ_{tree}. *TreeQSM* β_{tree} showed great disparity compared to the manually measured β_{tree}. *TreeQSM* β_{tree} values were greater than manually measured β_{tree}.

Table 5.4: *(continued).*

Trees	Length radius - β			
	TreeQSM		Measured	
GUY01	0.21	−0.06 – 0.60	−0.12	−0.32 – 0.25
GUY03	0.59	0.24 – 0.99	0.3	0.10 – 0.49
GUY04	0.35	−0.04 – 0.79	0.13	−0.23 – 0.42
GUY05	0.17	−0.31 – 1.04	−0.33	−0.71 – 0.59
GUY06	0.55	0.10 – 0.99	0.42	−0.11 – 0.99
GUY07	0.62	0.24 – 1.08	−0.19	−0.53 – 0.30
GUY08	0.44	0.12 – 0.74	0.28	−0.20 – 0.75
GUY09	0.57	0.26 – 0.83	0.05	−0.35 – 0.38
GUY10	0.23	0 – 0.50	−0.11	−0.51 – 0.32
plot-level	0.17 – 0.62		-0.33 – 0.42	

Table 5.4: *(continued).*

Trees	Metabolic rate - θ			
	TreeQSM		Measured	
GUY01	0.69	0.45 – 0.88	0.52	0.39 – 0.65
GUY03	0.56	0.38 – 0.84	0.64	0.53 – 0.76
GUY04	0.38	−0.27 – 0.56	0.47	0.41 – 0.59
GUY05	0.24	−0.39 – 0.65	0.38	−1.26 – 0.69
GUY06	0.51	0.34 – 0.84	0.38	0.23 – 0.92
GUY07	0.75	0.55 – 1.04	0.76	0.58 – 0.97
GUY08	0.53	0.37 – 0.67	0.27	−2.18 – 0.34
GUY09	0.59	0.48 – 0.83	0.71	0.54 – 0.96
GUY10	0.77	0.57 – 1.02	0.45	0.25 – 0.95
plot-level	0.24 – 0.77		0.27 – 0.76	

At plot-level, the range of (pseudo)median values for our *TreeQSM* estimated scaling exponent α_{plot} was from 0.33 to 0.52, while for the manually measured scaling values was from 0.53 to 0.69. For the estimated scaling exponent β_{plot}, *TreeQSM* (pseudo)median values ranged from 0.17 to 0.62 and −0.33 to 0.42 for the manually measured scaling values. For the estimated scaling exponent θ_{plot}, (pseudo)median values ranged from 0.24 to 0.77 for the *TreeQSM* and 0.27 to 0.77 for the manually measured scaling values (Table 5.4).

Theoretical scaling exponents inclusion

At branch-level (Table 5.3), all of the 95 % CI for *TreeQSM* and manually measured scaling exponents excluded the theoretical values ($\alpha = 1/2$, $\beta = 1/3$, and $\theta = 3/4$). Only *TreeQSM* β_{branch} included the theoretical values within its CI range. However, at tree-level, most of the individual trees included the theoretical values within their 95 % CI (Table 5.4). At plot-level, all scaling exponents from *TreeQSM* and manually measured values included the theoretical values within their ranges except the manually measured α_{plot}. It did not include α_{tree} prediction due to a small difference (0.53 compared to 0.50; Table 5.4).

5.4 Discussion

We first examine the results obtained for the *TreeQSM* and manually measured exponents, then we analyse the implications of using TLS and 3D models in the estimation of scaling exponents, and finally describe the implications of our results within the WBE context of metabolic scaling.

This study represents the first quantitative analysis of metabolic scaling rates based on WBE theory applied to tropical trees based on 3D models from point cloud and field measured data. Overall, we found that only architecture-based metabolic rate (θ) converged between our *TreeQSM* modelled and manually measured dataset at both, branch-level (with a (pseudo)median of 0.59 for *TreeQSM* and 0.50 for the manually measured exponent) and at tree-level (with a (pseudo)median of 0.56 for *TreeQSM* and 0.51 for the manually measured exponent). Our results did not support the same conclusion for branch radius scaling ratio (α) or branch length scaling ratio (β) - neither at branch-level nor at tree-level. The branch radius scaling ratio (α) diverged at branch-level (with a (pseudo)median of 0.45 for *TreeQSM* and 0.63 for the manually measured exponent) and at tree-level (with a (pseudo)median of 0.46 for *TreeQSM* and 0.64 for the manually measured exponent). The length scaling ratio (β) was the exponent which most deviated between *TreeQSM* and manually measured dataset at branch-level (with a (pseudo)median of 0.42 for *TreeQSM* and 0.07 for the manually measured exponent) and at tree-level (with a (pseudo)median of 0.41 for *TreeQSM* and 0.05 for the manually measured exponent).

The large divergence in the branch length scaling ratios was caused by the large absolute length error between the *TreeQSM* estimates and the manual measurements (Table 5.1). While for branches greater than 50 cm, the length of QSMs branches was overestimated by 1 %, for branches thinner than 50 cm, the average length of QSMs branches was underestimated by 20 % (See Table 5.1). As discussed in Chapter 4, a conceptual difference in the branch termination between the *TreeQSM* estimates and the manual measurements

was found. This conceptual difference has a direct impact in the branch length scaling ratio (Table 5.2). As length scaling is a ratio ($\frac{l_{\text{daughter}}}{l_{\text{parent}}}$), the larger the value of the length of the parent branch, the smaller the exponent value is. Since we had an underestimation of the length of QSMs branches, we expect that our *TreeQSM* exponent values would be higher than the measured exponents at branch-, tree- and plot-level, as in Table 5.3). As also discussed in Chapter 4, a correct definition of the branch measurements could avoid ambiguity and lower the absolute errors.

A trend can be observed in the cumulative scaling exponents between the *TreeQSM* and the manually measured branches (Fig. 5.4 and Table 5.A2 in Appendix). This concords with the tree metrics from Table 5.1. For radii, *TreeQSM* showed an underestimation; while for the lengths, *TreeQSM* showed an overestimation when compared to manually measured branches. However, while radius scaling exponents and the architecture-based metabolic rate had no significant variation while cumulating branch orders, the length scaling exponents had a high (pseudo)median in the first two cumulative branch orders and then decreasing until being steady from the 5^{th} cumulative branch order. We theorize that the length scaling ratio is high at this order due to the ratio between the length of father branch (in this case, the main stem) and the length of daughter branches. This difference can be up to several meters, having a direct effect on the length scaling exponent at this cumulative branch order.

WBE predicted values for plant scaling regarding the scaling of radius, length and architecture-based metabolic exponents were not in concordance with our results from the tropical trees assessed in this study. Our analysis showed that central values deviated from predictions and that WBE predicted values were included by a very small margin in the 95 % confidence intervals, only at plot-level. Moreover, this study found out that while *TreeQSM* branch ratio $\alpha_{\text{branch,tree}}$ were relatively close to the theoretical value, length ratio $\beta_{\text{branch,tree}}$ and architecture-based metabolic rate $\theta_{\text{branch,tree}}$ greatly deviated from WBE predictions, in both, *TreeQSM* and manually measured datasets.

The *TreeQSM* β exponents were closer to 1/2 than to the WBE theoretical estimate of 1/3. This finding is consistent with Bentley et al. (2013), who found that β estimates were closer to 1/2 than 1/3, and Muller-Landau et al. (2006), who also observed that observed exponents significantly differed from predicted theoretical values. Bentley suggested that $\beta = 1/3$ might only occur in large trees, but although our tree sample comprised trees ranging between 61.3 cm to 97.0 cm DBH, our results do not support this statement. As mentioned by Malhi et al. (2018); the tree's rapid response to the environment to maximize light capture through maximizing vertical height, maximize efficiency of resource distribution, and minimize the risk of breakage or overturning might be the reason why trees appear more plastic in their lengths than in their radius (Bentley et al., 2013; Price et al., 2007).

In addition to the deviation observed for length ratio β, our findings for *TreeQSM* architecture-based metabolic rate $\theta_{\text{branch,tree}}$ were lower than WBE prediction of 3/4 While Isaac & Carbone (2010) found strong support for 3/4 scaling of metabolism, our analysis does not support this statement. In fact, our results are more aligned with those by Petit & Anfodillo (2009); Bentley et al. (2013); and Smith et al. (2014b), whose estimates all deviated from predicted exponents. Our results at branch-level and tree-level were closer to 3/8 than 3/4 metabolic rate which supports the assumption of elastic similarity in large branching networks as mentioned by Price et al. (2007) and Bentley et al. (2013); and plastic response to environment, a common feature found in tropical trees.

Fractal branching and homogeneous length and diameter parameters within the same branch node were not found in our dataset. As mentioned by Petit & Anfodillo (2009), the fractal branching proposed by the WBE model is very unlikely to be found in real plants. The scaling exponents deviated significantly from the exponents predicted from symmetrical and self-similar branches as proposed by the WBE model. The WBE predictions might work on individual trees which grow in absence of competition and no nutrition limitation, such as on plantations (Muller-Landau et al., 2006); or might work on young trees with simple branching rules (Petit & Anfodillo, 2009; Loehle, 2016). Those trees would have enough nutrients and would be protected from environmental hazards (such as heavy wind or rainfall) and with small branch size distributions which might be easily measured. Our sample trees do not fall into those assumptions. Predictions for large trees, as explained by Loehle (2016), are still puzzling due to the architectural complexity of real trees, their susceptibility to damage and their rapid resilience; characteristics unfitted for the symmetrical branching geometry proposed by WBE model.

Our sample also showed a high variation, supporting Loehle's statement which says that optimal branching cannot be found in old trees or with increased exposure to the environment. We suggest a further study focusing on how asymmetrical branching changes WBE predictions and how to improve WBE predictions based on asymmetrical branching. As suggested by Smith et al. (2014b) and Price et al. (2009), the theoretical value for metabolic scaling in the WBE context might be more an approximate rather than an exact value when applied to real trees.

5.5 Conclusions

We present a novel approach to estimate scaling exponents and architecture-based metabolic rate within the context of the West, Brown and Enquist (WBE) model for tropical forest trees that relies on Terrestrial Laser Scanner (TLS) and *TreeQSM* modelling. While some limitations emerged that would still allow to further improve the scaling exponents estimations from TLS and *TreeQSM* modelling; our results show that

radius scaling exponents, length scaling exponents, and architecture-based metabolic rate can be estimated from 3D data of tree point clouds. Thus, a much easier way is identified to test metabolic scaling laws further with the use of large datasets collected in non-destructive ways in the field, rather than with the smaller datasets obtained from the tedious and time-consuming hand-collection of data.

Nevertheless, our results show that only architecture-based metabolic rate (θ) converged between *TreeQSM* and manually measured metabolic rate at branch- (0.59 and 0.50), tree- (0.56 and 0.51) and plot-level (0.24 to 0.77 and 0.27 to 0.76). Our results did not support the same conclusion for branch radius scaling ratio (α) or branch length scaling ratio (β) - neither at branch-, tree- nor at plot-level. The ability to estimate these scaling exponents is critical to estimate metabolic rate at tree-level and scale up to large-scale plots without the need of destructive sampling.

We highlight that our results are based on a limited sample of nine trees in Guyana and more research is needed. Nevertheless, the validation of our approach provides an insight into the potential of TLS and *TreeQSM* to account for individual tree structure, providing enough detailed architectural information to estimate scaling exponents at both, branch-level and tree-level and how this could be implemented for large-scale plant scaling assessments. Our approach can be used further to estimate plant-scaling exponents and metabolic rate from *TreeQSM* models from trees from different regions at a global scale. This new data might improve the current understanding of metabolic scaling without harvesting trees.

5.6 Acknowledgements

This research is supported by CIFOR's Global Comparative Study on REDD+, ERA-GAS NWO-3DforMod project 5160957540, ERC Advanced Investigator Award (GEM-TRAITS, 321131) and NERC grant NE/P012337/1.

5.A Appendix

WBE metabolic scaling exponents

The WBE theory holds that the scaling of metabolic rate and other biological functions has its origin in an optimal branching system network at both internal (vascular) and external (branching) components (West et al., 1997; West, 1999a). While the internal structure is composed by xylem and phloem conduits, the external structure is composed by branches. The WBE theory assumes that an idealized external tree branching network is symmetrical, self-similar and hierarchical (see Figure 3 in Malhi et al. 2018), organized in such a way that metabolic rate should not vary when comparing branch node-level to the whole tree-level (West, 1999a; Nygren & Pallardy, 2008; Sperry et al., 2012; Bentley et al., 2013). Nevertheless, real trees do not show an idealized external branching network. Self-similarity rarely holds true throughout a whole tree, branching order varies across tree-level, and stems taper and exhibit asymmetric branching (Nygren & Pallardy, 2008; Smith et al., 2014b; Price et al., 2012; Bentley et al., 2013).

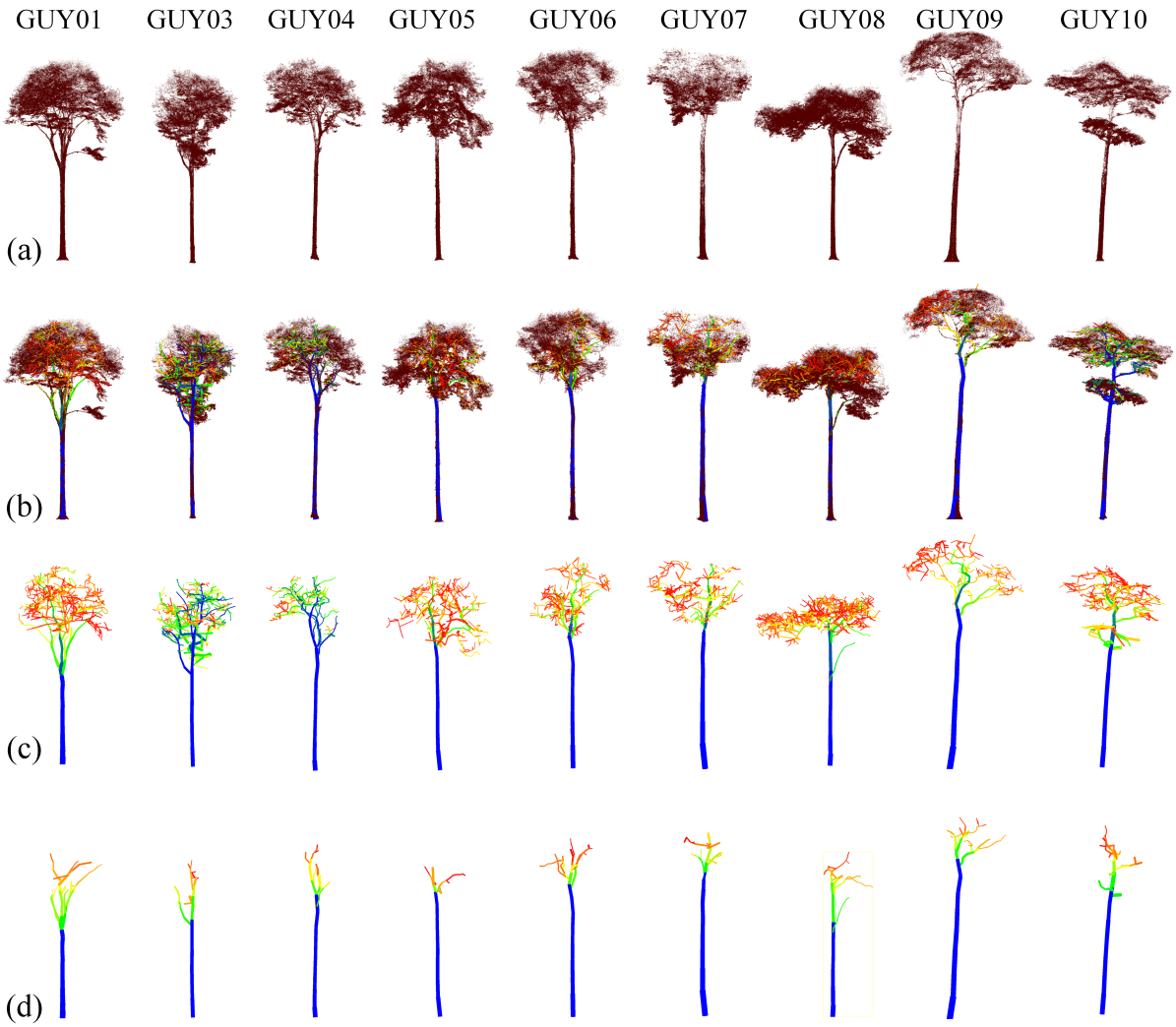

Figure 5.A1: Tree point clouds and *TreeQSM* models from the nine trees scanned in Guyana. (**a**) tree point clouds of the nine trees from Guyana, (**b**) One repetition of *TreeQSM* with branches > 10 cm diameter reconstructed along with the tree point clouds, (**c**) QSM branches classified by branching order, and (**d**) QSM branches which were paired with manually measured branches. GUY01 to GUY08 are *Eperua grandiflora* trees, GUY09 is a *Ormosia coutinhoi* tree, and GUY10 is a *Eperua falcata* tree.

Table 5.A1: Shapiro-Wilks p-values, (Pseudo)median and CI (95%) for scaling exponents at branch node-level and tree-level for QSM model trees and reference trees.

Scaling exponent and theoretical value		TLS-derived scaling exponent			Reference scaling exponent		
		p-value	(Pseudo)median and CI (95%)		p-value	(Pseudo)median and CI (95%)	
α_{node}	$1/2$	0.0325	0.45	0.43 – 0.48	1.913×10^{-9}	0.63	0.62 – 0.65
α_{tree}		-	0.46	0.38 – 0.53	-	0.64	0.59 – 0.69
β_{node}	$1/3$	0.0123	0.42	0.31 – 0.54	4.31×10^{-5}	0.07	−0.06 – 0.2
β_{tree}		-	0.41	0.06 – 0.84	-	0.05	−0.32 – 0.5
θ_{node}	$3/4$	1.345×10^{-41}	0.59	0.53 – 0.65	8.305×10^{-42}	0.5	0.44 – 0.56
θ_{tree}		-	0.56	0.28 – 0.81	-	0.51	−0.06 – 0.76

Table 5.A2: Accumulated (Pseudo)median and CI (95%) for branch order for scaling exponents at branch node-level for *TreeQSM* and manually measured branches.

Branch order accumulated	Branch radius - α			
	TreeQSM		Measured	
up to 2nd	0.70	0.63 – 0.75	0.61	0.57 – 0.65
up to 3rd	0.54	0.50 – 0.58	0.64	0.59 – 0.66
up to 4th	0.51	0.48 – 0.54	0.64	0.62 – 0.66
up to 5th	0.48	0.45 – 0.50	0.64	0.62 – 0.66
up to 6th	0.46	0.44 – 0.48	0.64	0.62 – 0.66
up to 7th	0.46	0.43 – 0.48	0.63	0.62 – 0.65
up to 8th	0.45	0.43 – 0.48	0.63	0.62 – 0.65

Table 5.A2: *(continued).*

Branch order accumulated	Length radius - β			
	TreeQSM		Measured	
up to 2nd	2.40	2.22 – 2.63	2.27	1.98 – 2.46
up to 3rd	1.01	0.80 – 1.23	0.84	0.59 – 1.03
up to 4th	0.60	0.46 – 0.75	0.32	0.17 – 0.47
up to 5th	0.48	0.36 – 0.61	0.07	−0.06 – 0.22
up to 6th	0.44	0.32 – 0.56	0.11	−0.01 – 0.26
up to 7th	0.43	0.31 – 0.54	0.07	−0.06 – 0.20
up to 8th	0.42	0.31 – 0.54	0.07	−0.06 – 0.20

Table 5.A2: *(continued).*

Branch order accumulated	Metabolic rate - θ			
	TreeQSM		Measured	
up to 2nd	0.28	0.26 – 0.29	0.30	0.28 – 0.31
up to 3rd	0.28	0.39 – 0.56	0.47	0.43 – 0.53
up to 4th	0.47	0.50 – 0.62	0.58	0.52 – 0.65
up to 5th	0.56	0.52 – 0.65	0.51	0.45 – 0.58
up to 6th	0.58	0.51 – 0.64	0.50	0.44 – 0.56
up to 7th	0.58	0.52 – 0.65	0.50	0.44 – 0.56
up to 8th	0.58	0.52 – 0.65	0.50	0.44 – 0.57

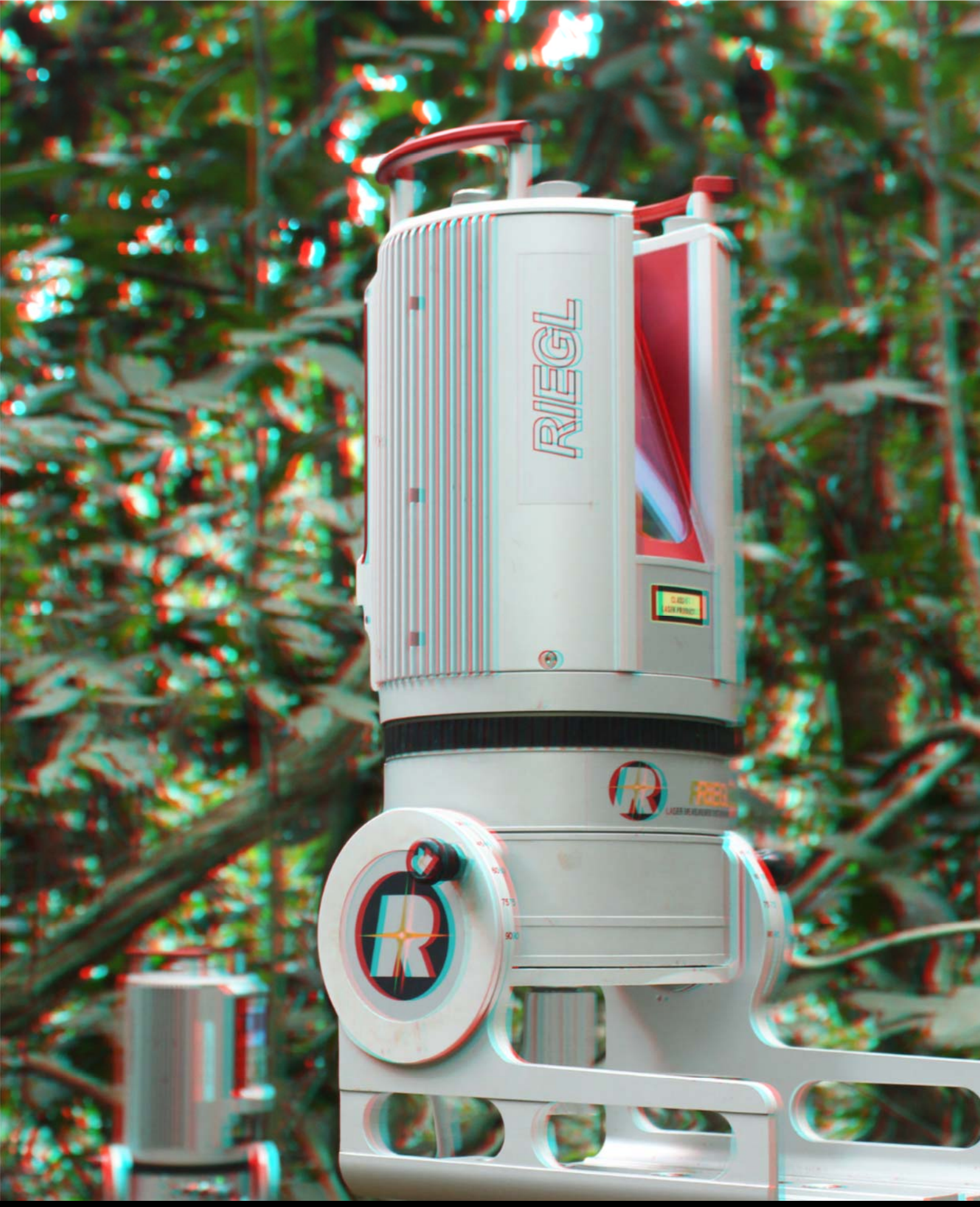

Ankasa Conservation Area, Ghana

Chapter 6

Synthesis

6.1 Main findings

The main objective of this thesis is to explore the use of 3D models from TLS point clouds to estimate above-ground biomass and architecture of tropical trees. From the estimations of AGB and tree architecture, I generated significant quality data for a better understanding of ecological challenges in tropical forests. Based on this objective, four research questions were defined in section 1.5. The previous chapters (2 to 5) addressed the research conducted in this thesis. In this chapter, I answer each of the research questions formulated in the Introduction based on my findings.

1. How accurately can above-ground biomass of tropical trees be estimated from TLS point clouds?

The key result from Chapter 2 and Chapter 3 is that **reconstructed tree volume with basic wood density values can estimate more accurately AGB that have less bias than pantropical allometric models**. In both chapters, I described an approach to estimate AGB based on tree volume and basic wood density values. The tree volume is reconstructed from 3D modelling of tropical trees TLS point clouds. AGB estimations were improved during this thesis. As a result, in Chapter 2 buttresses were assumed cylindrical, in Chapter 3 buttresses were modelled as meshes. Estimating the volume of buttresses reduced the uncertainties of buttresses modelling. The analysis in Chapter 2 was based on 29 trees across three pantropical regions (Peru, Indonesia, and Guyana) and in Chapter 3 the analysis was based on 26 trees in Guyana.

In Chapter 2, I demonstrated that AGB estimates from *TreeQSM* models had high agreement with the reference AGB and better agreement than when the pantropical models were assessed. AGB estimates from *TreeQSM* had an overall underestimation of 3.7 %, while AGB estimates from pantropical models had an overall underestimation ranging from 15.2 % to 35.7 % (Figure 2.5). Chapter 3 also demonstrated that AGB estimates from *TreeQSM* had the highest level of agreement, the highest R^2, and the smallest CV RMSE compared to the pantropical models assessed in this chapter. Both chapters demonstrated the systematic increasing AGB underestimation for large trees ($D > 70\,\text{cm}$) when estimated with allometric models (Figure 2.5). My results confirm the observations by Calders et al. (2015b) and show that this is also valid for tropical forests.

2. What is the capability of non-destructive TLS-based methods to derive allometric models for tropical trees?

The major result from Chapter 3 is that **allometric models can be built from TLS-derived tree volume and basic wood density with no need for destructive harvesting. The allometric models provide good agreement with reference data with almost unbiased estimates.** In Chapter 3, I developed allometric models to estimate AGB from trees in Guyana. These allometric models are based on TLS-derived

parameters, such as D, H, CD, and basic WD. I used *TreeQSM* to estimate AGB from TLS data in a similar approach as in Chapter 2. The TLS-derived allometric models were based on 72 scanned trees and I validated them with 26 harvested trees. To assess the ability of these TLS-derived allometric models, I compared my TLS-derived estimated AGB with AGB from five pantropical allometric models (Appendix 3A.2).

This approach not only evidenced the potential of TLS-derived allometric models to estimate accurately AGB from tropical forest in Guyana, but also that including CD provides a good agreement with reference data, while H worsens AGB estimates. I show that the pantropical models assessed in this study corroborated the systematic underestimation for small trees ($D \leq 70$ cm) with an increasing error for larger trees, as mentioned by Goodman et al. (2014) and Calders et al. (2015b). My findings contribute estimating tree metrics and TLS-derived methods to develop allometric models in Guyana. Although Chapter 3 is a case scenario for Guyana, the methodology presented is not dependent on the structure of the trees. My approach should accurately generate TLS-derived tree parameters from different types of forest and be able to build an allometric model that estimates AGB from any type of forest. An example is the assessment done by Stovall & Shugart (2018). In this study, they reconstructed 329 trees from a forest plot in Virginia, US in a similar approach as this chapter.

3. Can the branching architecture of tropical trees be linked to 3D models using their topological features?

Chapter 4 offered the first quantitative analysis branch-by-branch between *TreeQSM* models and manually measured branches. Chapter 4 demonstrated that **big branches (> 40 cm diameter) could be reconstructed accurately, while for smaller branches the accuracy decreased** when using *TreeQSM* and TLS approach. In Chapter 4, I reconstructed the branching architecture of tropical trees using TLS and *TreeQSM* and compared them to their manually measured counterparts. A total of 279 individual branches ($D > 10$ cm diameter) from 10 trees in Guyana were collected, scanned, and manually measured. To assess the accuracy of my approach, I analysed the following tree architecture parameters: branch length, branch diameter, branching order, absolute and cumulative tree length, and absolute and cumulative tree volume. An essential step in the methodology is that the manually measured branches and the QSM branches were visually paired branch-by-branch. By applying this step, I was able to match the QSM branches against their reference measurements to individual branch-level.

In Chapter 4, my approach identified and reconstructed 95 % of the measured branches thicker than 30 cm diameter, and correctly assigned the branching order in 99 % of the cases. Results also show that my approach overestimated branch length thicker than 50 cm by 1 % and underestimated diameter of branches between 20 cm to 60 cm by 8 %. A major limitation found in Chapter 4 was the conceptual difference where the main stem ends: between the manual measurements (Figure 4.1) and the *TreeQSM* model (Figure 4.2).

This ambiguous definition led to higher uncertainties in the length of the QSM models. An additional constraint was the low point density of the smaller branches. In response to these limitations, a series of recommendations were described to improve the accuracy of my approach. I recommended unifying the branch definitions between the TreeQSM branches and the measured branches. Although my results performed worse for smaller branches, my study still represents a breakthrough into studies of tree architecture based on TLS and *TreeQSM*. My findings can improve our understandings of tree architecture and how it may influence ecological processes or be shaped by those processes.

4. Does TLS-based branching architecture relate to metabolic scaling in tropical trees?

In Chapter 5, my analysis indicated that **only metabolic rate converged between the TLS-derived and manually measured values.** Results also indicated that neither branch radius nor branch length converged between the TLS-derived and manually measured values. From these two exponents, branch length was the exponent that deviated the most. The theoretical exponents from the WBE theory converged with TLS-derived and manually measured exponents only at tree-level. To estimate the metabolic scaling in tropical trees, I develop an approach to estimate these exponents from the TLS-derived branch architecture. The scaling exponents from the WBE model can be described using three parameters: branch radius scaling ratio, branch length scaling ratio, and branching ratios (West, 1999a). From these parameters, the architecture-based metabolic scaling ratio can be predicted. I used the results from Chapter 4 to estimate the scaling exponents. By applying the approach from Chapter 5, branch scaling ratio, length scaling ratio, and metabolic scaling can be estimated from TLS-derived branching architecture. To validate my analysis, I compared the TLS-derived scaling exponents against manually measured scaling exponents at three levels: branch-level, tree-level, and plot-level.

The major limitation found in Chapter 5 was the stem conceptual difference stated in the previous chapter. The large absolute error (70 cm) in the length between the TLS-derived and the manually measured branches caused a large divergence in the branch length scaling ratio (Table 5.3). Despite these results, my data did not show symmetrical fractal branching nor homogeneous branch and length parameters. Petit & Anfodillo (2009) argue that the symmetrical branching proposed by WBE theory cannot be found in real plants —my data can support their statement. Muller-Landau et al. (2006) and Petit & Anfodillo (2009) stated that WBE predictions might work on trees that grow in absence of competition or nutrient limitations, protected from environmental hazards, or in young trees. My dataset does not fall into these assumptions and might explain the divergence between my results and the WBE predictions. Despite the limitations, my findings contribute to a basis for a better understanding of the metabolic scaling and how I can estimate metabolic scaling using TLS-derived parameters.

6.2 Reflection and outlook

The research performed in this thesis was motivated by the need for estimating tree attributes for biomass and tree architecture that can help us increase the present collection of available tropical tree datasets. Within this context, this thesis revealed that tree attributes such as diameter, height, crown diameter, total volume, and branch lengths and diameters derived from TLS point clouds can be used to estimate biomass and define quantitatively the architecture of trees. Moreover, this thesis contributes scientifically to the development and assessment of new methods, and explores their practical use. In fact, I developed allometric models and calculated plant scaling exponents based on these TLS-derived parameters, and compared these estimates with those from traditionally inventoried data. Even though I found several limitations during this thesis, it offers great opportunities as an alternative for traditional forest inventory data and destructive sampling with ground-breaking results. In this section, I provide insight on some of the issues and limitations encountered, and an overview of current and upcoming developments on LiDAR research.

6.2.1 From traditional to digital fieldwork

Liang et al. (2016) indicated that three aspects shape the adaptation of any new technique for measuring trees in forest inventories: (i) the cost of the acquisition data, the post-processing, and interpretation of data should be affordable; (ii) the accuracy of the tree parameters estimation with the new technique should be at least at the same level or surpass the traditional technique; and (iii) the new technique should focus on tree attributes relevant for the decision-making process.

Regarding point (i); besides of the cost of the TLS instrument and licensed software, the fieldwork campaigns in this thesis were based on a strong cooperation between several institutions that provided logistics for before-, during-, and after-campaign. This cooperation allows us to share the costs and make efficient use of the resources allocated. Moreover, the gained experience from previous fieldworks incurs into a better use of resources by taking into account practical considerations when designing and executing a successfully fieldwork campaign. In this thesis, I used licensed software, and wherever possible, open-source software to perform analysis. Not only because of the extra cost for licensing software, but also because open-source software allows accessibility and usability for researchers with less resources, transparency, and greater shareability in the scientific community.

Concerning point (ii) and (iii); I demonstrated in Chapter 2 and 4 that tree attributes such as diameter, height, crown diameter, and branch lengths and diameters can be derived from TLS point clouds of tropical trees. Moreover; that not only these parameters can be

derived, but that the accuracy of these TLS-derived parameters have high agreement with reference data. Moreover, in Chapter 2, 3, and 4 I also showed that indirect estimates, such as AGB had also high agreement with reference data and allometric models can be built based on TLS-derived parameters. This thesis is a contribution towards an accurate estimation of tree parameters and derived estimates such as AGB, allometric models, and plant scaling. Destructive sampling is not an option at large-scale, and TLS-derived parameters could step in as an alternative to estimate tree parameters in tropical forests.

The miniaturization and mobilization of LiDAR instruments would allow a small team to scan forests plots within hours. Moreover, the up-scaling of tree algorithms from tree-level to plot-level would allow; not only to extract forest attributes such as diameter and height, but also to infer indirect attributes, such as tree volume, path length, and surface area in a semi-automatic way. In the near future, these technologies would be a basic component of any fieldwork campaign.

6.2.2 The art of tree modelling

The methods developed in this thesis employed *TreeQSM* modelling method to reconstruct quantitative structure models (QSMs) of tropical trees from point clouds. In Chapter 2, I evidenced that tree parameters could be derived from QSMs of tropical trees and in Chapter 4, I showed that the fine detail structure of tropical trees could be reconstructed. Both chapters evidenced the robustness of *TreeQSM* to model tropical trees. Nevertheless, *TreeQSM* is not the only modelling method available to model trees. Tree modelling is relevant in other fields, e.g., planning tree growth in agricultural projects, accurate representation of trees for video games, and tree models for urban planning (Bournez et al., 2017). Several algorithms, such as *PlantScan3D* (Boudon et al., 2014), *TreeArchitecture* (Landes et al., 2015), *SimpleTree* (Hackenberg et al., 2015a), and *VoxR* (Lecigne et al., 2018) were developed throughout these years and served different purposes.

Despite the great advances of these algorithms, challenges persist in the modelling process. A great challenge I found during the tree modelling process (besides extracting individual trees from the forest point cloud, which I discuss in the following section) is tuning the *TreeQSM* parameters to create the best representation of the tree point cloud. *TreeQSM* has several parameters that can be modified and the different combination of these parameters provide a different range of results. In Chapter 2, I developed an optimization for the most important parameter; and two years later, in Chapter 4, I used the semi-automatic optimization process developed by Burt (2017) to model tree point clouds. Whereas knowledge on *TreeQSM* is required for developing a manual optimization, no deep prior knowledge on *TreeQSM* is required for the semi-automatic optimization process. This

will enhance the usage of tree *TreeQSM* models among the scientific community.

Due to the random component of *TreeQSM* (Raumonen et al., 2013), it is suggested that a tree parameter should be used as the average value of 5 to 10 QSM models (Calders et al., 2015b). For the volume parameter in Chapter 2 and 3, we used the average of 20 QSMs to determine the volume value per tree. However, for detailed branch matching, as in Chapter 4, a manually branch-by-branch pairing was performed. One alternative approach used by Momo Takoudjou et al. (2018) was manually editing one single QSM model to closely resemble the tree point cloud. This approach could deal with point cloud issues, such as gaps due to occlusion, or noise in the point cloud. While editing a few trees is feasible, editing hundreds or thousands of trees at a plot-scale involve extensive hours of manual editing.

An important part of modelling tropical trees is the buttresses modelling. As stated before, the buttresses modelling improved from Chapter 2 to Chapter 3 (Figure 3.2). In Chapter 3, I used meshes to model the buttresses and estimate volume. Other studies also assessed the geometry of buttresses through meshes (Nölke et al., 2015; Bauwens et al., 2017; Momo Takoudjou et al., 2018). Nölke et al. (2015) analysed the geometry and allometry and Bauwens et al. (2017) used point clouds from terrestrial close-range photogrammetry for measuring and modelling buttresses with high concordance. My results in Chapter 3 and the results from Momo Takoudjou et al. (2018) also indicated high concordance between total tree volume with buttresses and their reference counterpart.

Throughout this thesis, I evidenced that the main stem and branches (until certain diameter) can be reconstructed with cylindrical features from TLS point clouds of tropical trees. Moreover, my results support similar research by Calders et al. (2015b); Rahman et al. (2017); Momo Takoudjou et al. (2018); and Disney et al. (2018) in tropical and evergreen trees. Nevertheless, a TLS tree point cloud also includes leaves. While on deciduous trees, one has the opportunity to scan a tree in a leaf-off condition; in evergreen trees, one does not have this chance. Analysing separately hard tissue (stem and branches) from soft tissue (leaves, fruits) is relevant for AGB estimation (this thesis), classification of vegetation elements (Li et al., 2018), gap fraction, and leaf area index (LAI; Zhu et al., 2018). In Chapter 3, I digitally defoliated the tree sample using a leaf/wood separation algorithm from Vicari (2017; Figure 3.1c). This algorithm detects trunk and larger branches first, and then unsupervised classification assigns the remaining points as leaves (Disney et al., 2018). Having a digital defoliated tree point cloud improves the *TreeQSM* reconstruction and reduces the chance of creating non-existent branches.

Other type of research needs to create a high realistic 3D virtual forest. Despite TLS point clouds include leaves, their reconstructing still (to my knowledge) not attainable. To cope with that, Åkerblom et al. (2018) developed an algorithm to insert leaves (broadleaves or needle leaves) into QSMs structures. Measuring individual leaves seems an impossible

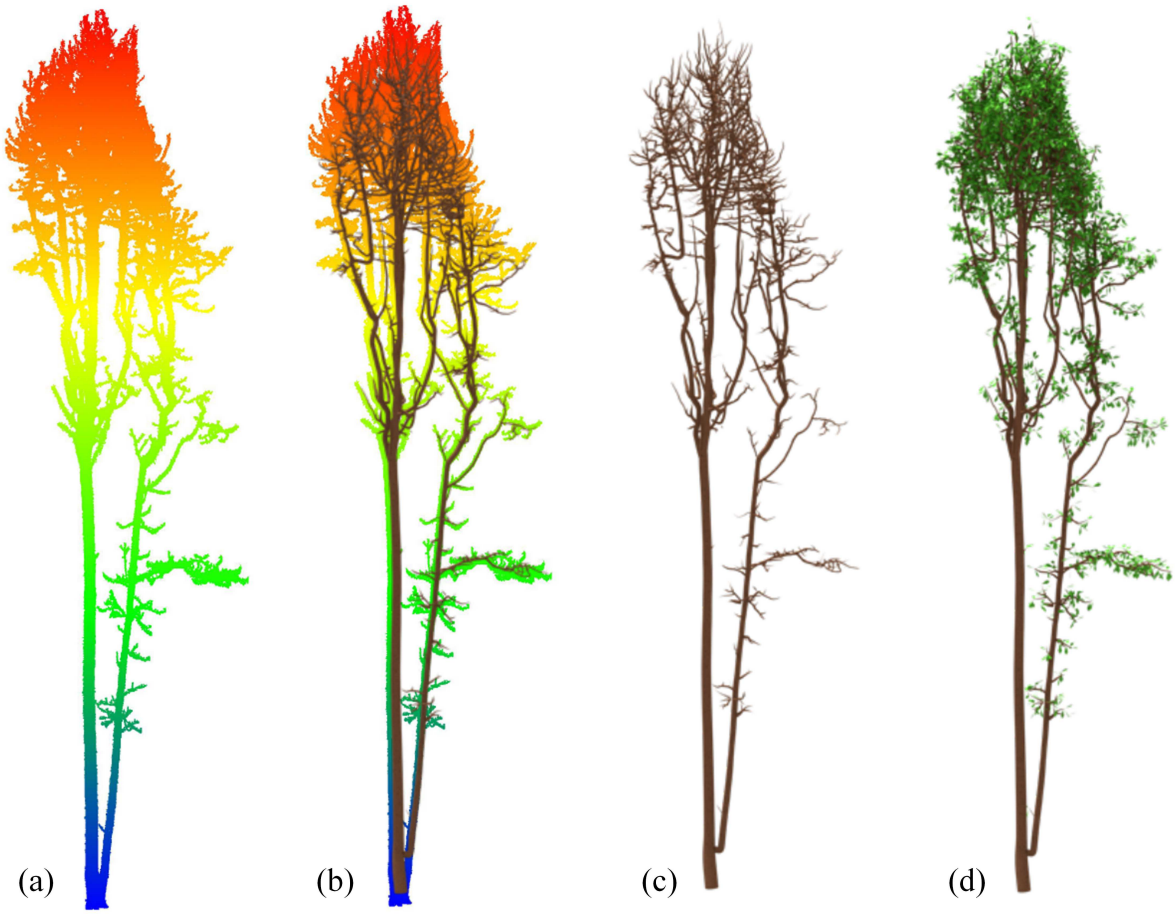

Figure 6.1: (a) TLS leaf-off point cloud of Sycamore (*Acer pseudoplatanus*) coloured by height from 0 m (blue) to 25.9 m (red), (b) TLS point cloud and QSM, (c) standalone QSM, and (d) QSM with added leaves; modified from Calders et al. (2018).

task. This algorithm generates digital leaves and insert them in a realistic way that certain leaf properties can be estimated. Calders et al. (2018) recreated a 3D virtual forest in Wytham Woods (Oxford, UK) and used this algorithm to generate digital leaves (Figure 6.1) for radiate transfer modelling. Although now seems an impossible task to reconstruct individual leaves from trees, it seems plausible that modelling individual leaves would be the next step in tree modelling. With enough points to define a leaf, algorithms might be able to detect leaves, either by shape or by colour, identify them, and model individually. This digital leaf would be inserted back to where the real leaf is and create a high realistic 3D virtual forest.

6.2.3 From trees to plots

One limitation I encountered in this thesis was the manual extraction of individual tree point clouds from the massive plot-level point cloud. Delineating and manually extracting

each tree point cloud is time-consuming and highly prone to errors due to the complexity of the forest structure. For Chapters 2, 4, and 5 a colleague and I manually extracted 29 trees. These chapters aimed to characterize individual trees and the 29 trees served their purpose. Nevertheless, Chapter 3 aimed to develop an allometric model based on TLS-derived parameters. For that, a greater number of trees was required. A total of 106 tree individual point clouds were extracted. To extract these trees, a semi-automatic tree segmentation algorithm, *treeseg*; Burt (2017), was applied.

Semi-automatic tree segmentations are needed to assist in the extraction of individual trees. A few studies have developed also other tree segmentation approaches. One of the pioneers was Raumonen et al. (2015). They developed an automated extraction of individual trees from point cloud data based point cloud segmentation into stem and branches. Ayrey et al. (2017) developed *layer stacking* algorithm. This segmentation method slices the entire forest point cloud and isolates trees in each slice later. In addition, Trochta et al. (2017) developed *3D forest*, an algorithm that uses the distance between points and clusters to segment trees. These algorithms were tested and performed well in particular forest type: deciduous forest in leaf-off stage.

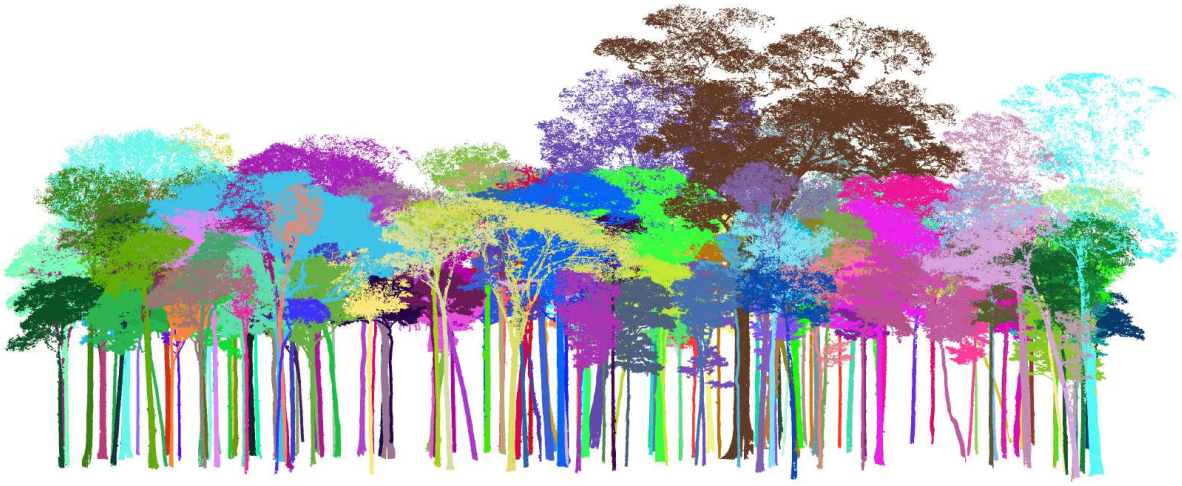

Figure 6.2: Individual tropical tree point clouds in Brazil using *treeseg*; from Burt (2017).

The algorithm I used in Chapter 3, *treeseg*, was developed by Burt (2017). His algorithm has been tested on deciduous forests (Disney et al., 2018; Calders et al., 2018), but also in tropical environments (Chapter 4 of this thesis, Burt, 2017; Disney et al., 2018) as shown in Figure 6.2. These segmentation algorithms are the next step in modelling tree point clouds. The extraction of tree parameters with little or no human interaction allow me to model entire forest plots within days and recreate a real 3D virtual forest with a detailed reconstruction of every tree.

Massive reconstruction of trees is particular relevant for plot-level research; such as Radiative Transfer Modelling (Calders et al., 2018), or developing allometric models, or

estimating forest AGB for calibration plot for space-born missions with more realistic features (individual leaves, branches, and stems). Having this quality of detail in a virtual forest would allow researchers to understand the dynamics of forests and be able to link between TLS-derived ground measurements and high-resolution remote sensing, or airborne LiDAR or, even spaceborne LiDAR.

I foresee that semi-automatic tree segmentation algorithms will have important developments within these five years. The number of tropical forests plots TLS scanned is increasing greatly and the demand for extracting hundreds of tropical trees is increasing exponentially. Most of the research done today with TLS are proof of concept research and the next step, up-scaling analysis, will require the extraction of hundreds or thousands of tree point clouds.

6.2.4 TLS-derived allometry for greenhouse inventories

The economical and policy framework of the United Nations' REDD+ is a global effort to create a monetary value for the carbon in forests (Hunter et al., 2013). This framework allows countries that demonstrate emissions reductions to access a (monetary or non-monetary) compensation from the international carbon market (Gibbs et al., 2007). However, to ensure a fair and adequate compensation based on the measurement, reporting, and verification (MRV) of carbon pools; it is essential to quantify carbon stocks with the lowest possible uncertainty (Hunter et al., 2013) within the country's capacities and capabilities (Henry et al., 2015).

In Chapter 3, I evidenced that TLS-derived allometric models can estimate less biased AGB than pantropical allometric models in Guyana. Although Chapter 3 is a case study in Guyana, I am confident that the methodology from Chapter 3 can be adapted to different forest types and produce the same results. One example is Momo Takoudjou et al. (2018). They applied a similar methodology using TLS point clouds from trees in Cameroon and *SimpleTree* algorithm to calibrate pantropical allometric models with good results. These findings might be the starting point to consolidate TLS-derived allometric models as a robust alternative approach to estimate AGB for countries that are working towards a national REDD+ MRV system.

This thesis and other TLS-related researches reviewed in this thesis revealed that using TLS and 3D modelling is an alternative approach to traditional pantropical allometric models to estimate AGB in tropics. Nevertheless, the consolidation of a TLS-derived approach as part of the design and implementation of a MMRV system remains a challenge. The TLS-derived approach is a novel methodology that needs to be tested and refined in different tropical environments before to be assessed as a robust approach for a MMRV system. Moreover, the methodology should be based on open-source software to enhance the accessibility and reachability by experts and non-experts. To improve the

understanding of non-experts, capacity development, and training workshops should be integral part of the MMRV system to explore the capabilities and potentialities of using TLS for their own benefit.

6.2.5 Integrating LiDAR in remote sensing

An accurate assessment of forests AGB at global level is vital for climate change modelling at global scale, greenhouse inventories, and terrestrial carbon accounting (Dittmann et al., 2017). Remote sensing is widely considered an essential tool for monitoring deforestation and forest degradation. Remote sensing can provide data for monitoring national-scale forest area change in tropics; and, along with ground measurements provide an objective and practical cost-effective solution for developing REDD+ MMRV systems (De Sy et al., 2012).

Spaceborne ESA's BIOMASS (Eitel et al., 2016) and NASA's GEDI (`https://science.nasa.gov/missions/gedi`) missions are being developed and will incorporate LiDAR technology to provide large scale detailed information from above the canopy to assess carbon stocks. Uncertainty regarding plot-level biomass is present due to inadequate and unrepresentative allometric models to estimate AGB. Chapters 2 and 3 evidenced the potential of TLS to estimate AGB from tropical trees *in-situ*. Recently, Stovall & Shugart (2018) used 243 trees reconstructed from TLS to calibrate SAR- and LiDAR-based empirical biomass models. They found that TLS reduced plot-level RMSE and revealed a systematic underestimation in the allometric models used.

LiDAR technology is overcoming its own limitations and with the new advances discussed in this thesis, TLS has the theoretical potential to provide accurate data to calibrate algorithms from space-born missions and link to ground observations. LiDAR-derived assessments could synergy with other two-dimension remote sensing imageries to provide high detailed vegetation metrics. This synergy would allow us to add explicitly structural 3D information to the remote sensing imagery and characterize individual tree attributes up scaling to plot-level analysis.

6.2.6 Beyond terrestrial LiDAR

As stated in the Introduction, the TLS point clouds analysed in this thesis were acquired using a RIEGL VZ-400 terrestrial LiDAR (Figure 1.2). Wilkes et al. (2017) presented their experience using RIEGL VZ-400 terrestrial LiDAR in 27 field campaigns, in which I contributed with three of them. Nevertheless, there are several commercial terrestrial LiDARs available, and picking the right one is a matter of budget and the aim of the research.

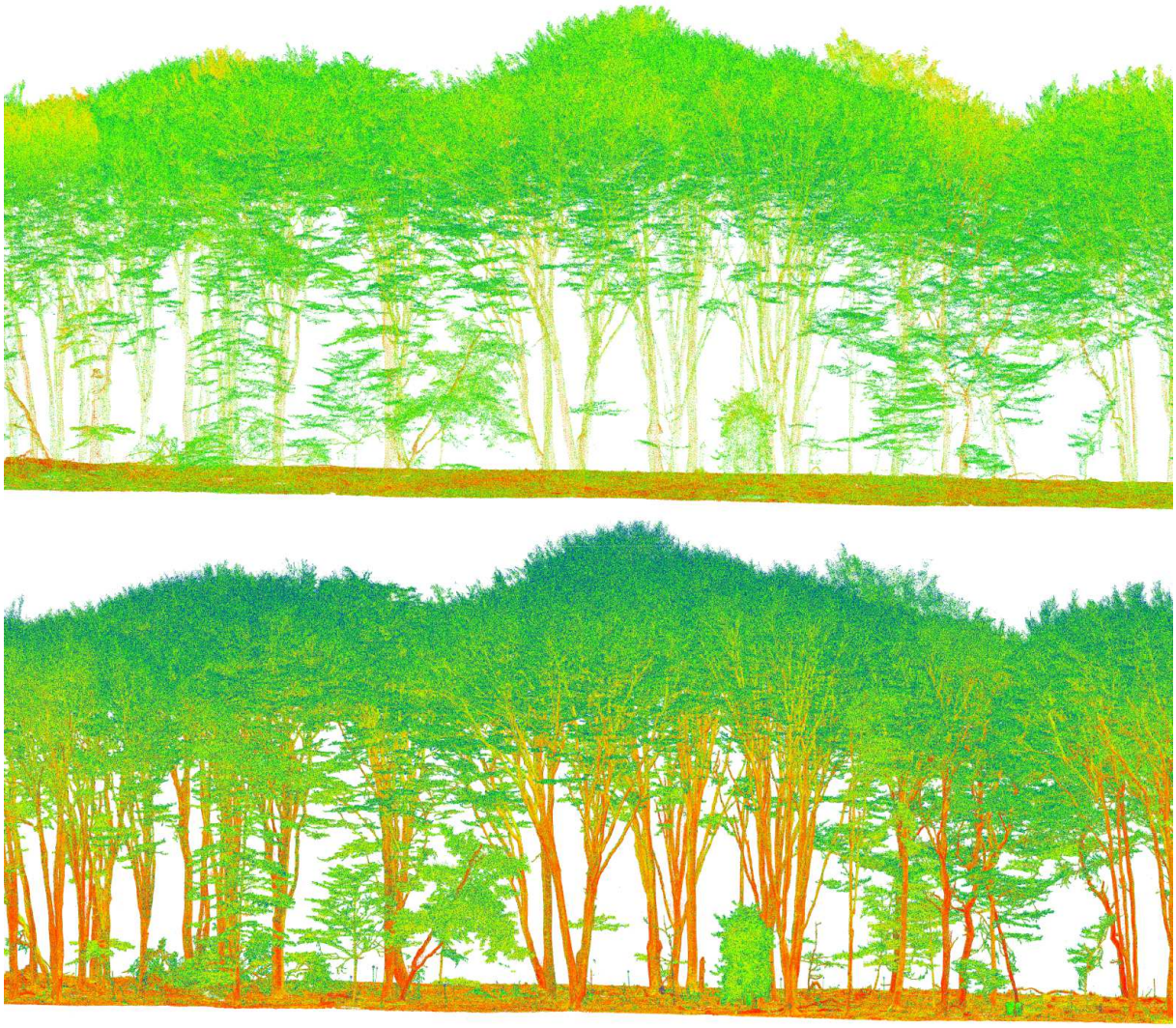

Figure 6.3: Point cloud composite from UAV LiDAR (top), and TLS (bottom) for an Old beech and Oak forest coloured by apparent reflectance from low (blue) to high (red); modified from Brede et al. (2017).

In addition to the commercial scanners available, other research groups have developed several experimental TLS instruments specifically for forestry applications. The single wavelength Echidna (Strahler et al., 2008), the Dual-Wavelength Echidna Laser scanner — DWEL (Douglas et al., 2015), the Compact Biomasss LiDAR — CBL (Paynter et al., 2016), the Salford Advanced Laser Canopy Analyser — SALCA (Danson et al., 2014), and the VEGgetation monitoring NETwork — VEGNET (Culvenor et al., 2014) are one of the few instruments developed by other research groups around the globe. These instruments have been designed for specific tree attributes: volumetric models for the CBL (Paynter et al., 2018), vegetation properties for the SALCA instrument (Hancock et al., 2017), and plant area index for the VEGNET (Portillo-Quintero et al., 2014) with successful results.

In the recent years, laser scanners have been mounted on different platforms to improve the effort acquisitions of medium to large areas. LiDAR instruments became more portable and with the raising popularity of Unmanned Aerial Vehicles (UAVs) for forest surveys, laser scanner has been mounted on UAVs and able to scan large areas in less time and use these point clouds to extract basic tree parameters with enough accuracy as TLS point clouds (Wallace et al., 2016; Brede et al., 2017). The RIEGL RiCOPTER with VUX® - 1UAV (RIEGL Laser Measurements Systems, GmbH, Horn, Austria) is a 2D laser scanner mounted on a UAV. However, the UAV-LiDAR incorporates the best features of both systems. As being an UAV system, it is able to scan in low altitude, closer to the canopy of trees compared to airborne LiDAR; which is mounted on airplanes. Moreover, due to the low altitude flight, it provides a better side view of the understory than airborne LiDAR. This is important for the structural description of forests. In addition, the UAV-LiDAR is able to scan larger areas in less time than using TLS with interesting results. In Brede et al. (2017), a comparison between the RIEGL RiCOPTER and the VZ-400 TLS concluded that RiCOPTER has the potential to acquire enough information (Figure 6.3) to perform comparable to TLS for estimating canopy height and diameter at breast height, under forest conditions. Future research should test the *TreeQSM* models with tree point clouds from UAV LiDAR.

Tambopata National Reserve, Peru

References

Åkerblom, M. (2017). Inversetampere/Treeqsm: Initial Release. doi:10.5281/zenodo.844626.

Åkerblom, M., Raumonen, P., Casella, E., Disney, M. I., Danson, F. M., Gaulton, R., Schofield, L. A., & Kaasalainen, M. (2018). Non-intersecting leaf insertion algorithm for tree structure models. *Interface Focus*, *8*, 20170045. doi:10.1098/rsfs.2017.0045.

Åkerblom, M., Raumonen, P., Mäkipää, R., & Kaasalainen, M. (2017). Automatic tree species recognition with quantitative structure models. *Remote Sensing of Environment*, *191*, 1–12. doi:10.1016/j.rse.2016.12.002.

Alvarez, E., Duque, A., Saldarriaga, J., Cabrera, K., de las Salas, G., del Valle, I., Lema, A., Moreno, F., Orrego, S., & Rodríguez, L. (2012). Tree above-ground biomass allometries for carbon stocks estimation in the natural forests of Colombia. *Forest Ecology and Management*, *267*, 297–308. doi:10.1016/j.foreco.2011.12.013.

Avitabile, V. et al. (2016). An integrated pan-tropical biomass map using multiple reference datasets. *Global Change Biology*, *22*, 1406–1420. doi:10.1111/gcb.13139.

Ayrey, E., Fraver, S., Kershaw, J. A., Kenefic, L. S., Hayes, D., Weiskittel, A. R., & Roth, B. E. (2017). Layer Stacking: A Novel Algorithm for Individual Forest Tree Segmentation from LiDAR Point Clouds. *Canadian Journal of Remote Sensing*, *43*, 16–27. doi:10.1080/07038992.2017.1252907.

Baccini, A., Goetz, S. J., Walker, W. S., Laporte, N. T., Sun, M., Sulla-Menashe, D., Hackler, J., Beck, P. S. A., Dubayah, R., Friedl, M. A., Samanta, S., & Houghton, R. A. (2012). Estimated carbon dioxide emissions from tropical deforestation improved by carbon-density maps. *Nature Climate Change*, *2*, 182–185. doi:10.1038/nclimate1354.

Baskerville, G. L. (1972). Use of Logarithmic Regression in the Estimation of Plant Biomass. *Canadian Journal of Forest Research*, *2*, 49–53. doi:10.1139/x72-009. `arXiv:arXiv:1011.1669v3`.

Bauwens, S., Bartholomeus, H., Calders, K., & Lejeune, P. (2016). Forest Inventory with Terrestrial LiDAR: A Comparison of Static and Hand-Held Mobile Laser Scanning. *Forests*, *7*, 127. doi:10.3390/f7060127.

Bauwens, S., Fayolle, A., Gourlet-Fleury, S., Ndjele, L. M., Mengal, C., & Lejeune, P.

(2017). Terrestrial photogrammetry: a non-destructive method for modelling irregularly shaped tropical tree trunks. *Methods in Ecology and Evolution*, *8*, 460–471. doi:10.1111/2041-210X.12670.

Bentley, L. P., Stegen, J. C., Savage, V. M., Smith, D. D., von Allmen, E. I., Sperry, J. S., Reich, P. B., & Enquist, B. J. (2013). An empirical assessment of tree branching networks and implications for plant allometric scaling models. *Ecology Letters*, *16*, 1069–1078. doi:10.1111/ele.12127.

Berger, A., Gschwantner, T., McRoberts, R. E., & Schadauer, K. (2014). Effects of Measurement Errors on Individual Tree Stem Volume Estimates for the Austrian National Forest Inventory. *Forest Science*, *60*, 14–24. doi:10.5849/forsci.12-164.

Bezdek, J. C. (1981). *Pattern Recognition with Fuzzy Objective Function Algorithms* volume 25. Boston, MA: Springer US. doi:10.1007/978-1-4757-0450-1.

Blanchard, E. et al. (2016). Contrasted allometries between stem diameter, crown area, and tree height in five tropical biogeographic areas. *Trees*, *30*, 1953–1968. doi:10.1007/s00468-016-1424-3.

Boudon, F., Preuksakarn, C., Ferraro, P., Diener, J., Nacry, P., Nikinmaa, E., & Godin, C. (2014). Quantitative assessment of automatic reconstructions of branching systems obtained from laser scanning. *Annals of Botany*, *114*, 853–862. doi:10.1093/aob/mcu062.

Bournez, E., Landes, T., Saudreau, M., Kastendeuch, P., & Najjar, G. (2017). From TLS point clouds to 3D models of trees: A comparison of existing algorithms for 3D tree reconstruction. *International Archives of the Photogrammetry, Remote Sensing and Spatial Information Sciences*, *XLII-2/W3*, 113–120. doi:10.5194/isprs-archives-XLII-2-W3-113-2017.

Brede, B., Lau, A., Bartholomeus, H. M., & Kooistra, L. (2017). Comparing RIEGL RiCOPTER UAV LiDAR Derived Canopy Height and DBH with Terrestrial LiDAR. *Sensors*, *17*, 2371. doi:10.3390/s17102371.

Bremer, M., Rutzinger, M., & Wichmann, V. (2013). Derivation of tree skeletons and error assessment using LiDAR point cloud data of varying quality. *ISPRS Journal of Photogrammetry and Remote Sensing*, *80*, 39–50. doi:10.1016/j.isprsjprs.2013.03.003.

Burt, A. (2017). *New 3D measurements of forest structure*. Doctoral thesis University College London.

Burt, A., Disney, M., Raumonen, P., Armston, J., Calders, K., & Lewis, P. (2013). Rapid characterisation of forest structure from TLS and 3D modelling. In *2013 IEEE International Geoscience and Remote Sensing Symposium - IGARSS* 128.197.168.195 (pp. 3387–3390). IEEE. doi:10.1109/IGARSS.2013.6723555.

Butt, N., Epps, K., Overman, H., Iwamura, T., & Fragoso, J. M. (2015). Assessing carbon stocks using indigenous peoples' field measurements in Amazonian Guyana.

Forest Ecology and Management, *338*, 191–199. doi:10.1016/j.foreco.2014.11.014.

Calders, K., Burt, A., Newnham, G. G., Disney, M., Murphy, S., Raumonen, P., Herold, M., Culvenor, D., Armston, J., Avitabile, V., & Kaasalainen, M. (2015a). Reducing uncertainties in above-ground biomass estimates using terrestrial laser scanning. In *Proceedings of Silvilaser* (pp. 197–199). La Grande Motte, France: IRSTEA, IGN.

Calders, K., Burt, A., Origo, N., Disney, M., Nightingale, M., Raumonen, P., Akerblom, M., & Lewis, P. (2018). Realistic Forest Stand Reconstruction from Terrestrial LiDAR for Radiative Transfer Modelling. *Remote Sensing; in press*, (pp. 1–15). doi:10.3390/rs10060933.

Calders, K., Newnham, G. G., Burt, A., Murphy, S., Raumonen, P., Herold, M., Culvenor, D., Avitabile, V., Disney, M., Armston, J., & Kaasalainen, M. (2015b). Nondestructive estimates of above-ground biomass using terrestrial laser scanning. *Methods in Ecology and Evolution*, *6*, 198–208. doi:10.1111/2041-210X.12301.

Calders, K., Newnham, G. G., Herold, M., Murphy, S., Culvenor, D., Raumonen, P., Burt, A., Armston, J., Avitabile, V., & Disney, M. (2013). Estimating above ground biomass from terrestrial laser scanning in Australian Eucalypt Open Forest. *Silvilaser 2013, October 9-11, Beijing, China*, *di*, 90–97.

Chambers, J. Q., dos Santos, J., Ribeiro, R. J., Higuchi, N., dos Santos, J., Ribeiro, R. J., & Higuchi, N. (2001). Tree damage, allometric relationships, and above-ground net primary production in central Amazon forest. *Forest Ecology and Management*, *152*, 73–84. doi:10.1016/S0378-1127(00)00591-0.

Chave, J. (2005). Measuring tree height for tropical forest trees-A field manual.

Chave, J. et al. (2005). Tree allometry and improved estimation of carbon stocks and balance in tropical forests. *Oecologia*, *145*, 87–99. doi:10.1007/s00442-005-0100-x.

Chave, J., Condit, R., Aguilar, S., Hernandez, A., Lao, S., & Perez, R. (2004). Error propagation and scaling for tropical forest biomass estimates. *Philosophical Transactions of the Royal Society B: Biological Sciences*, *359*, 409–420. doi:10.1098/rstb.2003.1425.

Chave, J., Coomes, D., Jansen, S., Lewis, S. L., Swenson, N. G., & Zanne, A. E. (2009). Towards a worldwide wood economics spectrum. *Ecology Letters*, *12*, 351–366. doi:10.1111/j.1461-0248.2009.01285.x.

Chave, J. et al. (2014). Improved allometric models to estimate the aboveground biomass of tropical trees. *Global change biology*, (pp. 3177–3190). doi:10.1111/gcb.12629.

Chéné, Y., Rousseau, D., Lucidarme, P., Bertheloot, J., Caffier, V., Morel, P., Belin, É., & Chapeau-Blondeau, F. (2012). On the use of depth camera for 3D phenotyping of entire plants. *Computers and Electronics in Agriculture*, *82*, 122–127. doi:10.1016/j.compag.2011.12.007.

Clark, D. B., & Kellner, J. R. (2012). Tropical forest biomass estimation and the

fallacy of misplaced concreteness. *Journal of Vegetation Science*, *23*, 1191–1196. doi:10.1111/j.1654-1103.2012.01471.x.

Côté, J.-F., Fournier, R. A., Frazer, G. W., & Olaf Niemann, K. (2012). A fine-scale architectural model of trees to enhance LiDAR-derived measurements of forest canopy structure. *Agricultural and Forest Meteorology*, *166-167*, 72–85. doi:10.1016/j.agrformet.2012.06.007.

Culvenor, D., Newnham, G., Mellor, A., Sims, N., & Haywood, A. (2014). Automated In-Situ Laser Scanner for Monitoring Forest Leaf Area Index. *Sensors*, *14*, 14994–15008. doi:10.3390/s140814994.

Danson, F. M., Gaulton, R., Armitage, R. P., Disney, M., Gunawan, O., Lewis, P., Pearson, G., & Ramirez, A. F. (2014). Developing a dual-wavelength full-waveform terrestrial laser scanner to characterize forest canopy structure. *Agricultural and Forest Meteorology*, *198-199*, 7–14. doi:10.1016/j.agrformet.2014.07.007.

Dassot, M., Barbacci, A., Colin, A., Fournier, M., & Constant, T. (2010). Tree architecture and biomass assessment from terrestrial LiDAR measurements: a case study for some Beech trees (Fagus Sylvatica).

Dassot, M., Colin, A., Santenoise, P., Fournier, M., & Constant, T. (2012). Terrestrial laser scanning for measuring the solid wood volume, including branches, of adult standing trees in the forest environment. *Computers and Electronics in Agriculture*, *89*, 86–93. doi:10.1016/j.compag.2012.08.005.

Dassot, M., Constant, T., & Fournier, M. (2011). The use of terrestrial LiDAR technology in forest science: application fields, benefits and challenges. *Annals of Forest Science*, *68*, 959–974. doi:10.1007/s13595-011-0102-2.

De Sy, V., Herold, M., Achard, F., Asner, G. P., Held, A., Kellndorfer, J., & Verbesselt, J. (2012). Synergies of multiple remote sensing data sources for REDD+ monitoring. doi:10.1016/j.cosust.2012.09.013.

Delagrange, S., Jauvin, C., & Rochon, P. (2014). PypeTree: A Tool for Reconstructing Tree Perennial Tissues from Point Clouds. *Sensors*, *14*, 4271–4289. doi:10.3390/s140304271.

Disney, M., Burt, A., Calders, K., Raumonen, P., Gonzalez de Tanago, J., Sanchez, A. C., Avitabile, V., Herold, M., Armston, J., Lewis, S., Lines, E., & Lewis, P. (2014). New applications of 3D measurement & modelling for quantifying forest structure & biomass. In *Proceedings of the IC Global Vegetation Monitoring and Modeling (GV2M)* (pp. 208 – 209). Avignon, France.

Disney, M. I., Boni Vicari, M., Burt, A., Calders, K., Lewis, S. L., Raumonen, P., & Wilkes, P. (2018). Weighing trees with lasers: advances, challenges and opportunities. *Interface Focus*, *8*, 20170048. doi:10.1098/rsfs.2017.0048.

Dittmann, S., Thiessen, E., & Hartung, E. (2017). Applicability of different non-invasive methods for tree mass estimation: A review. *Forest Ecology and Management*, *398*, 208–215. doi:10.1016/j.foreco.2017.05.013.

Djomo, A. N., & Chimi, C. D. (2017). Tree allometric equations for estimation of above, below and total biomass in a tropical moist forest: Case study with application to remote sensing. *Forest Ecology and Management*, *391*, 184–193. doi:10.1016/j.foreco.2017.02.022.

Doetterl, S., Kearsley, E., Bauters, M., Hufkens, K., Lisingo, J., Baert, G., Verbeeck, H., & Boeckx, P. (2015). Aboveground vs. Belowground Carbon Stocks in African Tropical Lowland Rainforest: Drivers and Implications. *PLOS ONE*, *10*, e0143209. doi:10.1371/journal.pone.0143209.

Douglas, E. S., Martel, J., Li, Z., Howe, G., Hewawasam, K., Marshall, R. A., Schaaf, C. L., Cook, T. A., Newnham, G. J., Strahler, A., & Chakrabarti, S. (2015). Finding Leaves in the Forest: The Dual-Wavelength Echidna Lidar. *IEEE Geoscience and Remote Sensing Letters*, *12*, 776–780. doi:10.1109/LGRS.2014.2361812.

Eitel, J. U. et al. (2016). Beyond 3-D: The new spectrum of lidar applications for earth and ecological sciences. *Remote Sensing of Environment*, *186*, 372–392. doi:10.1016/j.rse.2016.08.018.

Fayolle, A., Loubota Panzou, G. J., Drouet, T., Swaine, M. D., Bauwens, S., Vleminckx, J., Biwole, A., Lejeune, P., & Doucet, J.-L. (2016). Taller trees, denser stands and greater biomass in semi-deciduous than in evergreen lowland central African forests. *Forest Ecology and Management*, *374*, 42–50. doi:10.1016/j.foreco.2016.04.033.

Feldpausch, T. R. et al. (2012). Tree height integrated into pantropical forest biomass estimates. *Biogeosciences*, *9*, 3381–3403. doi:10.5194/bg-9-3381-2012.

Gaaliche, B., Aiachi-Mezghani, M., Trad, M., Costes, E., Lauri, P.-E., & Mars, M. (2016). Shoot Architecture and Morphology of Different Branch Orders in Fig Tree (Ficus carica L.). *International Journal of Fruit Science*, *16*, 378–394. doi:10.1080/15538362.2015.1126699.

Gibbs, H. K., Brown, S., Niles, J. O., & Foley, J. A. (2007). Monitoring and estimating tropical forest carbon stocks: making REDD a reality. *Environmental Research Letters*, *2*, 045023. doi:10.1088/1748-9326/2/4/045023.

Goetz, S. J., & Dubayah, R. (2011). Advances in remote sensing technology and implications for measuring and monitoring forest carbon stocks and change. *Carbon Management*, *2*, 231–244. doi:10.4155/cmt.11.18.

Gonzalez de Tanago, J., Lau, A., Bartholomeus, H., Herold, M., Avitabile, V., Raumonen, P., Martius, C., Goodman, R. C., Disney, M., Manuri, S., Burt, A., & Calders, K. (2017). Estimation of above-ground biomass of large tropical trees with terrestrial LiDAR. *Methods in Ecology and Evolution*, *2017*, 1–12. doi:10.1111/2041-210X.12904.

Gonzalez de Tanago, J., Lau, A., Bartholomeus, H., Herold, M., Raumonen, P., & Avitabile, V. (2016). Quantification of Tropical Forest Biomass with Terrestrial LiDAR and 3D Tree Quantitative Structure Modelling.

Goodman, R. C., & Herold, M. (2014). Why Maintaining Tropical Forests Is Essential and Urgent for a Stable Climate. . doi:10.2139/ssrn.2622749.

Goodman, R. C., Phillips, O. L., & Baker, T. R. (2012). Tightening up on tree carbon estimates. *Nature*, *491*, 527–527. doi:10.1038/491527b.

Goodman, R. C., Phillips, O. L., & Baker, T. R. (2013). Data from: The importance of crown dimensions to improve tropical tree biomass estimates. doi:10.5061/dryad.p281g.

Goodman, R. C., Phillips, O. L., & Baker, T. R. (2014). The importance of crown dimensions to improve tropical tree biomass estimates. *Ecological Applications*, *24*, 680–698. doi:10.1890/13-0070.1.

Grau, E., Durrieu, S., Fournier, R., Gastellu-Etchegorry, J.-P., & Yin, T. (2017). Estimation of 3D vegetation density with Terrestrial Laser Scanning data using voxels. A sensitivity analysis of influencing parameters. *Remote Sensing of Environment*, *191*, 373–388. doi:10.1016/j.rse.2017.01.032.

Guyana Lands and Surveys Commission (2013). *Guyana National Land Use Plan*. June. Georgetown: Guyana Lands and Surveys Commission.

Hackenberg, J., Morhart, C., Sheppard, J., Spiecker, H., & Disney, M. (2014). Highly Accurate Tree Models Derived from Terrestrial Laser Scan Data: A Method Description. *Forests*, *5*, 1069–1105. doi:10.3390/f5051069.

Hackenberg, J., Spiecker, H., Calders, K., Disney, M., & Raumonen, P. (2015a). SimpleTree —An Efficient Open Source Tool to Build Tree Models from TLS Clouds. *Forests*, *6*, 4245–4294. doi:10.3390/f6114245.

Hackenberg, J., Wassenberg, M., Spiecker, H., & Sun, D. (2015b). Non Destructive Method for Biomass Prediction Combining TLS Derived Tree Volume and Wood Density. *Forests*, *6*, 1274–1300. doi:10.3390/f6041274.

Hallé, F., & Oldeman, R. (1970). *Essai sur l'architecture et la dynamique de croissance des arbres tropicaux*. Monographie de Botanique et de Biologie Végétale. {M}asson.

Hallé, F., Oldeman, R. A. A., & Tomlinson, P. B. (1978). *Tropical Trees and Forests*. Berlin, Heidelberg: Springer Berlin Heidelberg. doi:10.1007/978-3-642-81190-6.

Hancock, S., Gaulton, R., & Danson, F. M. (2017). Angular Reflectance of Leaves With a Dual-Wavelength Terrestrial Lidar and Its Implications for Leaf-Bark Separation and Leaf Moisture Estimation. *IEEE Transactions on Geoscience and Remote Sensing*, *55*, 3084–3090. doi:10.1109/TGRS.2017.2652140.

Henning, J. G., & Radtke, P. J. (2006). Detailed stem measurements of standing trees from ground-based scanning lidar. *Forest Science*, *52*, 67–80.

Henry, M. et al. (2015). Recommendations for the use of tree models to estimate national forest biomass and assess their uncertainty. *Annals of Forest Science*, *72*, 769–777. doi:10.1007/s13595-015-0465-x.

Holopainen, M., Vastaranta, M., & Kankare, V. (2011). Biomass estimation of individual trees using stem and crown diameter TLS measurements. *International Archives of Photogrammetry, Remote Sensing and Spatial Information Sciences*, *XXXVIII*, 29–31.

Huang, H., Li, Z., Gong, P., Cheng, X., Clinton, N., Cao, C., Ni, W., & Wang, L. (2011). Automated Methods for Measuring DBH and Tree Heights with a Commercial Scanning Lidar. *Photogrammetric Engineering & Remote Sensing*, *77*, 219–227. doi:10.14358/PERS.77.3.219.

Hunter, M., Keller, M., Victoria, D., & Morton, D. C. (2013). Tree height and tropical forest biomass estimation. *Biogeosciences*, *10*, 8385–8399. doi:10.5194/bg-10-8385-2013.

IPCC (2006). *2006 IPCC Guidelines for National Greenhouse Gas Inventories*. Kanagawa: Institute for Global Environmental Strategies (IGES).

Isaac, N. J. B., & Carbone, C. (2010). Why are metabolic scaling exponents so controversial? Quantifying variance and testing hypotheses. *Ecology Letters*, *13*, 728–735. doi:10.1111/j.1461-0248.2010.01461.x.

Jaya, A., Siregar, U. J., Daryono, H., & Suhartana, S. (2007). Biomassa hutan rawa gambut tropika pada berbagai kondisi penutupan lahan. *Jurnal Penelitian Hutan dan Konservasi Alam*, *4*, 341–352.

Jiménez-Rojas, E. M., Londoño, a. C., & Vester, H. F. M. (2002). Descripción de la arquitectura de Iryanthera tricornis, Osteophloeum platyspermum y Virola pavonis (Myristicaceae). *Caldasia*, *24*, 65–94.

Jucker, T. et al. (2017). Allometric equations for integrating remote sensing imagery into forest monitoring programmes. *Global Change Biology*, *23*, 177–190. doi:10.1111/gcb.13388.

Kaasalainen, S., Krooks, A., Liski, J., Raumonen, P., Kaartinen, H., Kaasalainen, M., Puttonen, E., Anttila, K., & Mäkipää, R. (2014). Change detection of tree biomass with terrestrial laser scanning and quantitative structure modelling. *Remote Sensing*, *6*, 3906–3922. doi:10.3390/rs6053906.

Kankare, V., Vastaranta, M., Holopainen, M., Räty, M., Yu, X., Hyyppä, J., Hyyppä, H., Alho, P., & Viitala, R. (2013). Retrieval of Forest Aboveground Biomass and Stem Volume with Airborne Scanning LiDAR. *Remote Sensing*, *5*, 2257–2274. doi:10.3390/rs5052257.

Kempes, C. P., West, G. B., Crowell, K., & Girvan, M. (2011). Predicting maximum tree heights and other traits from allometric scaling and resource limitations. *PLoS ONE*, *6*. doi:10.1371/journal.pone.0020551.

Király, G., & Brolly, G. (2007). Tree height estimation methods for terrestrial laser scanning in a forest reserve. *International Archives of Photogrammetry, Remote Sensing and Spatial Information Sciences*, *XXXVI*, 211–215.

Kitajima, K., Mulkey, S. S., & Wright, S. J. (2004). Variation in Crown Light Utilization Characteristics among Tropical Canopy Trees. *Annals of Botany*, *95*, 535–547. doi:10.1093/aob/mci051.

Krooks, A., Kaasalainen, S., Kankare, V., Joensuu, M., Raumonen, P., & Kaasalainen, M. (2014). Tree structure vs. height from terrestrial laser scanning and quantitative structure models. *Silva Fennica*, *48*, 1–11. doi:10.14214/sf.1125.

Kuyah, S., Dietz, J., Muthuri, C., Jamnadass, R., Mwangi, P., Coe, R., & Neufeldt, H. (2012). Allometric equations for estimating biomass in agricultural landscapes: I. Aboveground biomass. *Agriculture, Ecosystems and Environment*, *158*, 216–224. doi:10.1016/j.agee.2012.05.011.

Landes, T., Saudreau, M., Najjar, G., Kastendeuch, P., Guillemin, S., Colin, J., & Luhahe, R. (2015). 3D tree architecture modeling from laser scanning for urban microclimate study. In *9th International Conference on Urban Climate, 12th Symposium on the Urban Environment* Figure 1 (p. 6).

Lecigne, B., Delagrange, S., & Messier, C. (2018). Exploring trees in three dimensions: VoxR, a novel voxel-based R package dedicated to analysing the complex arrangement of tree crowns. *Annals of Botany*, *121*, 589–601. doi:10.1093/aob/mcx095.

van Leeuwen, M., Coops, N., Newnham, G. G., Hilker, T., Culvenor, D., & Wulder, M. A. (2011). Stem detection and measuring DBH using terrestrial laser scanning. *Silvilaser, Full proceedings*, (pp. 1–6).

Lewis, S. L., Lloyd, J., Sitch, S., Mitchard, E. T., & Laurance, W. F. (2009). Changing Ecology of Tropical Forests: Evidence and Drivers. *Annual Review of Ecology, Evolution, and Systematics*, *40*, 529–549. doi:10.1146/annurev.ecolsys.39.110707.173345.

Li, Z., Schaefer, M., Strahler, A., Schaaf, C., & Jupp, D. (2018). On the utilization of novel spectral laser scanning for three-dimensional classification of vegetation elements. *Interface Focus*, *8*, 20170039. doi:10.1098/rsfs.2017.0039.

Liang, X., Kankare, V., Hyyppä, J., Wang, Y., Kukko, A., Haggrén, H., Yu, X., Kaartinen, H., Jaakkola, A., Guan, F., Holopainen, M., & Vastaranta, M. (2016). Terrestrial laser scanning in forest inventories. *ISPRS Journal of Photogrammetry and Remote Sensing*, *115*, 63–77. doi:10.1016/j.isprsjprs.2016.01.006.

Loehle, C. (2016). Biomechanical constraints on tree architecture. *Trees*, *30*, 2061–2070. doi:10.1007/s00468-016-1433-2.

Malhi, Y., Jackson, T., Patrick Bentley, L., Lau, A., Shenkin, A., Herold, M., Calders, K., Bartholomeus, H., & Disney, M. I. (2018). New perspectives on the ecology of tree

structure and tree communities through terrestrial laser scanning. *Interface Focus*, *8*, 20170052. doi:10.1098/rsfs.2017.0052.

Manuri, S. et al. (2014). Tree biomass equations for tropical peat swamp forest ecosystems in Indonesia. *Forest Ecology and Management*, *334*, 241–253. doi:10.1016/j.foreco.2014.08.031.

McMahon, T. A., & Kronauer, R. E. (1976). Tree structures: deducing the principle of mechanical design. *Journal of theoretical biology*, *59*, 443–466. doi:10.1016/0022-5193(76)90182-X.

Meyer, V. et al. (2018). Canopy Area of Large Trees Explains Aboveground Biomass Variations across Nine Neotropical Forest Landscapes. *Biogeosciences Discussions*, (pp. 1–38). doi:10.5194/bg-2017-547.

Miller, R. B., & Détienne, P. (2001). *Major Timber Trees of Guyana. Wood Anatomy*. Tropenbos series (volume 20 ed.). Wageningen, the Netherlands: Tropenbos International.

Mitchard, E. T. A. et al. (2014). Markedly divergent estimates of Amazon forest carbon density from ground plots and satellites. *Global Ecology and Biogeography*, *23*, 935–946. doi:10.1111/geb.12168.

Mitchard, E. T. A., Saatchi, S. S., Baccini, A., Asner, G. P., Goetz, S. J., Harris, N. L., & Brown, S. (2013). Uncertainty in the spatial distribution of tropical forest biomass: a comparison of pan-tropical maps. *Carbon Balance and Management*, *8*, 10. doi:10.1186/1750-0680-8-10.

Molto, Q., Rossi, V., & Blanc, L. (2013). Error propagation in biomass estimation in tropical forests. *Methods in Ecology and Evolution*, *4*, 175–183. doi:10.1111/j.2041-210x.2012.00266.x.

Momo Takoudjou, S., Ploton, P., Sonké, B., Hackenberg, J., Griffon, S., de Coligny, F., Kamdem, N. G., Libalah, M., Mofack, G. I. I., Le Moguédec, G., Pélissier, R., & Barbier, N. (2018). Using terrestrial laser scanning data to estimate large tropical trees biomass and calibrate allometric models: A comparison with traditional destructive approach. *Methods in Ecology and Evolution*, *9*, 905–916. doi:10.1111/2041-210X.12933. `arXiv:0608246v3`.

Muller-Landau, H. C. et al. (2006). Testing metabolic ecology theory for allometric scaling of tree size, growth and mortality in tropical forests. *Ecology Letters*, *9*, 575–588. doi:10.1111/j.1461-0248.2006.00904.x.

Muñoz, G., & Grieser, J. (2006). Climwat 2.0 for CROPWAT.

Newnham, G. G., Armston, J. D., Calders, K., Disney, M. I., Lovell, J. L., Schaaf, C. B., Strahler, A. H., & Danson, F. M. (2015). Terrestrial Laser Scanning for Plot-Scale Forest Measurement. *Current Forestry Reports*, *1*, 239–251. doi:10.1007/s40725-015-

0025-5.

Niklas, K. J. (1994). *Plant Allometry: The Scaling of Form and Process*. Chicago: University of Chicago Press.

Nogueira, E. M., Nelson, B. W., & Fearnside, P. M. (2005). Wood density in dense forest in central Amazonia, Brazil. *Forest Ecology and Management*, *208*, 261–286. doi:10.1016/j.foreco.2004.12.007.

Nölke, N., Fehrmann, L., I Nengah, S., Tiryana, T., Seidel, D., & Kleinn, C. (2015). On the geometry and allometry of big-buttressed trees - a challenge for forest monitoring: new insights from 3D-modeling with terrestrial laser scanning. *iForest - Biogeosciences and Forestry*, *8*, 574–581. doi:10.3832/ifor1449-007.

Nygren, P., & Pallardy, S. G. (2008). Applying a universal scaling model to vascular allometry in a single-stemmed, monopodially branching deciduous tree (Attim's model). *Tree physiology*, *28*, 1–10.

Olagoke, A., Proisy, C., Féret, J.-B., Blanchard, E., Fromard, F., Mehlig, U., de Menezes, M. M., dos Santos, V. F., & Berger, U. (2016). Extended biomass allometric equations for large mangrove trees from terrestrial LiDAR data. *Trees*, *30*, 935–947. doi:10.1007/s00468-015-1334-9.

Olivier, M.-D. D., Robert, S., & Richard A., F. (2017). A method to quantify canopy changes using multi-temporal terrestrial lidar data: Tree response to surrounding gaps. *Agricultural and Forest Meteorology*, *237-238*, 184–195. doi:10.1016/j.agrformet.2017.02.016.

Paynter, I., Genest, D., Peri, F., & Schaaf, C. (2018). Bounding uncertainty in volumetric geometric models for terrestrial lidar observations of ecosystems. *Interface Focus*, *8*, 20170043. doi:10.1098/rsfs.2017.0043.

Paynter, I., Saenz, E., Genest, D., Peri, F., Erb, A., Li, Z., Wiggin, K., Muir, J., Raumonen, P., Schaaf, E. S., Strahler, A., & Schaaf, C. (2016). Observing ecosystems with lightweight, rapid-scanning terrestrial lidar scanners. *Remote Sensing in Ecology and Conservation*, *2*, 174–189. doi:10.1002/rse2.26.

Petit, G., & Anfodillo, T. (2009). Plant physiology in theory and practice: An analysis of the WBE model for vascular plants. *Journal of Theoretical Biology*, *259*, 1–4. doi:10.1016/j.jtbi.2009.03.007.

Pfeifer, N., Gorte, B. H., & Winterhalder, D. (2004). Automatic reconstruction of single trees from terrestrial laser scanner data. *International Archives of Photogrammetry, Remote Sensing and Spatial Information Sciences*, *35*.

Phillips, O. L., Baker, T. R., Chao, K.-J., Jiménez, E., Lewis, S. L. S., Lloyd, J., Peacock, J., Lopez-Gonzalez, G., & Feldpausch, T. R. (2005). RAINFOR – Tree Field Work Database Codes.

Ploton, P. et al. (2016). Closing a gap in tropical forest biomass estimation: taking crown mass variation into account in pantropical allometries. *Biogeosciences*, *13*, 1571–1585. doi:10.5194/bg-13-1571-2016.

Portillo-Quintero, C., Sanchez-Azofeifa, A., & Culvenor, D. (2014). Using VEGNET In-Situ Monitoring LiDAR (IML) to Capture Dynamics of Plant Area Index, Structure and Phenology in Aspen Parkland Forests in Alberta, Canada. *Forests*, *5*, 1053–1068. doi:10.3390/f5051053.

Price, C. A., Enquist, B. J., & Savage, V. M. (2007). A general model for allometric covariation in botanical form and function. *Proceedings of the National Academy of Sciences*, *104*, 13204–13209. doi:10.1073/pnas.0702242104.

Price, C. A., Ogle, K., White, E. P., & Weitz, J. S. (2009). Evaluating scaling models in biology using hierarchical Bayesian approaches. *Ecology Letters*, *12*, 641–651. doi:10.1111/j.1461-0248.2009.01316.x.

Price, C. a. et al. (2012). Testing the metabolic theory of ecology. *Ecology Letters*, *15*, 1465–1474. doi:10.1111/j.1461-0248.2012.01860.x.

Pueschel, P., Newnham, G. G., Rock, G., Udelhoven, T., Werner, W., & Hill, J. (2013). The influence of scan mode and circle fitting on tree stem detection, stem diameter and volume extraction from terrestrial laser scans. *ISPRS Journal of Photogrammetry and Remote Sensing*, *77*, 44–56. doi:10.1016/j.isprsjprs.2012.12.001.

R Core Team (2017). R: A language and environment for statistical computing.

Rahman, M. Z. A. et al. (2017). Non-Destructive, Laser-Based Individual Tree Aboveground Biomass Estimation in a Tropical Rainforest. *Forests*, *8*, 86. doi:10.3390/f8030086.

Raumonen, P., Casella, E., Calders, K., Murphy, S., Åkerblom, M., & Kaasalainen, M. (2015). MASSIVE-SCALE TREE MODELLING FROM TLS DATA. *ISPRS Annals of Photogrammetry, Remote Sensing and Spatial Information Sciences*, *II-3/W4*, 189–196. doi:10.5194/isprsannals-II-3-W4-189-2015.

Raumonen, P., Kaasalainen, M., Åkerblom, M., Kaasalainen, S., Kaartinen, H., Vastaranta, M., Holopainen, M., Disney, M., & Lewis, P. (2013). Fast Automatic Precision Tree Models from Terrestrial Laser Scanner Data. *Remote Sensing*, *5*, 491–520. doi:10.3390/rs5020491.

Raumonen, P., Kaasalainen, S., Kaasalainen, M., & Kaartinen, H. (2011). Approximation of volume and branch size distribution of trees from laser scanner data. *International Archives of Photogrammetry, Remote Sensing and Spatial Information Sciences*, *XXXVIII*, 1–6.

Reinhardt, D., & Kuhlemeier, C. (2002). Plant architecture. *EMBO reports*, *3*, 846–51. doi:10.1093/embo-reports/kvf177.

Réjou-Méchain, M., Tanguy, A., Piponiot, C., Chave, J., & Hérault, B. (2017). biomass: An R package for estimating above-ground biomass and its uncertainty in tropical forests. *Methods in Ecology and Evolution*, (pp. 1163–1167). doi:10.1111/2041-210X.12753.

Rosati, A., Paoletti, A., Caporali, S., & Perri, E. (2013). The role of tree architecture in super high density olive orchards. *Scientia Horticulturae*, *161*, 24–29. doi:10.1016/j.scienta.2013.06.044.

Rosell, J. et al. (2009). Obtaining the three-dimensional structure of tree orchards from remote 2D terrestrial LIDAR scanning. *Agricultural and Forest Meteorology*, *149*, 1505–1515. doi:10.1016/j.agrformet.2009.04.008.

Saarinen, N. et al. (2017). Feasibility of Terrestrial laser scanning for collecting stem volume information from single trees. *ISPRS Journal of Photogrammetry and Remote Sensing*, *123*, 140–158. doi:10.1016/j.isprsjprs.2016.11.012.

Saatchi, S. S. et al. (2011). Benchmark map of forest carbon stocks in tropical regions across three continents. *Proceedings of the National Academy of Sciences*, *108*, 9899–9904. doi:10.1073/pnas.1019576108.

Savage, V. M., Bentley, L. P., Enquist, B. J., Sperry, J. S., Smith, D. D., Reich, P. B., & von Allmen, E. I. (2010). Hydraulic trade-offs and space filling enable better predictions of vascular structure and function in plants. *Proceedings of the National Academy of Sciences*, *107*, 22722–22727. doi:10.1073/pnas.1012194108.

Savage, V. M., Deeds, E. J., & Fontana, W. (2008). Sizing up allometric scaling theory. *PLoS computational biology*, *4*, e1000171. doi:10.1371/journal.pcbi.1000171.

Segura, M., & Kanninen, M. (2005). Allometric Models for Tree Volume and Total Aboveground Biomass in a Tropical Humid Forest in Costa Rica. *Biotropica*, *37*, 2–8. doi:10.1111/j.1744-7429.2005.02027.x.

Seidel, D., Fleck, S., & Leuschner, C. (2012). Analyzing forest canopies with ground-based laser scanning: A comparison with hemispherical photography. *Agricultural and Forest Meteorology*, *154-155*, 1–8. doi:10.1016/j.agrformet.2011.10.006.

Seidel, D., Fleck, S., Leuschner, C., & Hammett, T. (2011). Review of ground-based methods to measure the distribution of biomass in forest canopies. *Annals of Forest Science*, *68*, 225–244. doi:10.1007/s13595-011-0040-z.

Sheil, D., Eastaugh, C. S., Vlam, M., Zuidema, P. A., Groenendijk, P., van der Sleen, P., Jay, A., & Vanclay, J. (2017). Does biomass growth increase in the largest trees? Flaws, fallacies and alternative analyses. *Functional Ecology*, *31*, 568–581. doi:10.1111/1365-2435.12775.

Slik, J. W. F. et al. (2013). Large trees drive forest aboveground biomass variation in moist lowland forests across the tropics. *Global Ecology and Biogeography*, *22*, 1261–

1271. doi:10.1111/geb.12092.

Smith, A., Astrup, R., Raumonen, P., Liski, J., Krooks, A., Kaasalainen, S., Åkerblom, M., & Kaasalainen, M. (2014a). Tree Root System Characterization and Volume Estimation by Terrestrial Laser Scanning and Quantitative Structure Modeling. *Forests*, *5*, 3274–3294. doi:10.3390/f5123274.

Smith, D. D., Sperry, J. S., Enquist, B. J., Savage, V. M., McCulloh, K. A., & Bentley, L. P. (2014b). Deviation from symmetrically self-similar branching in trees predicts altered hydraulics, mechanics, light interception and metabolic scaling. *New Phytologist*, *201*, 217–229. doi:10.1111/nph.12487.

Sperry, J. S., Smith, D. D., Savage, V. M., Enquist, B. J., McCulloh, K. a., Reich, P. B., Bentley, L. P., & von Allmen, E. I. (2012). A species-level model for metabolic scaling in trees I. Exploring boundaries to scaling space within and across species. *Functional Ecology*, *26*, 1054–1065. doi:10.1111/j.1365-2435.2012.02022.x.

Srinivasan, S., Popescu, S., Eriksson, M., Sheridan, R., & Ku, N.-W. (2015). Terrestrial Laser Scanning as an Effective Tool to Retrieve Tree Level Height, Crown Width, and Stem Diameter. *Remote Sensing*, *7*, 1877–1896. doi:10.3390/rs70201877.

Stegen, J. C., Swenson, N. G., Enquist, B. J., White, E. P., Phillips, O. L., Jørgensen, P. M., Weiser, M. D., Monteagudo Mendoza, A., & Núñez Vargas, P. (2011). Variation in above-ground forest biomass across broad climatic gradients. *Global Ecology and Biogeography*, *20*, 744–754. doi:10.1111/j.1466-8238.2010.00645.x.

Stovall, A. E., Anderson-Teixeira, K. J., & Shugart, H. H. (2018). Assessing terrestrial laser scanning for developing non-destructive biomass allometry. *Forest Ecology and Management*, *427*, 217–229. doi:10.1016/j.foreco.2018.06.004.

Stovall, A. E., Vorster, A. G., Anderson, R. S., Evangelista, P. H., & Shugart, H. H. (2017). Non-destructive aboveground biomass estimation of coniferous trees using terrestrial LiDAR. *Remote Sensing of Environment*, *200*, 31–42. doi:10.1016/j.rse.2017.08.013.

Stovall, A. E. L., & Shugart, H. H. (2018). Improved Biomass Calibration and Validation With Terrestrial LiDAR: Implications for Future LiDAR and SAR Missions. *IEEE Journal of Selected Topics in Applied Earth Observations and Remote Sensing*, (pp. 1–11). doi:10.1109/JSTARS.2018.2803110.

Strahler, A. H., Jupp, D. L. B., Woodcock, C. E., Schaaf, C. B., Yao, T., Zhao, F., Yang, X., Lovell, J. L., Culvenor, D., Newnham, G. G. J., Ni-Meister, W., & Boykin-Morris, W. (2008). Retrieval of forest structural parameters using a ground-based lidar instrument (Echidna ®). *Canadian Journal of Remote Sensing*, *34*, S426—-S440. doi:10.5589/m08-046.

Sullivan, M. J. P. et al. (2018). Field methods for sampling tree height for tropical forest biomass estimation. *Methods in Ecology and Evolution*, *2018*, 1–11. doi:10.1111/2041-210X.12962.

Tansey, K., Selmes, N., Anstee, A., Tate, N. J., & Denniss, A. (2009). Estimating tree and stand variables in a Corsican Pine woodland from terrestrial laser scanner data. *International Journal of Remote Sensing*, *30*, 5195–5209. doi:10.1080/01431160902882587.

The MathWorks Inc. (2014). MatLab 2013a and Statistics Toolbox.

Thies, M., Pfeifer, N., Winterhalder, D., & Gorte, B. H. (2004). Three-dimensional reconstruction of stems for assessment of taper, sweep and lean based on laser scanning of standing trees. *Scandinavian Journal of Forest Research*, *19*, 571–581. doi:10.1080/02827580410019562.

Tredennick, A. T., Bentley, L. P., & Hanan, N. P. (2013). Allometric Convergence in Savanna Trees and Implications for the Use of Plant Scaling Models in Variable Ecosystems. *PLoS ONE*, *8*, e58241. doi:10.1371/journal.pone.0058241.

Trochta, J., Kruček, M., Vrška, T., & Kraâl, K. (2017). 3D Forest: An application for descriptions of three-dimensional forest structures using terrestrial LiDAR. *PLoS ONE*, *12*, 1–17. doi:10.1371/journal.pone.0176871.

Van der Zande, D., Hoet, W., Jonckheere, I., van Aardt, J., & Coppin, P. (2006). Influence of measurement set-up of ground-based LiDAR for derivation of tree structure. *Agricultural and Forest Meteorology*, *141*, 147–160. doi:10.1016/j.agrformet.2006.09.007.

Vicari, M. (2017). TLSeparation. doi:10.5281/ZENODO.802233.

Wallace, L., Lucieer, A., Malenovský, Z., Turner, D., & Vopěnka, P. (2016). Assessment of Forest Structure Using Two UAV Techniques: A Comparison of Airborne Laser Scanning and Structure from Motion (SfM) Point Clouds. *Forests*, *7*, 62. doi:10.3390/f7030062.

West, G. B. (1999a). The Fourth Dimension of Life: Fractal Geometry and Allometric Scaling of Organisms. *Science*, *284*, 1677–1679. doi:10.1126/science.284.5420.1677.

West, G. B. (1999b). The origin of universal scaling laws in biology. *Physica A: Statistical Mechanics and its Applications*, *263*, 104–113. doi:10.1016/S0378-4371(98)00639-6.

West, G. B., Brown, J. H., & Enquist, B. J. (1997). A General Model for the Origin of Allometric Scaling Laws in Biology. *Science*, *276*, 122–126. doi:10.1126/science.276.5309.122.

West, G. B., Enquist, B. J., & Brown, J. H. (2009). A general quantitative theory of forest structure and dynamics. *Proceedings of the National Academy of Sciences of the United States of America*, *106*, 7040–7045. doi:10.1073/pnas.0812294106.

Wilkes, P., Lau, A., Disney, M., Calders, K., Burt, A., Gonzalez de Tanago, J., Bartholomeus, H., Brede, B., & Herold, M. (2017). Data acquisition considerations for Terrestrial Laser Scanning of forest plots. *Remote Sensing of Environment*, *196*, 140–153. doi:10.1016/j.rse.2017.04.030.

Williamson, G. B., & Wiemann, M. C. (2010). Measuring wood specific gravity...correctly.

American Journal of Botany, *97*, 519–524. doi:10.3732/ajb.0900243.

Xi, Z., Hopkinson, C., & Chasmer, L. (2016). Automating Plot-Level Stem Analysis from Terrestrial Laser Scanning. *Forests*, *7*, 252. doi:10.3390/f7110252.

Yao, T. et al. (2011). Measuring forest structure and biomass in New England forest stands using Echidna ground-based lidar. *Remote Sensing of Environment*, *115*, 2965–2974. doi:10.1016/j.rse.2010.03.019.

Zanne, A. E., Lopez-Gonzalez, G., Coomes, D. a., Ilic, J., Jansen, S., Lewis, S. L. S., Miller, R. B., Swenson, N. G., Wiemann, M. C., & Chave, J. J. J. J. (2009). Data from: Towards a worldwide wood economics spectrum. doi:10.5061/dryad.234.

Zhao, F., Guo, Q., & Kelly, M. (2012). Allometric equation choice impacts lidar-based forest biomass estimates: A case study from the Sierra National Forest, CA. *Agricultural and Forest Meteorology*, *165*, 64–72. doi:10.1016/j.agrformet.2012.05.019.

Zhu, X., Skidmore, A. K., Darvishzadeh, R., Niemann, K. O., Liu, J., Shi, Y., & Wang, T. (2018). Foliar and woody materials discriminated using terrestrial LiDAR in a mixed natural forest. *International Journal of Applied Earth Observation and Geoinformation*, *64*, 43–50. doi:10.1016/j.jag.2017.09.004.

Zuidema, P. a., Baker, P. J., Groenendijk, P., Schippers, P., van der Sleen, P., Vlam, M., & Sterck, F. (2013). Tropical forests and global change: filling knowledge gaps. *Trends in plant science*, *18*, 413–419. doi:10.1016/j.tplants.2013.05.006.

Wayqecha, Peru

Acknowledgements

I truly believe nothing happens by chance and the fact that I am now, standing here and defending my PhD today is because of the impact you all had on me throughout my life and on every aspect of it. Although this seems to be the easiest part to write of a thesis (and maybe, the most read one) it is certainly hard to, within these lines, express all the gratitude I have for each and every one of you. Every person I met in my life had enriched me in every aspect, from the professional, to the academic, and personal. For that, I thank you from the bottom of my heart.

First of all, I would like to thank my promotor Martin Herold. I appreciate all the guidance and support during all these years; not only during the PhD, but also during the MSc. thesis and the upcoming years. Thanks for being committed to my research and for shaping our brainstorming sessions into scientific papers. Your leadership in the chair group is clearly and very much appreciated.

Second, I would like to thank my co-promotors Harm Bartholomeus and Kim Calders for all the support throughout my academic life in Wageningen. I would like also to thank Christopher Martius for his guidance and support. I appreciate all the countless "daily supervisor" meetings which contributed greatly to the successful completion of my PhD and all the brainstorming and discussion sessions I had with all of you. Harm, I am very grateful that I could always run into your office for any type of question, and you always had an answer.

I would like to thank my PhD opponents for their time and dedication for reading this thesis, attending the defence and that they could discuss it here today with me. Moreover, I would like to thanks all my co-authors and especially the anonymous reviewers who made science possible. Special thanks to Andy B., Allie, Lisa PB, Mat, Phil, Rosa G., Shijo, and Yadvinder for enriched me academically. This thesis would not have been completed without all the support I had before, during and after the fieldwork campaigns. For that, I want to acknowledge and thank the hard work of Andy S., Cornelis, Filio, Carey, Hans S., Jens, Jeremy, Justice, Uji, Neil, Walter, and specially the GFC team (specially Pradeepa and Nasheta). A special thanks for my paranymphs Sarah Carter and Sarahi Nuñez for standing with me on the podium and your attentive and detailed support for the very last part of my PhD: the party!

A todos mis amigos en Perú, quienes siempre me dan la bienvenida, ya sea con una cena o con un Sargento. ¡Me disculpan si es que no logro ver a todos cada vez que regreso! Un abrazo a Domingo, Fabiola E., Gilda, Lesly, Liz H., Lucía P., Mayumi, Naomi, y Vera. Especialmente quiero agradecer a mis amigos del cole, tantos recuerdos juntos: Caro S., César A., Cynthia T., el chino JuanCa, Machie, Moni, Mori, Pame C., Patty B., Ronald, Sileng, Silvia C., Luxia, Giovi, Tamy, Elia, Maribel, y Wendy. Y a mi querido grupex, no sé que hubiera sido de la UNALM sin ustedes: Ale F., Alonso, Bruno, Carlos Q., Claus, Diana I., Giuli, Hajime, Lorena G., Manolín, y Ruy.

Quisiera agradecer a las personas que me han formado profesionalmente en Perú. Al Sr. Percy G., por darme la oportunidad de mi primer trabajo. También al Laboratorio de Pastizales de la UNALM, especialmente al Dr. E. Flores y a la Dr. Lucrecia A. por formarme profesional y académicamente. Tambien quiero agradecer a Reynaldo, y al Dr. Javier Ñ. Y finalmente al Insituto Rural Valle Grande - IRVG y de manera especial al "Equipo Sierra" por todo el apoyo durante nuestra temporada en la Reserva paisajística Nor Yauyos-Cochas y en LLapay. Gracias Eduardo R., Jonay J., Juan Pablo A., Mario A., Mark P., Rodolfo M., y Yayo.

I always say that every new day in the Netherlands is a new adventure for me. I am very happy to have met so many wonderful people; people who had showed me that we have more in common than I ever thought of. Thanks Alessandra C., Amalia C., Anne E., Anton, Begoña, Careli, Charlotte, Daisy, Diana K., Djakhongir, Evelien VT, Giulia C. Gvantsa, Jana H., Jeroen, Jhon J., Juanma, Kiki, Laura G., Laura P., Luchito J., Luz, Marie-José (bedankt voor het Nederlandse lessen), María L., Marta W., Mirja, Montserrat & Duda, Nadine, Pierre, Sean, Simona, Sruthi, Sven, Trini, Victor D., and Zi-Hua & Mathieu P. Θέλω να ευχαριστήσω ιδιαίτερα την ελληνική οικογένειά μου. Ευχαριστώ την Ιουλία, τον Ηρακλή, τον Γιώργο και την Χαρά, την Δήμητρα, τη Βίκυ Α., τη Χριστίνα Φ., τον Βασίλη Κ., Τον Νικόλα Π. την Adri, τη Μαρία Π., την Ειρήνη Τ., Τη Ρούλα, τον Άκη και τον Δημήτρη Κ. που μου έδειξαν τον ελληνικό τρόπο ζωής. Ποτέ δεν περίμενα να νιώθω στην Ευρώπη, σαν το σπίτι μου. Είμαι πολύ ευγνώμων που σας γνώρισα όλους και ιδιαίτερα για την ελληνική κουζίνα!

A phrase says: "Home is where the heart is". Staying in Bennekom and especially in the "Corridor above the Clouds" would've not been the same without you guys. Thanks Aslihan, Carmen B., César N., Ceylan, Chetna, Claudia R. (el trío latino), Daniela Potočnjak, Eleonora P., Emma, Emilio L., Jose Alejandro T., Josue F., Luz, Margarita & Marek, Maria Laura M., Paul, and Prarthana for all the dinners, parties, and funny moments in the building. Moving from Bennekom to Wageningen was tough, but special. I am pleased to say that after fieldwork in some tropical country or just a whole day of work is always nice to be "back home". And I feel fortunate to have shared it with my housemates. Thank Claus, Lore, Silvia, Sonia, Justine, Julia, Marion and Leo for the everyday life I spent with you and all the moments we shared together; breakfasts, lunches, dinners,

parties, Netflix marathons and countless times together. You made me called that place “home” and you “family”.

Quiero agradecer a mi peruvian crew en Wageningen y alrededores. Estar con ustedes es como estar de regreso en Perú. Gracias por mi épica bienvenida Ale y Claus, siempre me acordaré de mi primera noche en Europa. Gracias Ale F., Alejo & Cris, Andrea F., Claudia S., Claudia V., Cristian T., Daniella Rojas, Deborah, Diana M., Ekatherina, Eli, Fanny, Gaby L., Gaby R., Giuli, Hugo, Jimmy, John L., Juanita, Julia C., Laura E., Lorena DP & Peter, Matías & Florie (merci pour les cours de français donnés à mon père!) Martín C., Mili, Moises C., Mylu, Ornella, Pame A., Renato C., Rik, Rosa C., Sergio, Yngrid, y Vero O. Siempre son bienvenidos a la “Peruvian Embassy”, especialmente para los potluck kipfeestjes!

From lunches, coffee breaks, afternoon cakes (especially on March), borrels, dinners, outings, Nederlandse koffie pauzes, and even, one-day fieldworks to Dassenbos and Speulderbos; life in office would be sooo boring without my colleagues and staff of our lovely chair group. For that, I want to thank Agnieszka, Aldo, Anne H. & Tom, Arnold, Arend, Arun & Puja, Astrid & Mark, Ben B. & Anna, Ben K., Ben DV., Brice, Christelle, Corne V., Dainius, Danaë, Dani Requena, Devis & Laure, Diego, Eliakim, Eskender, Erika R., Erika S., Giulia S., Jalal, Jan C., Jan V., Joao, Johannes B., Johannes R., John S., John V., Jose G., Juha, Kalkidan, Konstantin, Lala, Lammert, Loïc, Lucasz, Marcello, Maria P., Marian V., Marston, Mathieu D., Michi, Nandika & Sukhad, Niki, Patric, Peter & Marcela, Qijun, Richard F., Roberto, Ron, Rosa Maria., Sabina R. & Andrei, Samantha, Shivangi, Simon, Sylvain, Sytze, Tsoefiet, Valerio, Willy, and Yang, Special thanks goes to Antoinette and Truus for their endless support on the administrative side, especially on the first years translating all the Dutch for me (niet meer!!). I want to thank also Claudius and Lennart for all the support from PE & RC during these four years.

Finally, I would like to give a big thanks and a lot of love to my amazing family. A mis padres: Julia y Ricardo y mi hermana Fabiola por todo el apoyo desde que tengo uso de razón. Quiero agradecerles el soporte incondicional en todo momento, creyendo en mí aún cuando yo no tenia fé en mí mismo. Agradezco cada día de tenerlos a mi lado, aunque un océano de distancia nos separa, nunca los he sentido más cerca. Gracias a mi Apo, Acun, abuelito Victor y al chato por cuidarme desde el cielo. Quiero agradecer de la misma manera a todos mis tíos y tías que me han apoyado y especialmente a mi tía Gloria y mi tío Victor, a quienes los considero mi parte de mi familia. Agradezco tambien a mis tíos Juan del Risco, Pepe y mis padrinos Carlos y Dannis. Gracias por todo el apoyo incondicional y yo no estaría acá si no fuera por todos ustedes. Ik wil dit hoofdstuk niet afsluiten zonder jou, Rianne, te noemen. Bedankt voor alle geweldige momenten samen en alles wat nog komen gaat!

¡Gracias totales!

Central Kalimantan, Indonesia

About the author

Alvaro Lau, son of Mr. Ricardo Lau and Mrs. Julia Sarmiento de Lau, was born in Lima, Peru on March 25th, 1985. He completed his primary and secondary education at Colegio Peruano Chino Juan XXIII, in Lima. As a child, Alvaro was fascinated with dinosaurs and decided he would become a scientist to clone dinosaurs.

He wanted to study biology; however, destiny lead him to study animal science. Alvaro began his BSc. in Animal Science at the Universidad Nacional Agraria La Molina - UNALM, Lima, Peru in 2003. One year before culminating his BSc. studies, he decided that animal science was not fulfilling his life, so he took environmental science courses. He completed his BSc. in Animal Science with honours in 2008.

Right after his bachelors, he started working in the Ecology and Rangeland Utilization Laboratory - UNALM, under the supervision of Dr. Enrique Flores Mariazza. He worked as a research assistant in natural resource management of Peruvian highlands and became involved with GIS and remote sensing tools for the first time. In addition, he started a minor in Quality Management and Environmental Auditing Professional, which he also completed with honours.

After working two years at UNALM, he started working in Valle Grande Rural Institute - IRVG; a Peruvian NGO dedicated to improving the quality of life of local communities through forestry, animal husbandry, natural resource, and women's empowerment projects in Nor-Yauyos Cochas National Reserve, in Lima region. Here, he was in charge of the Geo-Information System and Decision Support office. After working in IRVG for more than two years, he realized that his almost-self-taught knowledge on GIS and remote sensing was not enough and decided to pursue master studies in GIS and remote sensing.

Knowing the reputation of Wageningen University and Research, and having some close friends studying there, he applied for MSc. studies. Alvaro was awarded the NUFFIC scholarship in 2012 and travelled to the Netherlands to begin his MSc. studies in the Geo-Information Science MSc. programme. When looking for a thesis topic, Alvaro always wanted to do his thesis research with data from Peru. By chance, he ran into Martin Herold, who just had a talk with Yadvinder Malhi (University of Oxford) and discussed

the possibility of a fieldwork in Peru. Alvaro accepted immediately —free flight ticket to Peru. The topic: terrestrial laser scanning (TLS) in the Peruvian Amazon. This is how he became involved in the TLS world. After the successful fieldwork, he wrote his major and minor thesis with the TLS data collected in Peru.

Right after MSc. studies, Alvaro was invited to continue his research in the Laboratory of Geo-Information Science and Remote Sensing at Wageningen University and Research as a PhD candidate. His PhD thesis entitled: "Assessing biomass and architecture of tropical trees with terrestrial laser scanning" is part of the "Global comparative study on REDD+" of the Center for International Forestry Research (CIFOR). During his PhD research, he successfully led several fieldwork campaigns in tropical countries and presented his research in important international conferences and symposia. Alvaro is an active member of the TLS research community and co-authored several publications.

Alvaro's current research interests are related to the estimation of tree parameters from TLS point clouds of tropical trees. Following his PhD, and after some deserved holidays, he will continue his research career as a post-doctoral researcher at Wageningen University and Research.

List of publications

Peer-reviewed publications

Lau, A., Bentley, L.P., Martius, C., Shenkin, A., Bartholomeus, H., Raumonen, P., Malhi, Y., Jackson, T. & Herold, M. (2018). Quantifying branch architecture of tropical trees using terrestrial LiDAR and 3D modelling. *Trees - Structure and Function*, 13. DOI: 10.1007/s00468-018-1704-1

Malhi, Y., Jackson, T., Patrick Bentley, L., **Lau, A.**, Shenkin, A., Herold, M., Calders, K., Bartholomeus, H. & Disney, M.I. (2018). New perspectives on the ecology of tree structure and tree communities through terrestrial laser scanning. *Interface Focus*, 8, DOI: 10.1098/rsfs.2017.0052

Gonzalez de Tanago, J., **Lau, A.**, Bartholomeus, H., Herold, M., Avitabile, V., Raumonen, P., Martius, C., Goodman, R.C., Disney, M., Manuri, S., Burt, A. & Calders, K. (2018). Estimation of above-ground biomass of large tropical trees with terrestrial LiDAR. *Methods in Ecology and Evolution*, 9, 223–234. DOI: 10.1111/2041-210X.12904

Pfeifer, M., Gonsamo, A., Woodgate, W., Cayuela, L., Marshall, A.R., Ledo, A., Paine, T.C.E., Marchant, R., Burt, A., Calders, K., Courtney-Mustaphi, C., Cuni-Sanchez, A., Deere, N.J., Denu, D., de Tanago, J.G., Hayward, R., **Lau, A.**, Macía, M.J., Olivier, P.I., Pellikka, P., Seki, H., Shirima, D., Trevithick, R., Wedeux, B., Wheeler, C., Munishi, P.K.T., Martin, T., Mustari, A. & Platts, P.J. (2018). Tropical forest canopies and their relationships with climate and disturbance: results from a global dataset of consistent field-based measurements. *Forest Ecosystems*, 5, 7. DOI: 10.1186/s40663-017-0118-7

Brede, B., **Lau, A.**, Bartholomeus, H. & Kooistra, L. (2017). Comparing RIEGL RiCOPTER UAV LiDAR Derived Canopy Height and DBH with Terrestrial LiDAR. *Sensors*, 17, 2371. DOI: 10.3390/s17102371

Wilkes, P., **Lau, A.**, Disney, M., Calders, K., Burt, A., Gonzalez de Tanago, J., Bartholomeus, H., Brede, B. & Herold, M. (2017). Data acquisition considerations for Terrestrial Laser Scanning of forest plots. *Remote Sensing of Environment*, 196, 140–153.

DOI: 10.1016/j.rse.2017.04.030

Other scientific publications

Lau, A., Gonzalez de Tanago, J., Bartholomeus, H., Herold, M., Avitabile, V., Raumonen, P., Martius, C., Goodman, R.C., Disney, M.I., Manuri, S., Burt, A. & Calders, K. (2017). Above-ground biomass assessment of tropical trees with Terrestrial LiDAR and 3D architecture models. *SilviLaser*, pp. 123–124. Blacksburg, Virginia, US.

Bartholomeus, H., **Lau, A.**, Gonzalez de Tanago, J., Herold, M., Brede, B., Kooistra, L. & Calders, K. (2017). Capturing forest structure and change–5 years of laser scanning and future perspectives using UAV based LiDAR. *SilviLaser*, pp. 61–62. Blacksburg, Virginia, US.

Bartholomeus, H., Brede, B., **Lau, A.** & Kooistra, L. (2017). Capturing forest structure using UAV based LiDAR.

Lau, A., Bartholomeus, H., Herold, M., Martius, C., Malhi, Y., Bentley, L.P., Shenkin, A. & Raumonen, P. (2017). Application of terrestrial LiDAR and modelling of tree branching structure for plant-scaling models in tropical forest trees. *The terrestrial laser scanning revolution in forest ecology*. Buckinghamshire, UK.

Gonzalez de Tanago, J., **Lau, A.**, Bartholomeus, H., Herold, M., Raumonen, P., Avitabile, V., Martius, C. & Joseph, S. (2016). Quantification of Tropical Forest Biomass with Terrestrial LiDAR and 3D Tree Quantitative Structure Modelling. *ESA Living Planet Symposium*. European Space Agency (ESA), Prague, Czech republic.

Lau, A., Gonzalez de Tanago, J., Bartholomeus, H., Herold, M., Raumonen, P., Avitabile, V., Martius, C., Goodman, R.C. & Manuri, S. (2016). Terrestrial LiDAR and 3D Reconstruction Models for Estimation of Large Tree Biomass in the Tropics. *ForestSat*. Santiago de Chile, Chile.

Lau, A., Herold, M., Bartholomeus, H. & Gonzalez de Tanago, J. (2016). Terrestrial LiDAR and 3D Reconstruction Models for Large Individual Tree Biomass Estimation in Tropics. *NCG Symposium*. Enschede, the Netherlands.

Lau, A., Bartholomeus, H., Herold, M., Martius, C., Malhi, Y., Bentley, L.P., Shenkin, A. & Raumonen, P. (2016). Application of Terrestrial LiDAR and Modelling of Tree Branching Structure for Plant-scaling Models in Tropical Forest Trees. *Living Planet Symposium*. Prague, Czech republic.

Herold, M., García Esteban, M., **Lau, A.**, Hoosbeek, M., Adam, K., Morton, D., Martorano, L.G., Lisboa, L.S., Muniz, R., Sotta, E., Beltrão, N.E.S., Vettorazzi, C.A., do Nascimento, N.C., Guadalupe, V., de Aguiar, L.J.G., dos Santos, V.F., Simoes, M. &

Ferraz, R. (2015). Effects of land use changes on ecosystem processes, carbon storage and climate change mitigation.

Lau, A., Calders, K., Herold, M., Avitabile, V., Raumonen, P., Gonzalez de Tanago, J. & Bartholomeus, H. (2015). Terrestrial Laser Scanning for measuring forest biomass change. *1st BIOMASS Science Workshop*. European Space Agency (ESA), Frascati, Italy.

Lau, A., Bartholomeus, H., Herold, M., Martius, C., Malhi, Y., Bentley, L.P., Shenkin, A. & Raumonen, P. (2015). Application of terrestrial LiDAR and modelling of tree branching structure for plant-scaling models in tropical forest trees. *SilviLaser*. La Grande Motte, France.

Bartholomeus, H., Gonzalez de Tanago, J., Calders, K., **Lau, A.** & Herold, M. (2014). Acquisition of terrestrial LIDAR in tropical forest to support ecological research. *NAEM*. Lunteren.

Lau, A., Bartholomeus, H. & Gonzalez de Tanago, J. (2014). Evaluation of different scan configurations for an effective field procedure on a terrestrial LiDAR scanner in tropical forest. *ForestSat*. Riva del Garda, Italy.

Gonzalez de Tanago, J., Joseph, S., Herold, M., Goodman, R.C., Bartholomeus, H., Avitabile, V., Raumonen, P., Calders, K., **Lau, A.** & Janovec, J. (2014). Terrestrial LiDAR and 3D tree reconstruction modeling for quantification of biomass loss and characterization of impacts of selective logging in tropical forest of Peruvian Amazon. Multi-sensor assessment, combining near and remote sensing. *ForestSat*. Riva del Garda, Italy.

Lau, A. (2014). Evaluation of different scan configurations for an effective field procedure on a Terrestrial LiDAR Scanner in Tropical Forest. *MSc thesis*, Wageningen University and Research.

Lau, A. (2014). Using T-LiDAR as an alternative measurement technique for plant-scaling modelling in tropical forest. *MSc thesis*, Wageningen University and Research.

Lau, A. (2010). Evaluación económica ambiental de un plan de manejo y gestión de la granja comercial de la C.C. Huantan - Lima. *BSc thesis*, Universidad Nacional Agraria La Molina.

Aula - Wageningen Campus, the Netherlands

PE&RC Training and Education Statement

With the training and education activities listed below the PhD candidate has complied with the requirements set by the C.T. de Wit Graduate School for Production Ecology and Resource Conservation (PE&RC) which comprises of a minimum total of 32 ECTS (= 22 weeks of activities)

Review of literature (6 ECTS)

- An overview of current methods to reconstruct tropical tree architecture from terrestrial LiDAR point clouds (2014)

Writing of project proposal (4.5 ECTS)

- Asssessing tropical forest characteristics with terrestrial laser scanning

Post-graduate courses (4 ECTS)

- REDD+ Monitoring, and measurement, reporting and verification workshop: Training the trainers; Lima, Peru (2016)
- Programming in Matlab; BioSB & PE&RC (2017)
- R & Big Data; PE&RC (2017)
- Workshop of CIFOR's global Comparative Study; Guyana Forestry Commission & CIFOR (2018)

Laboratory training and working visits (3.3 ECTS)

- Quantitative Structure Models; University of Tampere, Finland (2014)
- Tree extraction algorithm; University College London, UK (2015)
- Plant scaling modelling; University of Oxford, UK (2015)
- ERA GAS meeting; AMAP - IRD, France (2018)

Invited review of (unpublished) journal manuscript (3 ECTS)

- Remote Sensing: upscaling TLS using world-view 2 images (2015)
- International Journal of Geographical Information Science: 3D tree modelling from incomplete point clouds via optimization and L1-MST (2016)
- Remote Sensing: parsing building facades from TLS point cloud data (2016)

Competence strengthening / skills courses (6.1 ECTS)

- Project and Time Management; WGS (2015)
- Techniques for writing and presenting scientific papers; WGS (2015)
- Scientific writing SW6; Wageningen into Languages (2015)
- Reviewing a scientific paper; Wageningen UR Library (2015)
- Data Management planning; WGS (2016)
- Presenting with Impact; Wageningen into Languages (2016)
- Writing grant proposals; WGS (2016)
- Version management for data files and documents; Wageningen UR Library (2016)
- Interpersonal Communication for PhD candidates; Wageningen UR (2017)

PE&RC Annual meetings, seminars and the PE&RC weekend (3.6 ECTS)

- PE&RC PhD First year weekend (2015)
- Wageningen PhD Council (2015)
- PE&RC day (2015)
- 3rd WGS PhD Workshop Carousel (2016)
- 3rd PhD Symposium + convenor session (2016)
- PhD Day (2016)
- PhD Midterm weekend (2017)
- PhD Last year weekend (2018)

Discussion groups / local seminars or scientific meetings (7.5 ECTS)

- RCN Initiative + 1 meeting in UCL (2015–2018)
- REDD+ & CAS discussion group (2015–2018)
- Remote sensing thematic group (2015–2018)

International symposia, workshops and conferences (13.2 ECTS)

- ESA Biomass Workshop; Frascati, Italy (2015)
- Silvilaser; La Grande Motte, France (2015)
- 2nd Storymap workshop; Wageningen, the Netherlands (2015)
- Global Landscape Forum, part of COP21; Paris, France (2015)
- 3rd PhD Symposium "Diversity in Science"; Wageningen, the Netherlands (2016)
- Living planet symposium; Prague, Czech Republic (2016)
- CIFOR M3 Project Meeting; Bonn, Germany (2016)

- NGC Symposium; Enschede, the Netherlands (2016)
- ForestSat; Santiago de Chile, Chile (2016)
- The Terrestrial Laser Scanner Revolution in Forest Ecology; Chicheley Hall, United Kingdom (2017)
- Silvilaser; Virginia, US (2017)

Lecturing / supervision of practical's / tutorials (3.6 ECTS)

- Advanced earth observation
- Geo Media & design
- Geo-Information introduction for planning

Supervision of MSc students (5 ECTS)

- Above Ground Biomass Estimation in palm trees using terrestrial LiDAR and tree modelling; Adriana Caballero

This research is part of CIFOR's Global Comparative Study on REDD+ with financial support from the donors to the CGIAR Fund, SilvaCarbon research project 14IG-11132762-350 and ERA-GAS NWO-3DforMod project 5160957540.

Financial support from Wageningen University and Research for printing this thesis is gratefully acknowledged.

Photos (left and right) in page 3 by Jose Gonzalez de Tanago.
Photos in page 3 (center) and page 4 by Alvaro Lau.
Photos in page xii, 10, 32, 70, 90, 114, 128, 114, 148, and 154 by Alvaro Lau and edited by Eleonora Fiorin.

Cover design by Alvaro Lau and Eleonora Fiorin from a TLS point cloud in Guyana.

Printed by: DigiForce || ProefschriftMaken

Propositions

1. Terrestrial laser scanning of tropical trees captures more detail than manual measurements.
   (this thesis)

2. Terrestrial laser scanning will improve national tropical forest inventories.
   (this thesis)

3. Version control systems are a silent hero in scientific research.

4. Big data is like a thrift shop: a researcher's noise data is another's input data.

5. A PhD advances thanks to educated "educated guesses".

6. Clear judgement is inversely proportional to your deadline.

Propositions belonging to the thesis, entitled

"Assessing biomass and architecture of tropical trees using terrestrial laser scanning"

Alvaro Ivan Lau Sarmiento

Wageningen, 30 October 2018